DTIC FILE COPY

NAVAL POSTGRADUATE SCHOOL
Monterey, California

THESIS

WIND FORCING OF EDDIES AND
JETS IN THE
CALIFORNIA CURRENT SYSTEM

by

Terrance A. Tielking

June 1988

Thesis Advisor: Mary L. Batteen

DTIC
SELECTED
DEC 0 6 1988
E

88 12 6 025

NAVAL POSTGRADUATE SCHOOL
Monterey, California

Rear Admiral R. C. Austin   K. T. Marshall
Superintendent   Acting Provost

Released by:

GORDON E. SCHACHER
Dean of Science and Engineering

REPORT DOCUMENTATION PAGE

1a. REPORT SECURITY CLASSIFICATION	1b RESTRICTIVE MARKINGS
UNCLASSIFIED	

2a. SECURITY CLASSIFICATION AUTHORITY	3 DISTRIBUTION AVAILABILITY OF REPORT
	Approved for public release.
2b. DECLASSIFICATION / DOWNGRADING SCHEDULE	Distribution is unlimited.

4. PERFORMING ORGANIZATION REPORT NUMBER(S)	5 MONITORING ORGANIZATION REPORT NUMBER(S)
NPS 68-88-006	

6a. NAME OF PERFORMING ORGANIZATION	6b OFFICE SYMBOL (If applicable)	7a NAME OF MONITORING ORGANIZATION
Naval Postgraduate School	68	Office of Naval Research

6c. ADDRESS (City, State, and ZIP Code)	7b ADDRESS (City, State, and ZIP Code)
Monterey, California 93943-5000	800 N. Quincy St. Arlington, VA 22217-5000

8a. NAME OF FUNDING / SPONSORING ORGANIZATION	8b. OFFICE SYMBOL (If applicable)	9. PROCUREMENT INSTRUMENT IDENTIFICATION NUMBER
Naval Postgraduate School	68	O&MN, Direct Funding

8c. ADDRESS (City, State, and ZIP Code)	10 SOURCE OF FUNDING NUMBERS			
	PROGRAM ELEMENT NO	PROJECT NO	TASK NO	WORK UNIT ACCESSION NO
Monterey, California 93943-5000				

11. TITLE (Include Security Classification)

Wind Forcing of Eddies and Jets in the California Current System

12. PERSONAL AUTHOR(S)
Tielking, Terrance A. in conjunction with M.L. Batteen

13a TYPE OF REPORT	13b TIME COVERED	14. DATE OF REPORT (Year, Month, Day)	15 PAGE COUNT
Master's Thesis	FROM _____ TO _____	June 1988	118

16. SUPPLEMENTARY NOTATION The views expressed in this thesis are those of the author and do not reflect the official policy or position of the Department of Defense or the U.S. Government.

17	COSATI CODES		18 SUBJECT TERMS (Continue on reverse if necessary and identify by block number)
FIELD	GROUP	SUB-GROUP	PE ocean model eddies and jets
			California Current System wind forcing
			wind stress curl coastal jet and undercurrent

19. ABSTRACT (Continue on reverse if necessary and identify by block number)

A high-resolution, multi-level, primitive equation ocean model is used to examine the response to wind forcing of an idealized flat-bottomed oceanic regime along an eastern ocean boundary. A band of steady winds, either with or without a curl, is used as forcing on both an f-plane and a β-plane. In addition, a stability analysis is made to determine if the necessary and sufficient conditions for instability processes to occur are satisfied. It is seen that when the wind driven coastal jet and undercurrent are unstable (which occurs in the cases of wind with no curl), eddies and jets are generated. In the case of wind with curl, since the Davidson Current develops rather than the coastal jet and undercurrent, no eddies develop. A comparison of model results with available observations shows that both the time-averaged and instantaneous model simulations of the coastal jet, undercurrent and eddies are consistent with available observational data. The results of this study support the hypothesis that wind forcing can be an important eddy generation mechanism for the California Current System.

20 DISTRIBUTION / AVAILABILITY OF ABSTRACT	21 ABSTRACT SECURITY CLASSIFICATION
☒ UNCLASSIFIED/UNLIMITED ☐ SAME AS RPT ☐ DTIC USERS	UNCLASSIFIED

22a NAME OF RESPONSIBLE INDIVIDUAL	22b TELEPHONE (Include Area Code)	22c OFFICE SYMBOL
M.L. Batteen	(408) 646-3265	68Bv

i

Wind Forcing of Eddies and Jets
in the
California Current System

by

Terrance A. Tielking
Lieutenant Commander, United States Navy
B.S., United States Naval Academy, 1976

Submitted in partial fulfillment of the
requirements for the degree of

MASTER OF SCIENCE IN METEOROLOGY AND OCEANOGRAPHY

from the

NAVAL POSTGRADUATE SCHOOL
June 1988

Author: _____

Terrance A. Tielking

Approved by: _____

Mary L. Batteen, Thesis Advisor

_____

Robert L. Haney, Second Reader

_____

Curtis A. Collins, Chairman,
Department of Oceanography

_____

Gordon E. Schacher,
Dean of Science and Engineering

ii

ABSTRACT

A high-resolution, multi-level, primitive equation ocean model is used to examine the response to wind forcing of an idealized flat-bottomed oceanic regime along an eastern ocean boundary. A band of steady winds, either with or without a curl, is used as forcing on both an f-plane and a β-plane. In addition, a stability analysis is made to determine if the necessary and sufficient conditions for instability processes to occur are satisfied. It is seen that when the wind driven coastal jet and undercurrent are unstable (which occurs in the cases of wind with no curl), eddies and jets are generated. In the case of wind with curl, since the Davidson Current develops rather than the coastal jet and undercurrent, no eddies develop. A comparison of model results with available observations shows that both the time-averaged and instantaneous model simulations of the coastal jet, undercurrent and eddies are consistent with available observational data. The results of this study support the hypothesis that wind forcing can be an important eddy generation mechanism for the California Current System.

iii

TABLE OF CONTENTS

LIST OF TABLES

LIST OF FIGURES

I. INTRODUCTION

A. OBJECTIVES

The demand for dependable, accurate ocean prediction models has increased. For example, for U.S. Naval battle group anti-submarine warfare (ASW) tactics, an accurate description of ocean variability is required in strategic areas of the world. In particular, the ability to generate spatial and temporal forecasts of ocean fronts, currents and eddies is of crucial importance if the United States is to maintain superiority in the ASW arena. One promising numerical ocean model has already been developed by Miller et al. (1983) for the Gulf Stream and is presently being used by the Navy. This model, which is quasigeostrophic, can be initiated with real-time infra-red satellite and bathythermograph data and can subsequently develop a dynamical forecast for regional Gulf Stream areas (O'Brien, 1986).

In addition to the Gulf Stream, the eastern Pacific Ocean, specifically the California Current System (CCS), has been designated as an area of high ASW interest. Models of the CCS and other eastern boundary current regions are important not only for military applications, but also for civilian applications such as fisheries, oil recovery, waste disposal and search/rescue operations.

Current numerical modeling efforts of the CCS at the Naval Postgraduate School involve the use of a multi-level, eddy-resolving primitive equation (PE) ocean model to investigate generation

1

mechanisms for the synoptic-mesoscale variability of the CCS. Three generation mechanisms currently being investigated for eddy and jet formations in the CCS are wind forcing; topographic forcing due to the presence of the Mendocino Escarpment; and baroclinic, barotropic or mixed instability of the mean CCS.

The primary objective of this thesis is to investigate the role of wind forcing in the dynamics of the mean CCS, and in the generation of eddies and jets in the region. The organization of the thesis is as follows. The following section gives a brief background for the CCS, while Section II describes the numerical model used. The results of the wind forcing experiments along with a stability analysis are presented in Section III. The results are compared with available observations in Section IV. Both a summary and recommendations are presented in Section V.

B. THE CALIFORNIA CURRENT SYSTEM

The CCS, according to Hickey (1979), consists of four currents: the California Current, a broad southward flowing surface current; the California Undercurrent, a northward flowing subsurface flow; the Davidson Current, a surface, poleward flow found north of Point Conception; and the Southern California Countercurrent, a northward-flowing surface current found south of Point Conception in the California Bight. The ocean circulation along the California coast is forced by the atmospheric circulation around the North Pacific High, the position and strength of which varies seasonally so that the offshore pressure gradient along the west coast is strongest in summer (Huyer, 1983). These northerly winds are responsible for the coastal

2

upwelling observed from ~April to October by driving an offshore
Ekman flux, which requires a compensating vertical flow to conserve
mass (Gill, 1982), resulting in a two-dimensional (cross-shore and
vertical) circulation. Brink (1983) emphasized upwelling as a three-
dimensional process, particularly the role of horizontal advection of
heat and momentum in the near-surface dynamics of coastal upwelling.

Both wind stress and wind stress curl are thought to play
important roles in the dynamics of the mean CCS. At seasonal
frequencies, the alongshore component of the wind stress and the wind
stress curl have been hypothesized as driving the seasonal circulation
of the eastern ocean (Carton and Philander, 1984). Bryan and Ripa
(1978), Hickey (1979), Chelton (1984) and McCreary et al. (1987) have
stated that wind stress curl through Ekman pumping is responsible for
coastal upwelling events and forces the pressure field to establish
associated pressure gradients. Carton and Philander (1984) and
Philander and Yoon (1982) discussed, respectively, how wind stress
curl and alongshore wind stress could be important forcing mechanisms
that contribute to the seasonal variability in the CCS near the coast.
Anderson and Gill (1975) studied the oceanic adjustment resulting from
alongshore wind stress forcing and concluded that planetary Rossby
waves carry the coastal upwelling westward, contributing to the ocean
variability. McCreary et al. (1987), using a flat-bottom ocean model
with steady, equatorward, curl-free wind, showed that an equatorward
surface coastal jet can develop due to the wind forcing along with a
poleward undercurrent due to the presence of an alongshore variation
in the wind field. When wind stress curl was used in the model of

3

McCreary et al. (1987), a poleward surface current (i.e., the Davidson Current) developed in response to the curl near the coast along with an equatorward offshore flow approximately 150-175 km from the coast (consistent with Chelton's (1984) vertical cross-sections of alongshore geostrophic velocity).

Recent observations have shown that the CCS can consist of intense meandering current filaments (i.e., jets) with peak velocities of ~50 cm/sec intermingled with synoptic-mesoscale eddies with wavelengths of several hundred kilometers (Mooers and Robinson, 1984). These jets can entrain cold, upwelled coastal waters and advect them hundreds of kilometers offshore. Ikeda and Emery (1984) have shown that baroclinic instability associated with the vertical shear between the surface current and the undercurrent can be responsible for the growth of offshore meander patterns in the regions of capes (alongshore variations in the coastline).

The role of wind forcing in the generation of eddies and jets in the CCS has not yet been systematically investigated and may be the most important generation mechanism for eddy and jet formations. Satellite infra-red imagery has shown evidence of eddies and jets in the CCS during periods of winds favorable for upwelling. These observations provide evidence for wind forcing as a possible important role in eddy and jet formation. If wind-forced, eddies and jets could be caused by either a seasonal response to the wind field or short-lived, strong wind events occurring during the upwelling season.

Although wind events may be important eddy generation mechanisms (Carton, 1984; Carton and Philander, 1984), in this study we will

4

examine eddy and jet formations due to the response to the seasonal wind field and leave for future research the investigation of time-dependent wind forcing. The important results of McCreary et al. (1987) will be used as a guide for the selection of model experiments. In particular, the roles of both wind stress and wind stress curl will be examined in the generation of eddies and jets in the CCS.

II. NUMERICAL MODEL OF THE CALIFORNIA CURRENT SYSTEM

A. MODEL DESCRIPTION

1. Model Equations

The numerical model used in this research was developed by Haney (1985), modified by Batteen (1988a), and is a multi-level, PE model. The model has β-plane capability, and uses the hydrostatic and Boussinesq approximations. The model also has a topographic capability, but in this study only a flat-bottom will be used in order to ensure that the role of wind forcing will be isolated from the possible coupled role of wind forcing with bottom topography. The governing equations, written in sigma coordinates, are as follows:

a. Momentum Equations:

$$\frac{du}{dt} = \frac{-1}{\rho_0}\frac{\partial p'}{\partial x} + \frac{\sigma}{\rho_0 D}\frac{\partial p'}{\partial \sigma}\frac{\partial D}{\partial x} + fv - A_m \nabla^4 u$$

$$+ \frac{K_m}{D^2}\frac{\partial^2 u}{\partial \sigma^2} + \delta_d(u) \tag{2.1}$$

$$\frac{dv}{dt} = \frac{-1}{\rho_0}\frac{\partial p'}{\partial y} + \frac{\sigma}{\rho_0 D}\frac{\partial p'}{\partial \sigma}\frac{\partial D}{\partial y} - fu - A_m \nabla^4 v$$

$$+ \frac{K_m}{D^2}\frac{\partial^2 v}{\partial \sigma^2} + \delta_d(v) \tag{2.2}$$

b. Continuity Equation:

$$\frac{\partial w}{\partial \sigma} + \frac{\partial u}{\partial x} + \frac{\partial v}{\partial y} = 0 \tag{2.3}$$

6

c. **Vertically Integrated Hydrostatic Equation:**

$$p' = D \int_\sigma^0 B \, d\xi - \int_{-1}^0 \left[D \int_\sigma^0 B \, d\xi \right] d\sigma \tag{2.4}$$

d. **Equation of State:**

$$B = \alpha g (T - T_0) \tag{2.5}$$

e. **Thermodynamic Equation:**

$$\frac{dT}{dt} = -A_H \nabla^4 T + \frac{K_H \partial^2 T}{D^2 \partial \sigma^2} + \frac{\partial}{D \partial \sigma} [S(z) - (w'T')]$$
$$+ \delta_d(T) \tag{2.6}$$

In the above equations, sigma, denoted by σ, is equal to z/D. Equation (2.4) for the pressure includes the assumption that the depth-averaged pressure, i.e., the barotropic mode, is zero. All horizontal partial derivatives are on constant sigma surfaces. Table 1 defines the variables used in the above equations, while Table 2 provides other symbols in the model equations as well as values of constants used throughout this study.

2. Model Domain and Resolution

The domain of the model is the rectangular region extending from 124°W to 130°W and from 36.5°N to 42.5°N, covering an area of 6° longitude by 6° latitude (Figure 2.1). The region extends approximately 500 km offshore from the west coast of North America, and it spans the California coastline from Point Sur in the south to Cape Blanco in the north (640 km). The horizontal resolution is 8 km in the east-west direction and 10 km in the north-south direction. This horizontal grid resolution should allow realistic, spatial

7

TABLE 1

DEFINITIONS OF VARIABLES
USED IN THE MODEL

SYMBOL	DEFINITION
z	height (positive upwards)
t	time
p'	pressure perturbation from a vertical average
T	temperature
u,v,w	eastward, northward, and vertical (sigma) velocity components, respectively
B	buoyancy
δ_d	dynamic adjustment term
S	solar radiation in the ocean
$w'T'$	turbulent vertical heat flux

TABLE 2
VALUES OF CONSTANTS USED IN THE MODEL

	VALUE	NAME
Ω	2π day^{-1}	earth rotation rate
C_p	0.958 cal gm^{-1}($^\circ$K)$^{-1}$	specific heat of sea water
C_D	1.3×10^{-3}	drag coefficient
L	595. cal gm^{-1}	latent heat of sea water
T_0	278.2°K	constant reference temperature
ρ_a	1.23×10^{-3} gm cm^{-3}	density of air
ρ_o	1.0276 gm cm^{-3}	density of sea water at T_0
α	2.01×10^{-4}($^\circ$K)$^{-1}$	thermal expansion coefficient
K	10	number of levels in vertical
ΔX	$8. \times 10^5$ cm	meridional grid spacing
ΔY	$1. \times 10^6$ cm	zonal grid spacing
D	4.5×10^5 cm	total ocean depth
ϕ_o	36.5°N	latitude of southern boundary
ϕ_m	42.5°N	latitude of northern boundary
λ_0	124.0°W	longitude of eastern boundary
λ_m	130.0°W	longitude of western boundary
Δt	800. sec	time step
f	0.93×10^{-4} sec^{-1}	Coriolis parameter
g	980. cm sec^{-2}	acceleration of gravity
A_M	$2. \times 10^{17}$ cm^4 sec^{-1}	biharmonic momentum diffusion coefficient
A_H	$2. \times 10^{17}$ cm^4 sec^{-1}	biharmonic heat diffusion coefficient
K_M	0.5 cm^2 sec^{-1}	vertical eddy viscosity
K_H	0.5 cm^2 sec^{-1}	vertical eddy conductivity
P_{sfc}	1013.25 mb	surface air pressure
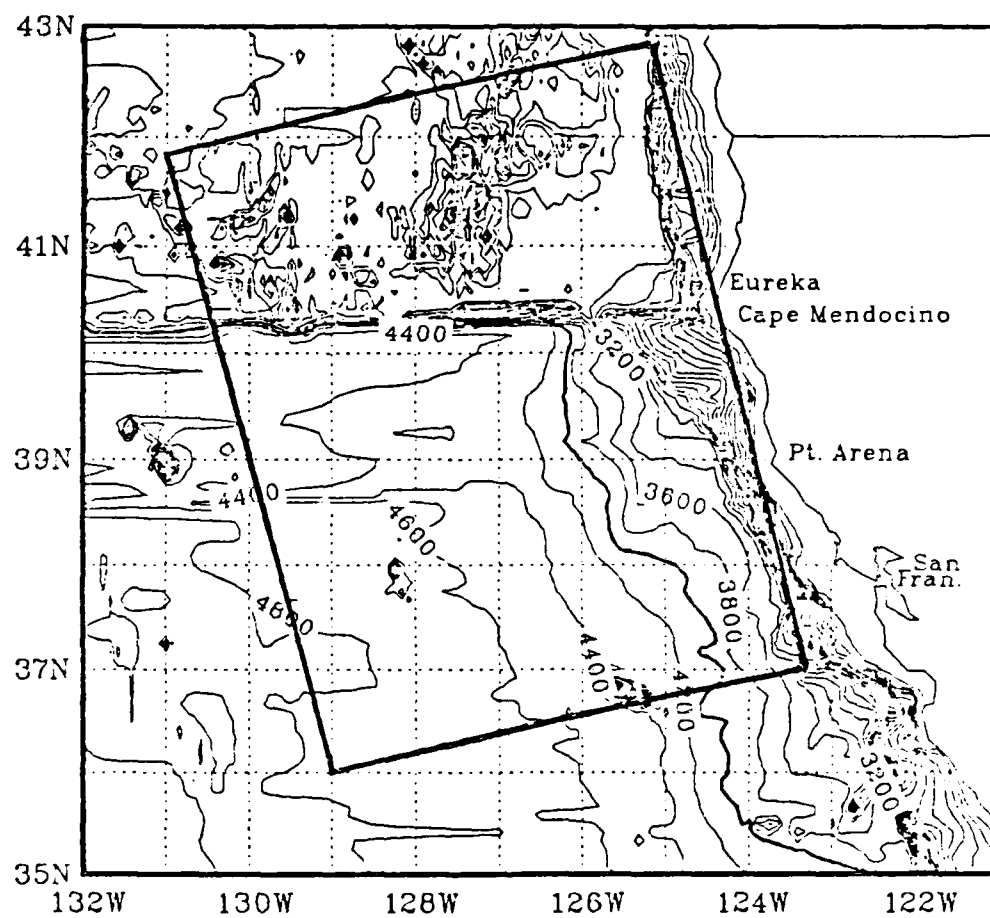
Figure 2.1   Model domain area.

10

resolution of mesoscale features in the CCS, which typically are on the order of 100 km (Breaker and Mooers, 1986).

3. Finite Difference Scheme

In the horizontal, a space-staggered B-scheme (Arakawa and Lamb, 1977; Batteen and Han, 1981) is used while a sigma (non-dimensional) coordinate system is used in the vertical, which has ten levels. The noise free version of the hydrostatic equation in sigma coordinates advocated by Arakawa and Suarez (1983) and Batteen (1988b) has been implemented.

4. Forcing Capabilities

The model can either be spun up from rest by a surface wind stress or heat flux, or it can be initialized with a specified current field. In this study, as in Renaud (1986), the model is spun up using the climatological wind fields of Nelson (1977), and a surface heat flux is computed and used to damp the temperature field towards the mean climatological value.

5. Boundary Conditions

The northern, southern and western boundaries are open using a modified version of the radiation boundary condition of Camerlengo and O'Brien (1980). The eastern boundary, representing the west coast of North America, is closed and straight, with zero or free-slip capability.

6. Heat and Momentum Diffusion

The model uses biharmonic lateral momentum and heat diffusion with the choice of coefficients listed in Table 2. This formulation of biharmonic, rather than Laplacian lateral diffusion, along with the

choice of coefficients should allow mesoscale eddies to be generated via baroclinic and/or barotropic instability processes (Holland and Batteen, 1986).

B. SPECIFIC EXPERIMENTAL CONDITIONS

1. Wind Forcing Determination

The key to obtaining successful model results from wind forcing compared with CCS observations is to accurately represent the wind field over the model domain. Using ship observations in 1-degree square areas, Nelson (1977) compiled a complete description of monthly wind stress and wind stress curl off the west coast of the United States. These historical marine wind observations are utilized in the PE model to determine the required wind forcing. Since upwelling has been observed primarily during periods of equatorward winds (Mooers et al., 1976; Huyer, 1983), which are dominant during the summer season in the central CCS region, we will incorporate in the model wind stress and wind stress curl data for the months of June, July and August.

a. Incorporation of Wind Stress

From Figures 2.2 through 2.4, which show wind stress data for the months of June through August, one can observe in the surface stress field a large variability in the offshore direction and a small variability in the alongshore direction. In the latter case, the winds are less variable and parallel to the coast within 10-20%. Based on these observations, following Renaud (1986), an idealized alongshore wind stress can be developed, and made a function of the offshore direction. Since the model domain has a straight, north-

12

south oriented coastline and the California coastline is neither straight nor north-south oriented (see Figure 2.1), the one-degree squares of Nelson (1977) were chosen such that they were parallel to the coast. In addition, the alongshore component of Nelson's wind stress along the coast was used as the model wind stress, while the offshore component was chosen to be zero for all experiments.

b. Incorporation of Wind Stress Curl

The wind stress curl data for the months of June through August are shown in Figures 2.5 through 2.7. A negative curl is observed offshore, while a positive curl is observed inshore, resulting in a line of zero wind stress curl parallel to the coast approximately 200-300 km offshore. These observations are consistent with Chelton (1984), who observed that the winds appear to be strongest approximately 200 km offshore so that there is a nearshore positive wind stress curl year round. The magnitude of this curl varies seasonally approximately in phase with the alongshore wind stress.

Following Renaud (1986), wind stress curl was extracted from Nelson's climatological data for the region of the PE model domain. The wind stress curl points were then averaged in the alongshore direction and time-averaged for the three summer months. The climatological curve resulting from the averaging procedures is shown in Figure 2.8. An analytical, Gaussian function was then found and used to represent the averaged curl:

$$\partial \tau / \partial x = 0.77 \exp[-0.5(XR/95.0)^2]-.11. \qquad (2.7)$$

13
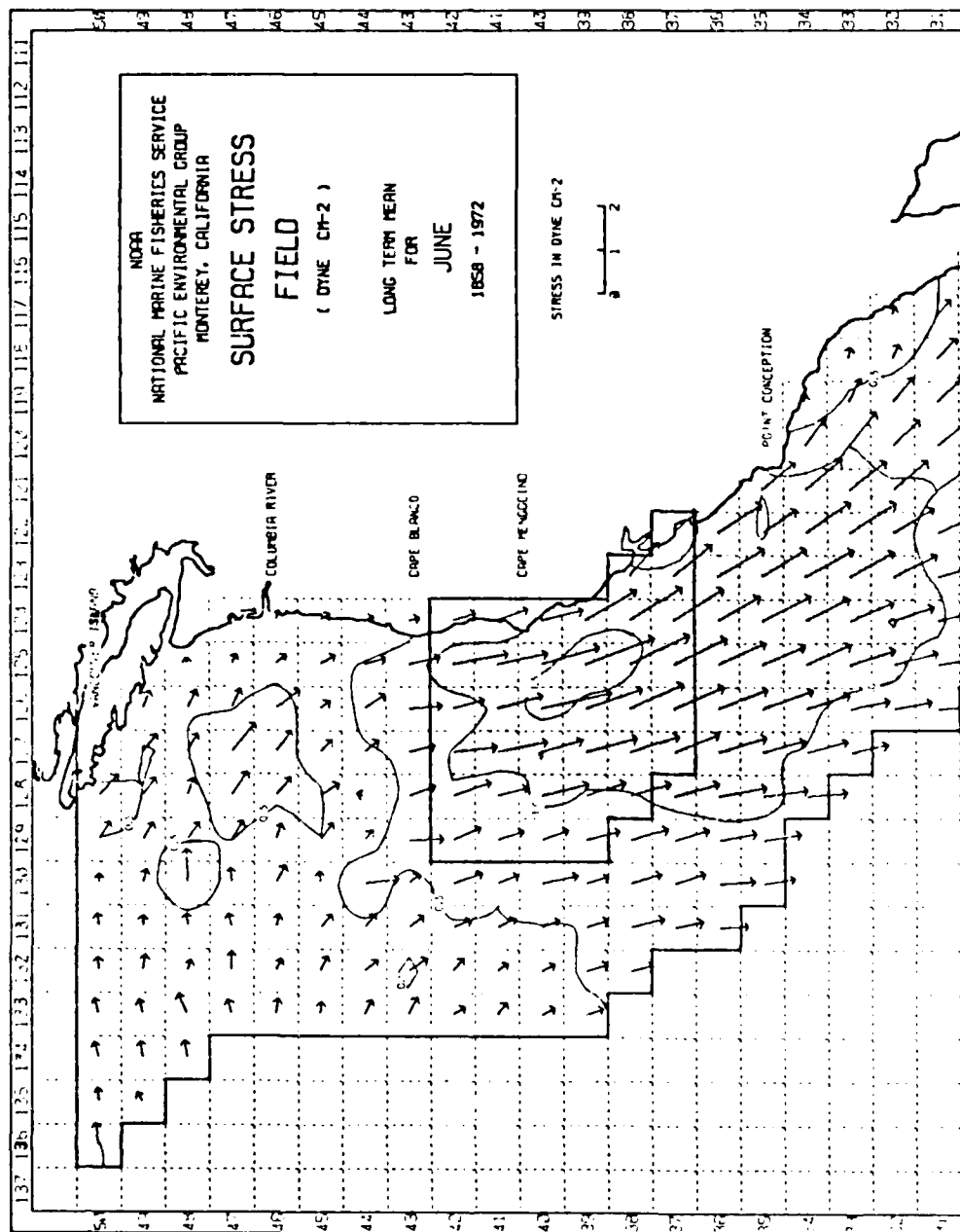
Figure 2.2   Climatological wind stress for June (from Nelson, 1977).   The inside box outlines the model domain.
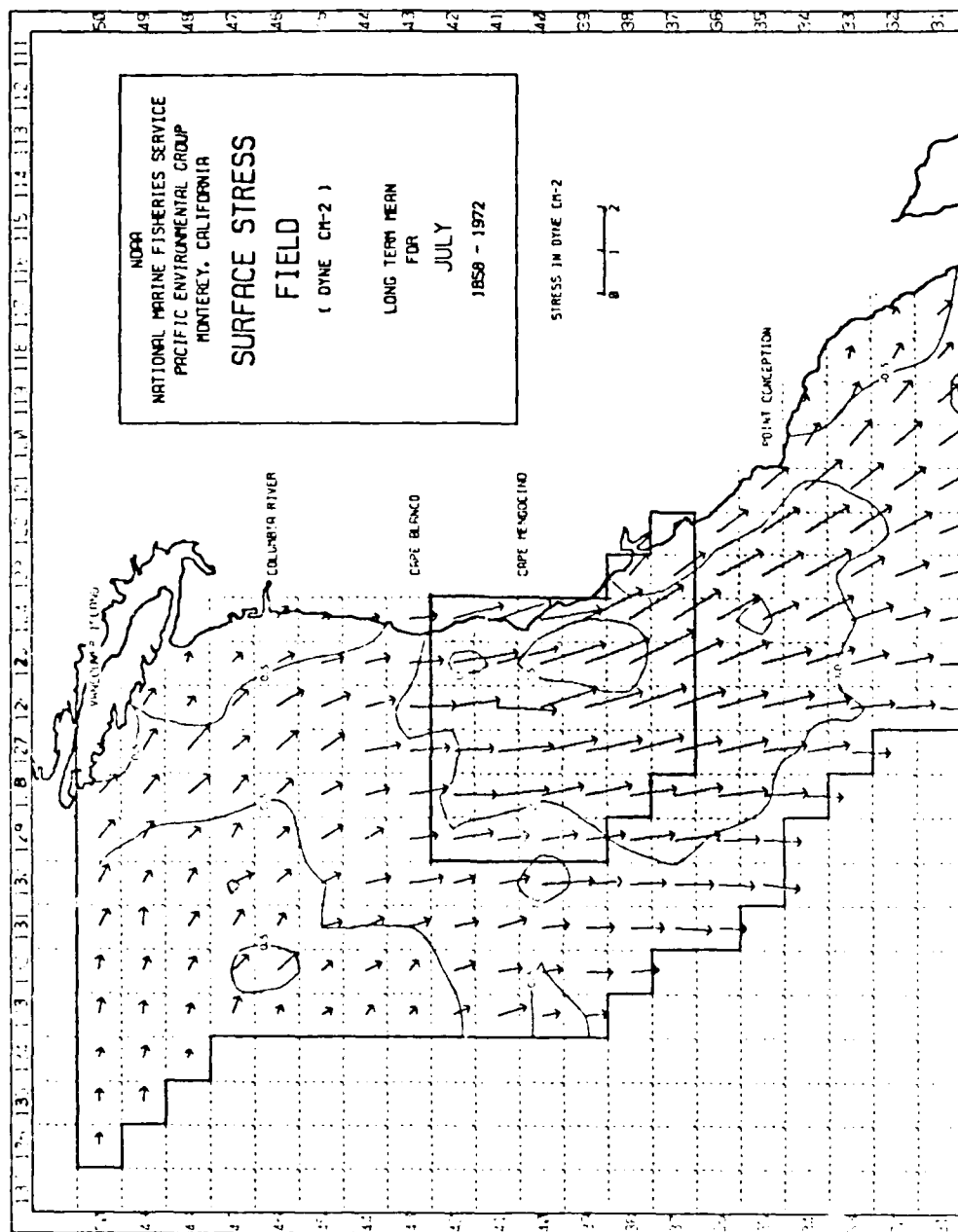
Figure 2.3   Climatological wind stress for July (from Nelson, 1977). The inside box outlines the model domain.

15
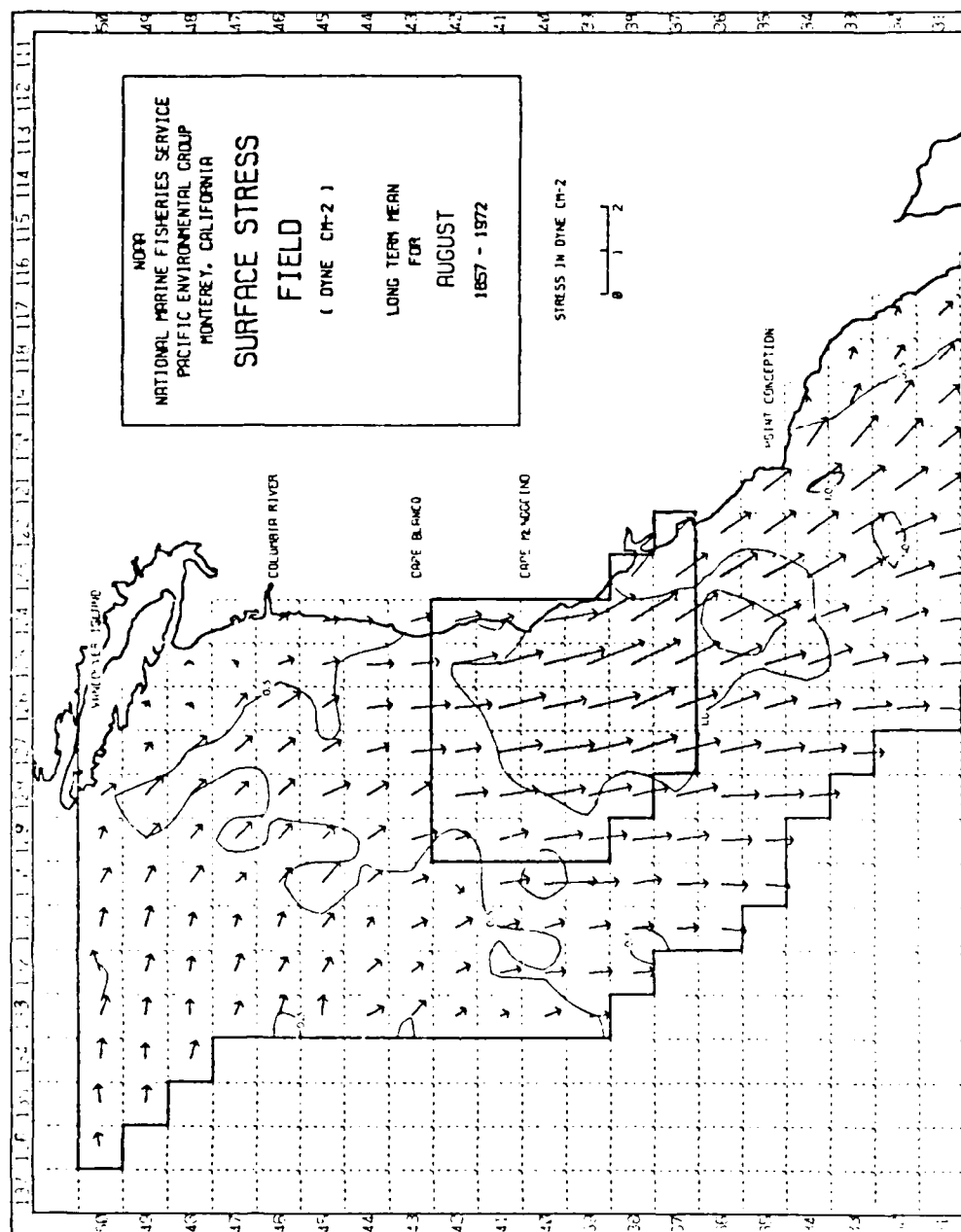
Figure 2.4   Climatological wind stress for August (from Nelson, 1977). The inside box outlines the model domain.

16
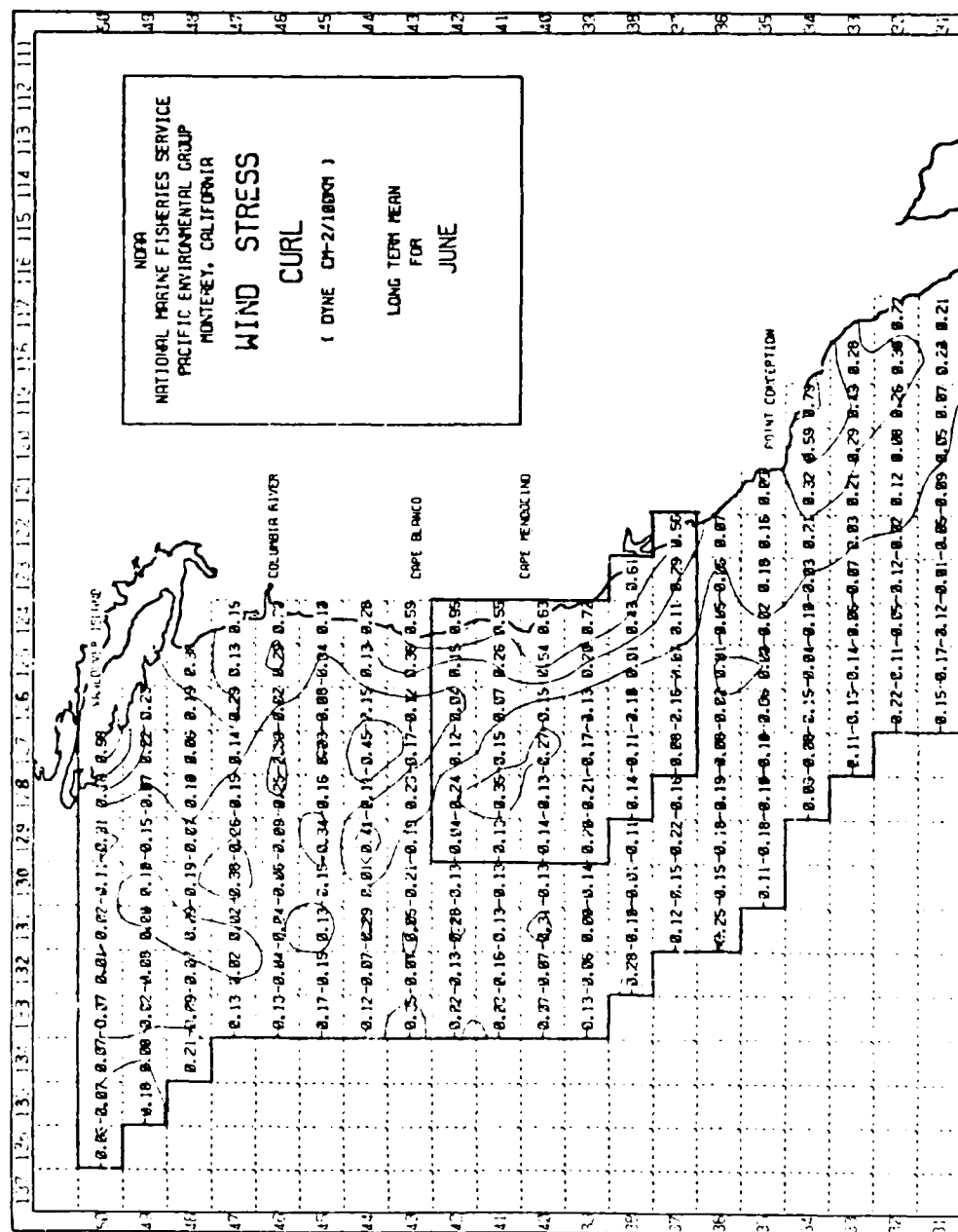
Figure 2.5   Climatological wind stress curl for June (from Nelson. 1977). The inside box outlines the model domain.

17
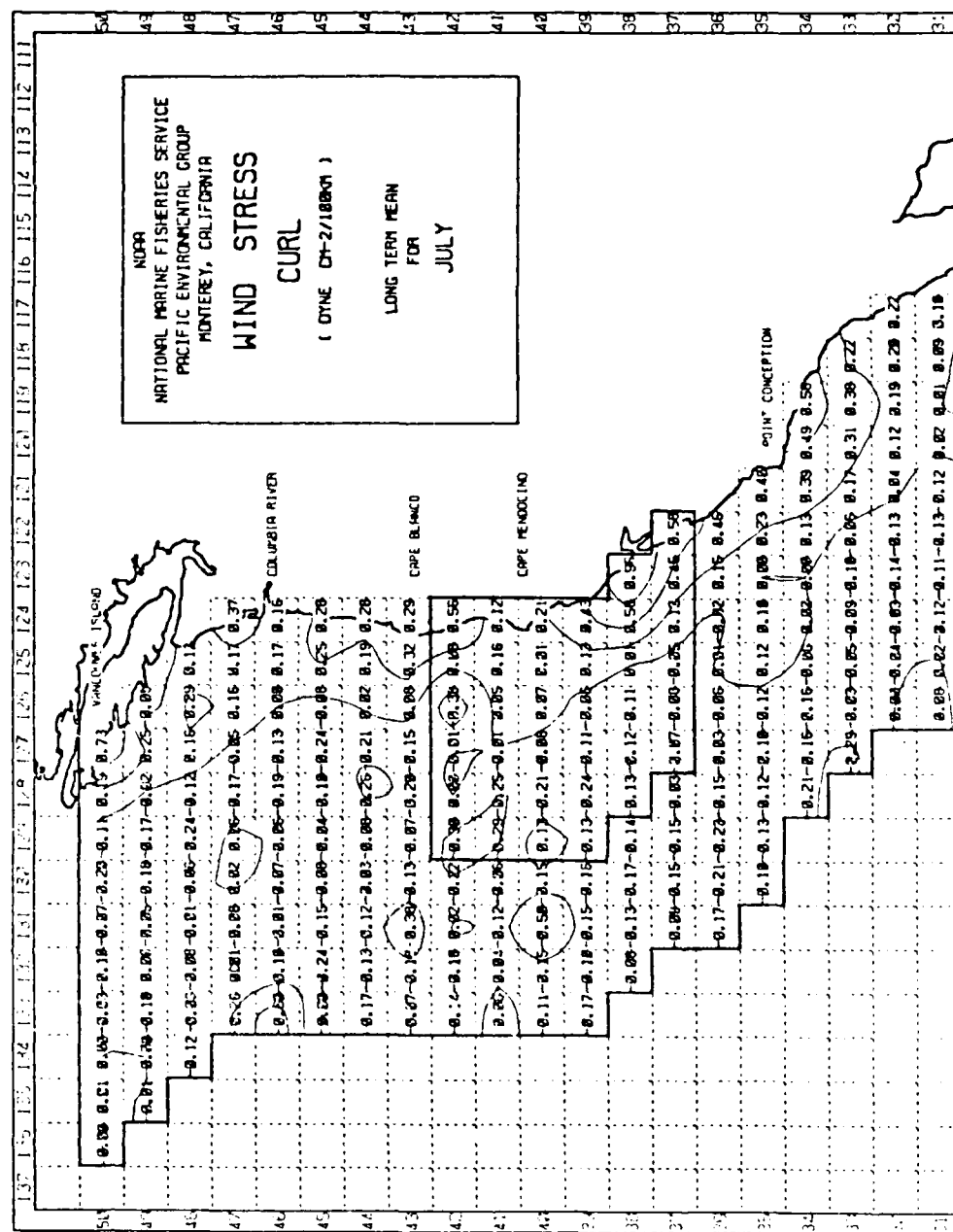
Figure 2.6   Climatological wind stress curl for July (from Nelson, 1977). The inside box outlines the model domain.

18
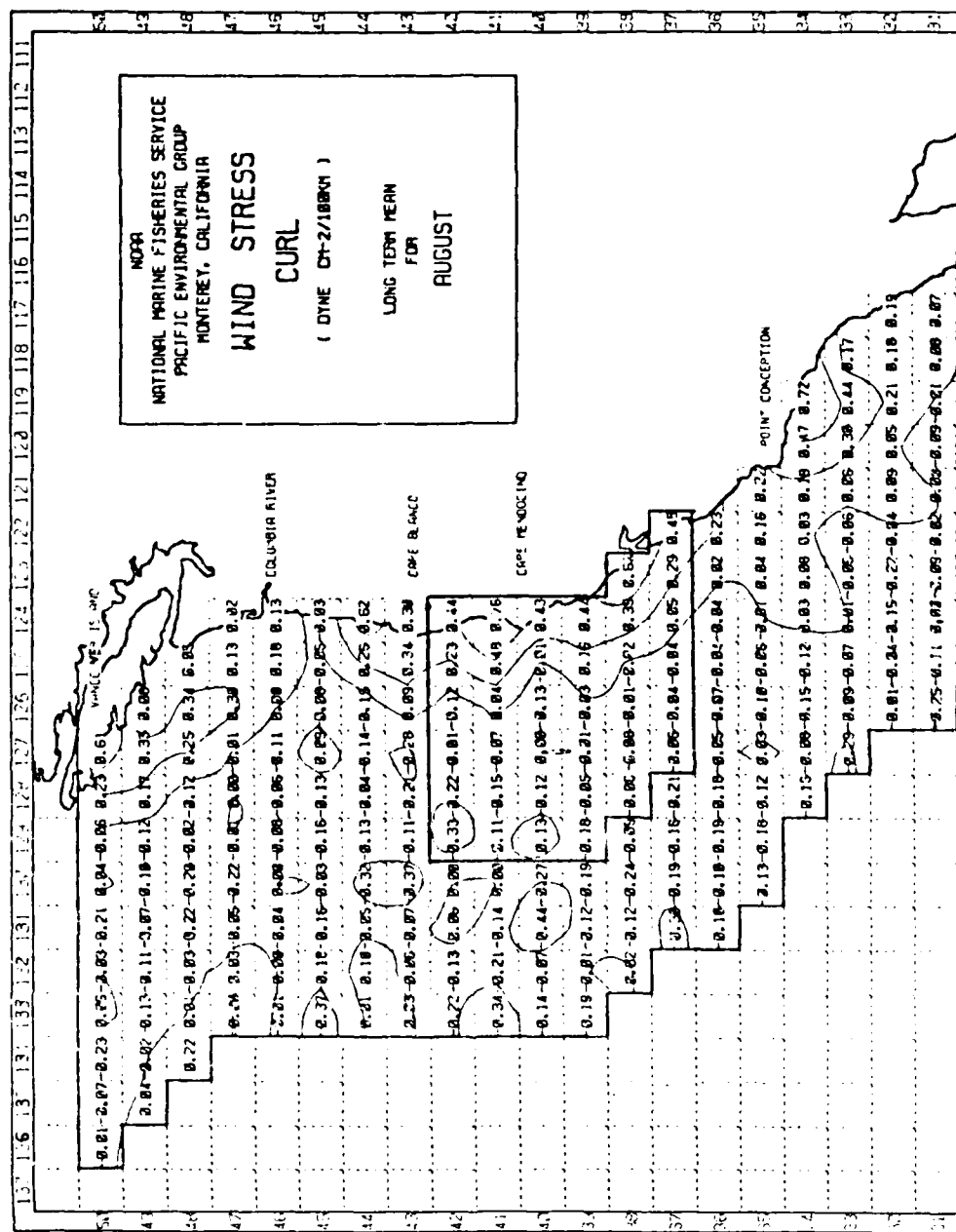
Figure 2.7 Climatological wind stress curl for August (from Nelson, 1977). The inside box outlines the model domain.

19

where XR is the distance in kilometers. The analytical model curve is superimposed over the climatological curve in Figure 2.8 and the two correlate well.

Since the PE model uses wind input rather than curl (for ease of heat flux and wind stress calculations), values for the wind stress were obtained at the temperature gridpoints from integration offshore of the analytical curl function at the u, v gridpoints, as in Renaud (1986). Finally, winds were derived from the analytical stress at the temperature gridpoints using the bulk aerodynamic formula. Plots of the derived wind stress and alongshore component wind (model versus climatology) are shown in Figures 2.9 and 2.10, respectively.

c. Incorporation of Alongshore Variation in Wind Stress

Anderson and Gill (1975) and Philander and Yoon (1982) have pointed out that variation in the alongshore winds, even if their curl is zero, can result in the development of a complex system of currents and contribute to the seasonal variability of the CCS. To examine the role of alongshore wind variability, the climatological alongshore wind stress from Nelson (1977) was zonally averaged for the summer season to provide the necessary alongshore variation. Figures 2.11 and 2.12 show plots of latitude versus wind stress and alongshore wind velocity, respectively. These values will be directly applied in two experiments (i.e., experiments 3 and 6) as model stress vice the use of an analytical function for the other experiments.

2. Surface Thermal Damping

The CCS can be a major upwelling area during the spring and summer seasons. Since the upwelled, cold water reduces both the

20
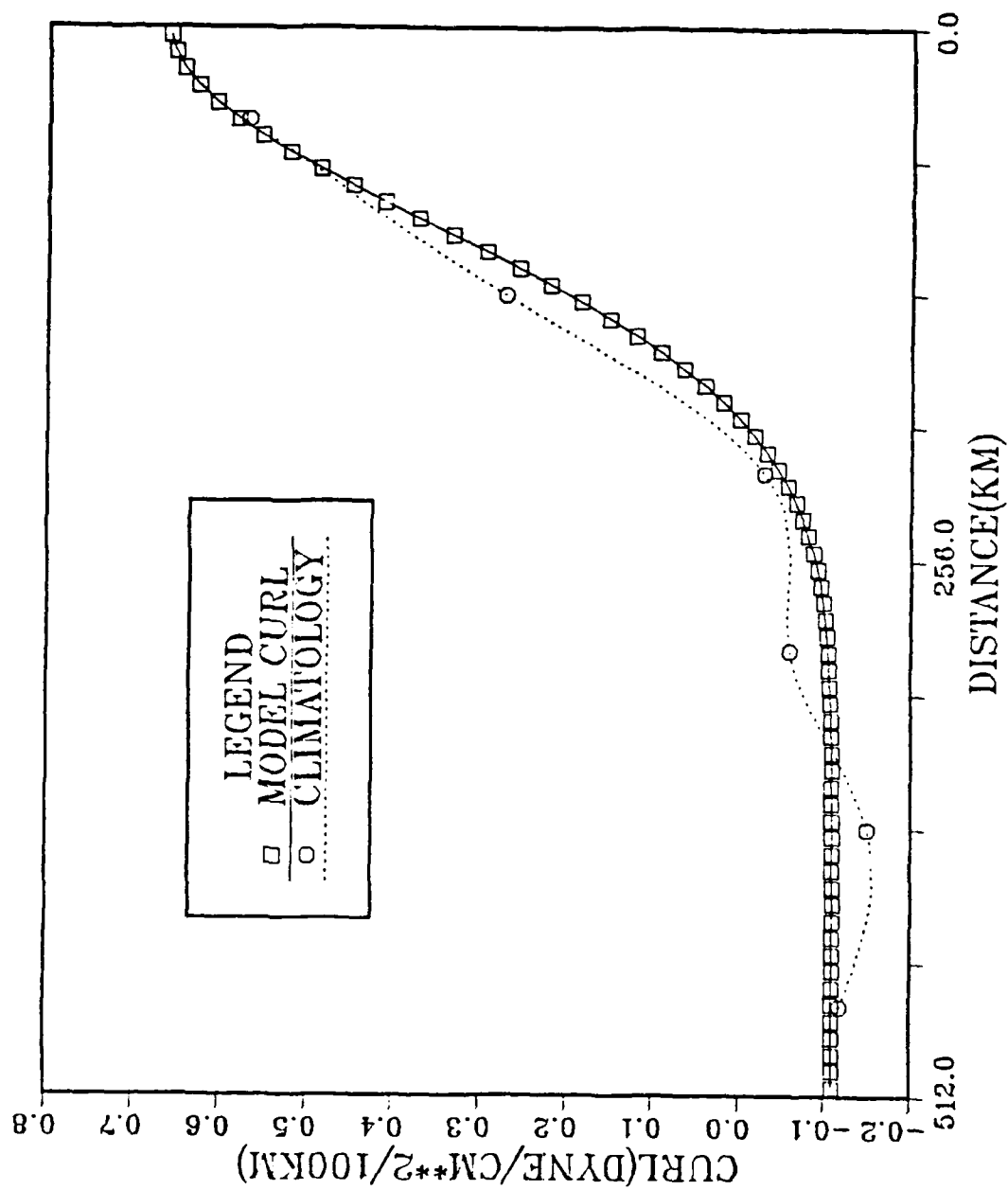
Figure 2.8   Wind stress curl versus offshore distance (from
              Renaud, 1986).
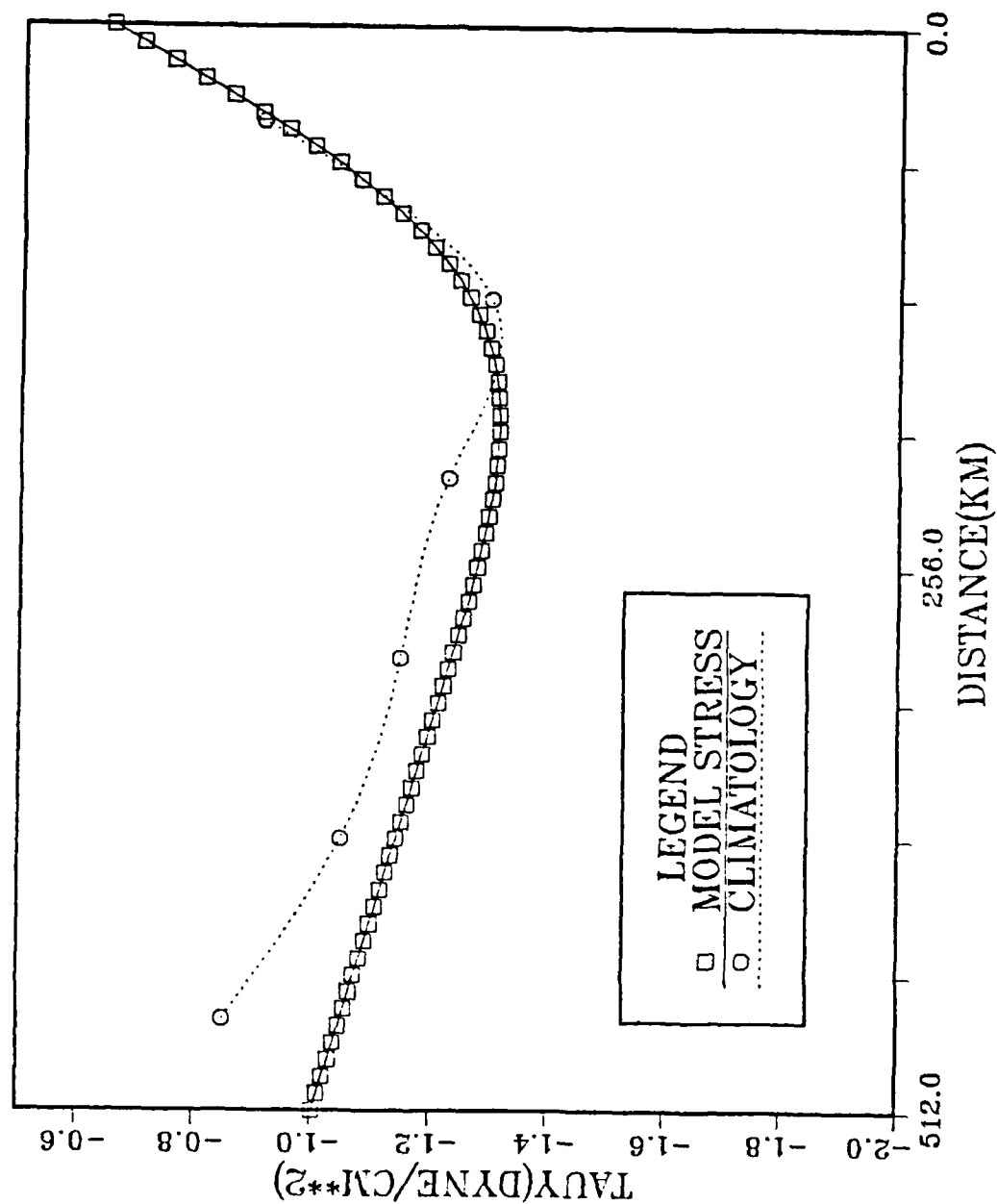
Figure 2.9   Wind stress versus offshore distance (from Renaud. 1986).

22
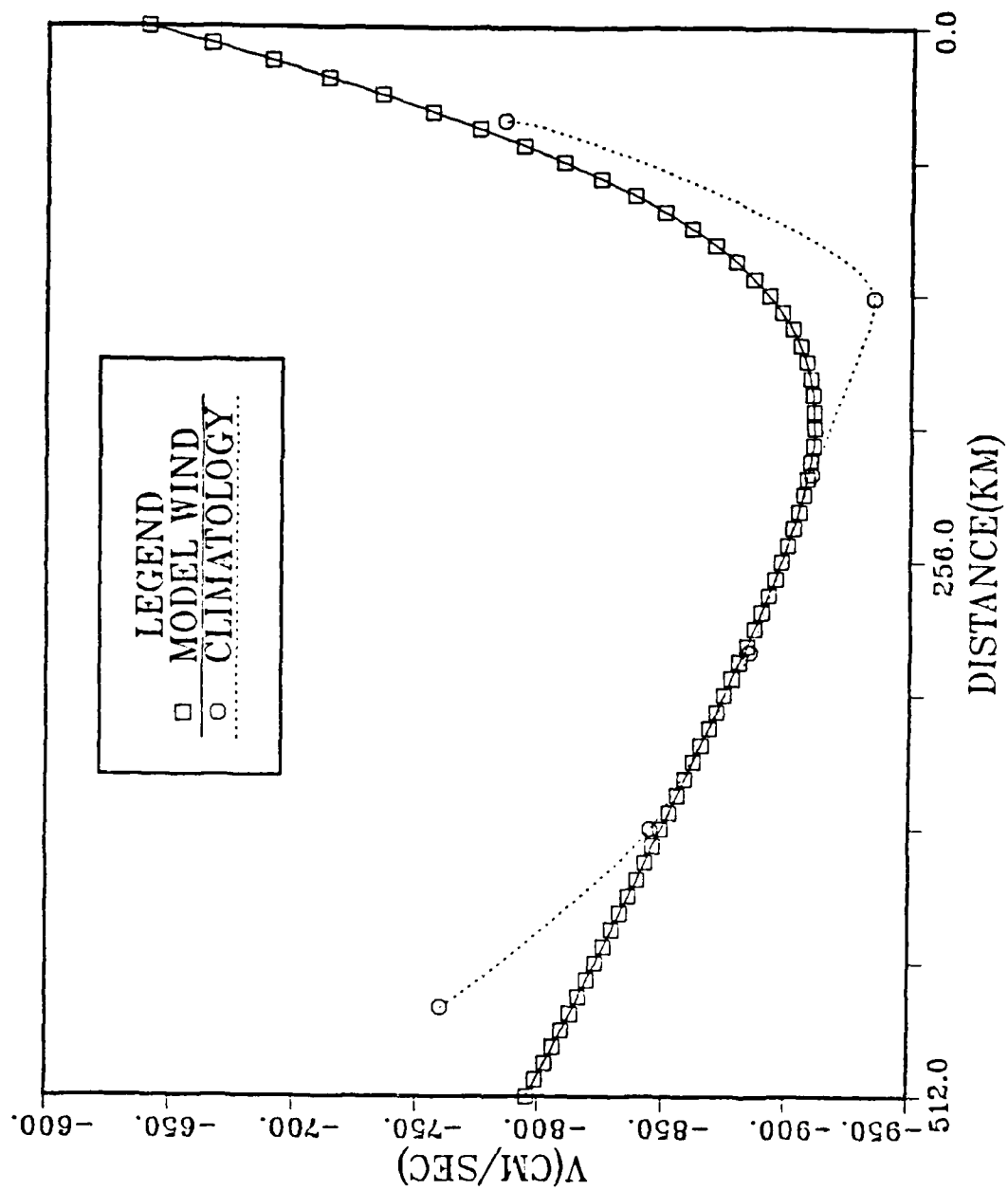
Figure 2.10   Alongshore component wind versus offshore distance (from Renaud, 1986).

23
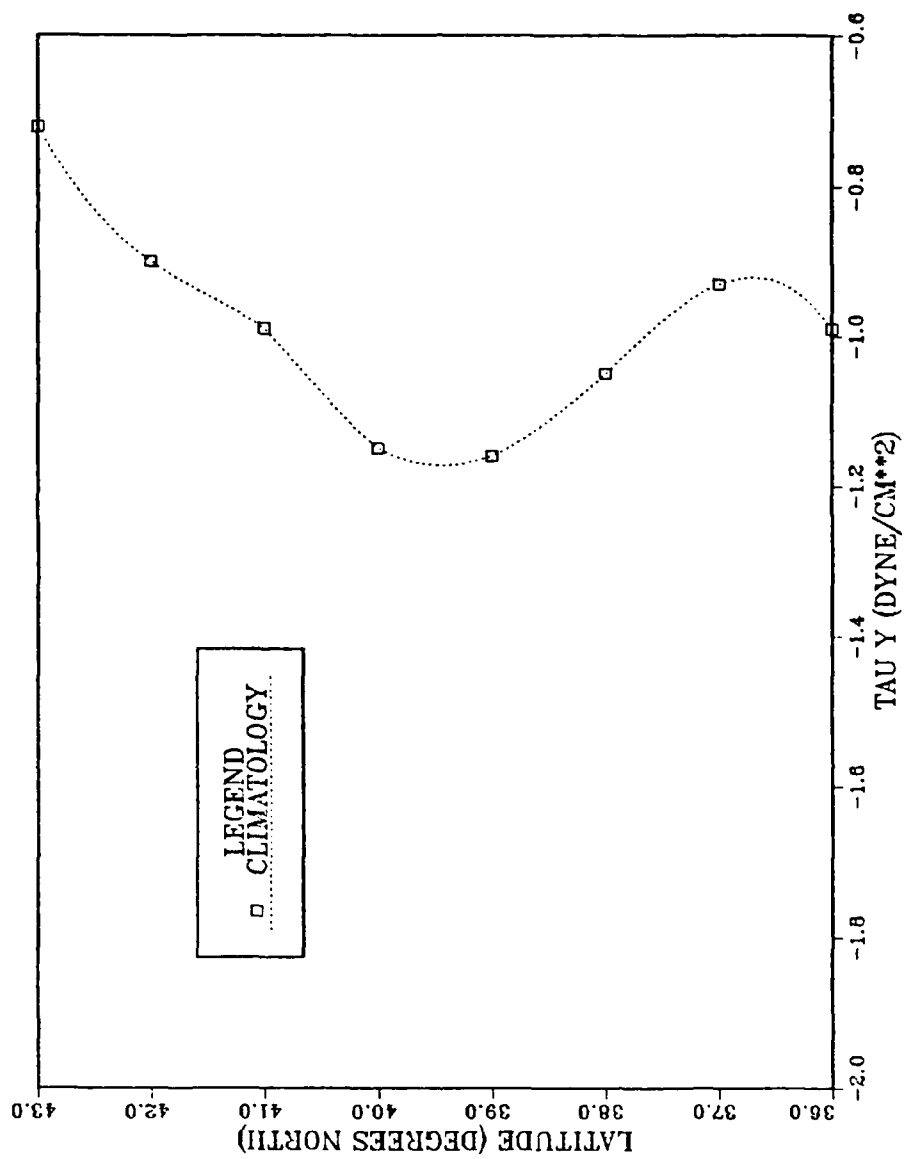
Figure 2.11   Latitude versus wind stress.
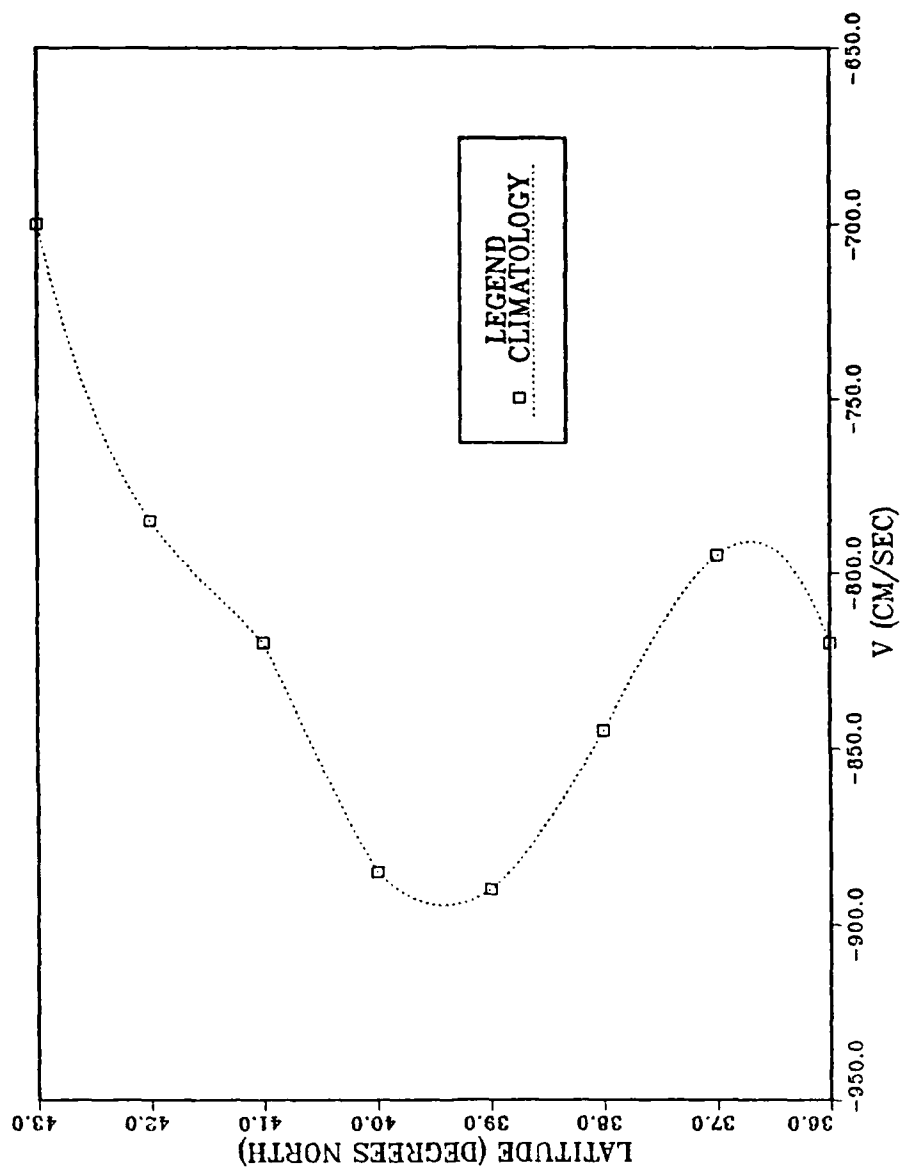
Figure 2.12   Latitude versus alongshore wind speed.

25

sensible and latent heat fluxes, the heat flux during the upwelling season is a downward flux or a damping factor. As a result, the model ocean temperature fields must be modified by surface thermal damping. Because atmospheric variations in clouds or air temperature are not a significant forcing (compared to the wind) mechanism in the CCS, summer mean values of solar insolation, cloud cover and relative humidity can be used in conjunction with computing sensible and latent heat fluxes from bulk formulae (Haney et al., 1978). The initial sea surface and air temperatures used were 15°C and 13°C, respectively. Following Renaud (1986), the air temperature was chosen so that there was not initially any heat flux at the surface when a steady wind speed was used. This maintained the model heat budget as a thermal damper based on a uniform surface wind forcing of ~850 cm/sec, and was a function of the changing sea surface temperature.

Following Haney (1971), a linearized form of the model equations was used for the downward surface flux Q:

$$Q = \gamma \ (T_A^* - T_S).$$

(2.8)

where T_A^* is the apparent atmospheric equilibrium temperature. T_S the model surface-layer temperature and γ is a coupling coefficient which is strongly dependent on the surface wind speed (Haney, 1985). Following Haney (1985), the relaxation time (λ^{-1}) for the surface temperature can be related to the density of sea water (ρ), the specific heat of sea water (C_p), the depth of the mixed layer (h) and the winds (γ) by the equation:

$$\lambda^{-1} = \rho C_p h \gamma^{-1}.$$

(2.9)

26

Using mean climatological winds of 25 $Wm^{-2}K^{-1}$ (Haney, 1971) and a mixed layer depth of 50 m, the relaxation time value of around 100 days was computed. As a result of this long damping time, any surface temperature anomaly that may develop due to wind forcing should be observed long before complete thermal damping by the computed surface heat flux occurs.

3. Open Boundary Conditions

Numerical models of coastal ocean regions typically involve the treatment of three open boundary conditions (OBCs): two cross-shelf and one offshore. According to Røed and Cooper (1985), the objective requirements for a successful, ideal open boundary condition are the following: the OBC should be numerically stable, mathematically well-posed, have adequate accuracy and allow unrestricted fluid motions such as propagating waves. Furthermore, the time evolution of the model's dependent variables at the open boundary and in the interior domain should develop and advect in harmony, so that no disturbances or reflections develop at the open boundary.

Chapman (1985) also investigated OBCs using a barotropic, coastal ocean model with a straight coastline and tested seven different cross-shelf OBCs. He concluded that there is no ideal way to handle the numerical treatment of open boundaries for models with the following features: two or three dimensions, rotation, variable depth, bottom friction or wind stress forcing.

Røed and Smedstad (1984) found that the OBCs of Camerlengo and O'Brien (1980) worked reasonably well for long, dispersive edge

27

waves. For experiments using alongshore wind stress, the modified Orlanski radiation OBC of Camerlengo and O'Brien (1980) provided the best results in Chapman's (1985) study.

Based on these previous investigations, we have chosen to use the modified OBCs of Camerlengo and O'Brien (1980). In a previous study of the CCS, Renaud (1986) used the same OBCs and applied both uniform and offshore-varying wind forcing not only in the interior, but on both the northern and southern open boundaries of the model domain. Although an equatorward flowing coastal jet and poleward flowing undercurrent developed, neither compared well with observations and no instability of the mean flow occurred.

In this study, we found that, as in Renaud (1986), if a uniform wind forcing is applied not only over the whole domain, but also on the northern and southern open boundaries, a coastal jet developed that was too deep. We also found that, if uniform wind forcing was applied everywhere except at the northern boundary, coastal Kelvin waves would not be able to propagate northward due to the presence of forcing on the southern boundary. If uniform wind forcing was applied everywhere except at the southern boundary, the coastal Kelvin waves would not be able to exit due to the presence of forcing on the northern boundary.

McCreary (1987) showed that if a uniform wind stress, as in Renaud (1986), is used, a steady alongshore current will result that is too strong, too deep and directed equatorward at all depths. In order to generate a realistic undercurrent, he concluded that either an alongshore pressure gradient or a variation in the alongshore wind

28

stress is necessary. He recommended and used wind band forcing, such that:

$$\tau^y = \tau_0 Y(y), \qquad\qquad (2.10)$$

where the meridional profile of the wind is confined in a band away from the northern and southern boundaries. Here τ^y is the wind band forcing, τ_0 is the wind strength for steady forcing, and $Y(y)$ is the latitudinal distribution of the stress. The use of wind band forcing allows an alongshore variation in the alongshore stress, with the result that a relatively realistic undercurrent can be set up by the poleward propagation of coastally trapped waves.

Following McCreary (1987), we have also imposed a band of wind forcing in the interior of the domain in the north-south direction away from both the northern and southern boundaries. As we will see, when wind band forcing is used, both a realistic coastal jet and undercurrent can be generated (compared to the deep jet of Renaud, 1986).

III. RESULTS OF WIND FORCING EXPERIMENTS

A. EXPERIMENTS ON AN F-PLANE

1. Experiment 1 (Uniform Wind Stress)

Experiment 1 was run on an f-plane with a constant Coriolis parameter of $f_0 = 9.3 \times 10^{-5}$ sec^{-1} based on the center of the domain. The wind forcing for this experiment was uniform, both in the alongshore and cross-shore directions and steady for a 90-day period. The constant wind forcing value of -830.0 cm/sec was determined from the time-, cross-shore- and alongshore-averaged summertime, climatological winds of Nelson (1977), as described in Section II.B. Although the model had both free-slip and zero-slip capability, all experiments had the eastern boundary condition (west coast of the United States) set as a zero-slip condition, i.e., the tangential velocity was set equal to zero at the coast. This choice was based on the results of Renaud (1986), who found that the zero-slip eastern boundary results compared more favorably with observations (Kosro, 1987; Huyer and Kosro, 1987) than the free-slip results. The same type of thermal damping, as described in Section II.B, was used in all experiments.

The initial temperature stratification used in all experiments was a pure exponential temperature profile as a function of height (z). The profile (Figure 3.1) had a length-scale of 450 m with a temperature at the first sigma level (surface ocean level) of 15°C and a value at great depth of 2°C. The exact form of this temperature function was:

$$T(z) = 2 + 13e^{z/450}. \qquad (3.1)$$
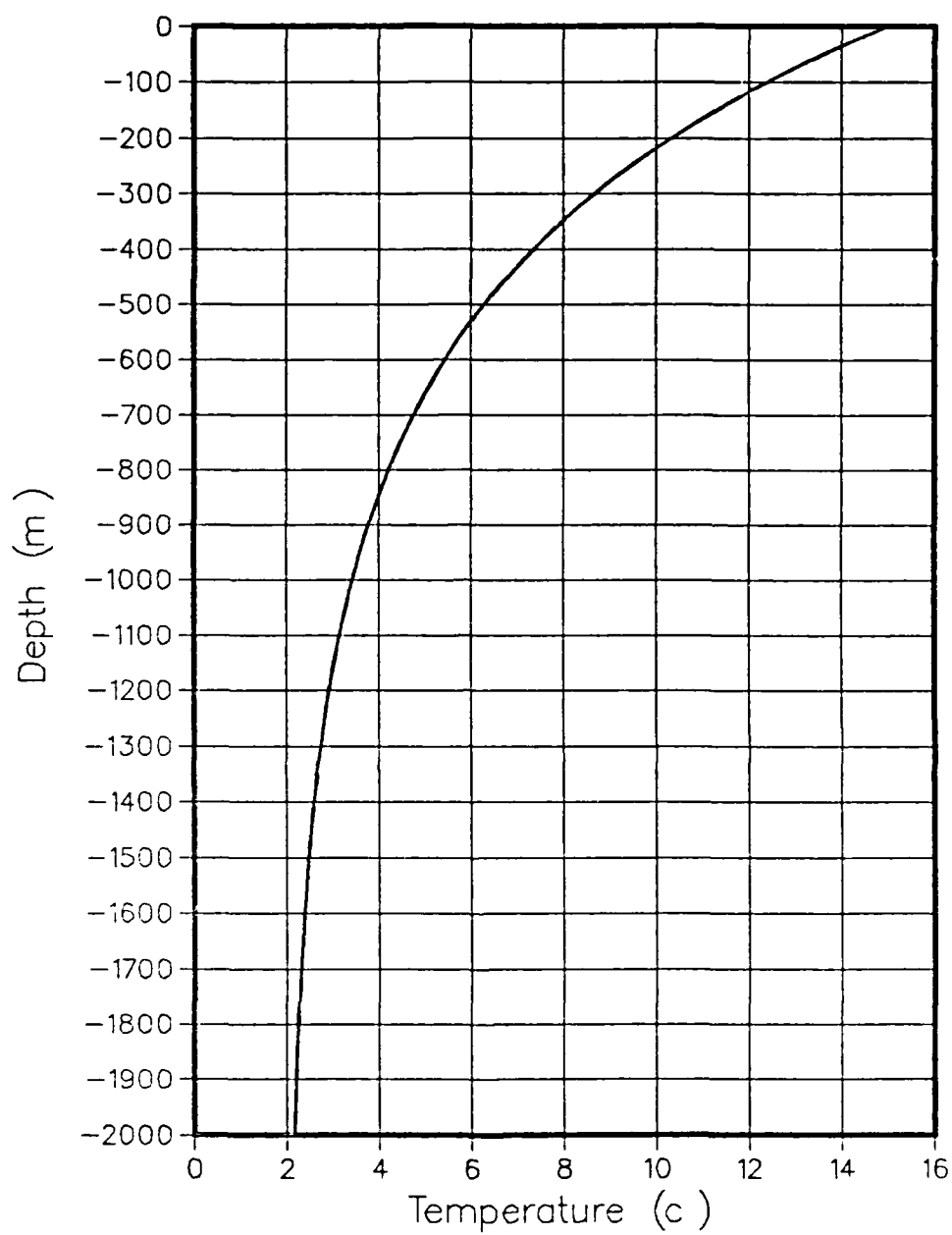
Figure 3.1   Model initial temperature profile.

31

This temperature profile was derived from observations used to support the Princeton Dynalysis model (Blumberg et al., 1987) and is representative of the long-term, mean climatological temperature stratification for the California coastal region. In addition, the Brunt-Vaisala frequency profile, $N^2(z)$, was calculated analytically using the temperature function in equation (3.1) from:

$$N^2 = \alpha g \partial T / \partial z. \tag{3.2}$$

The resultant N^2 profile (Figure 3.2) was incorporated for all experiments.

The model was initialized at day 0 with full magnitude winds and, as expected, inertial oscillations of near-surface ocean currents developed. These oscillations soon damped, leaving quasi-steady Ekman offshore transport to the right of the wind stress (Figure 3.3). As explained by Ekman (1905), an equatorward wind parallel to an eastern ocean coast can cause the surface layer to move offshore due to the Coriolis force. To maintain continuity of mass, colder water from below the surface must move upward to replace the water that moves offshore. As a result, the region near the coast, which has Ekman transport as a major driving mechanism (Pares-Sierra, 1987), can be considered a divergence area.

The subsequent progression of offshore movement of cold temperatures, seen in Figure 3.4, is caused by the cold, upwelled water, replacing the offshore movement of coastal waters due to Ekman transport. Surface temperature gradients near the coast are
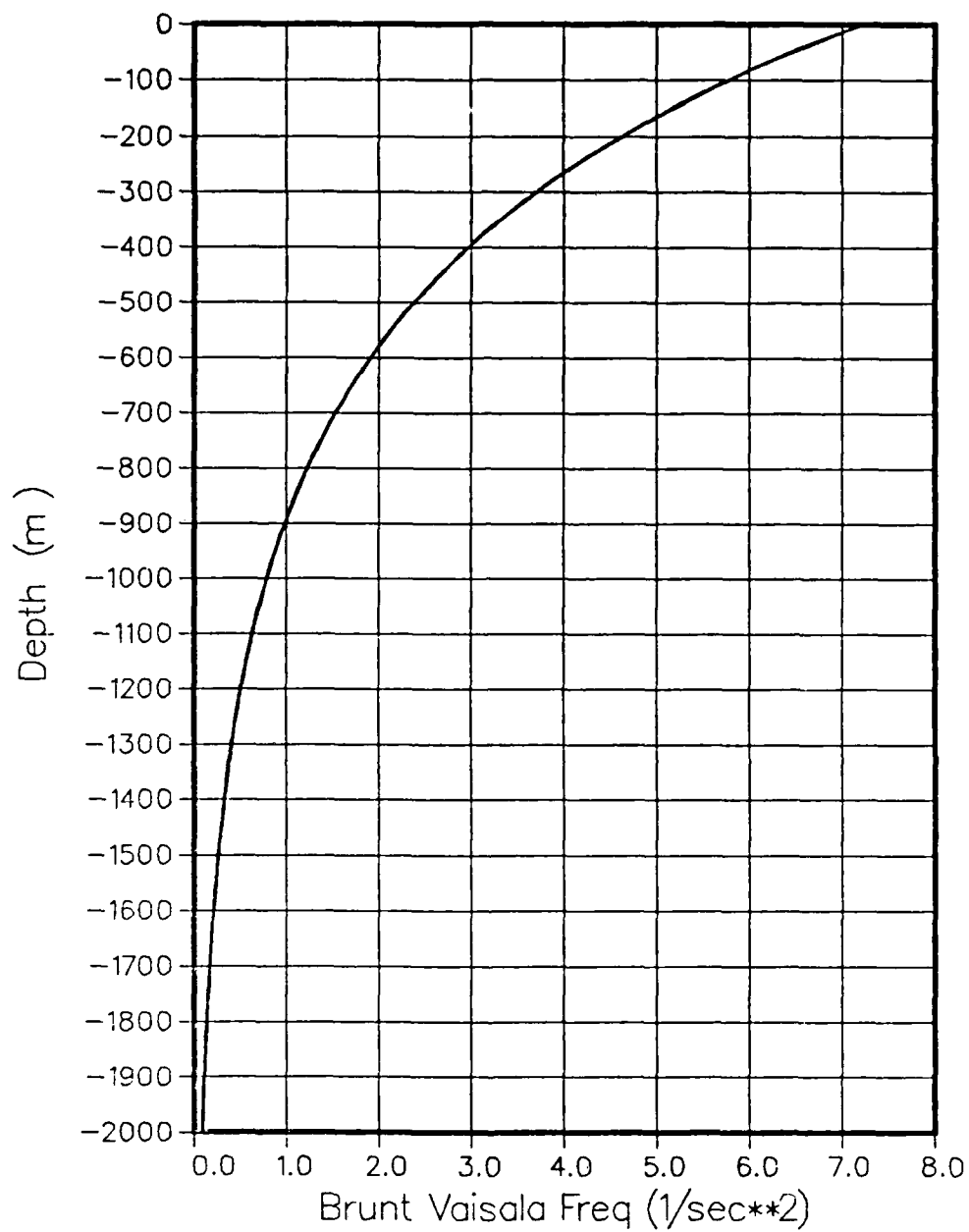
Figure 3.2   Initial profile of square Brunt-Vaisala frequency, N².

33
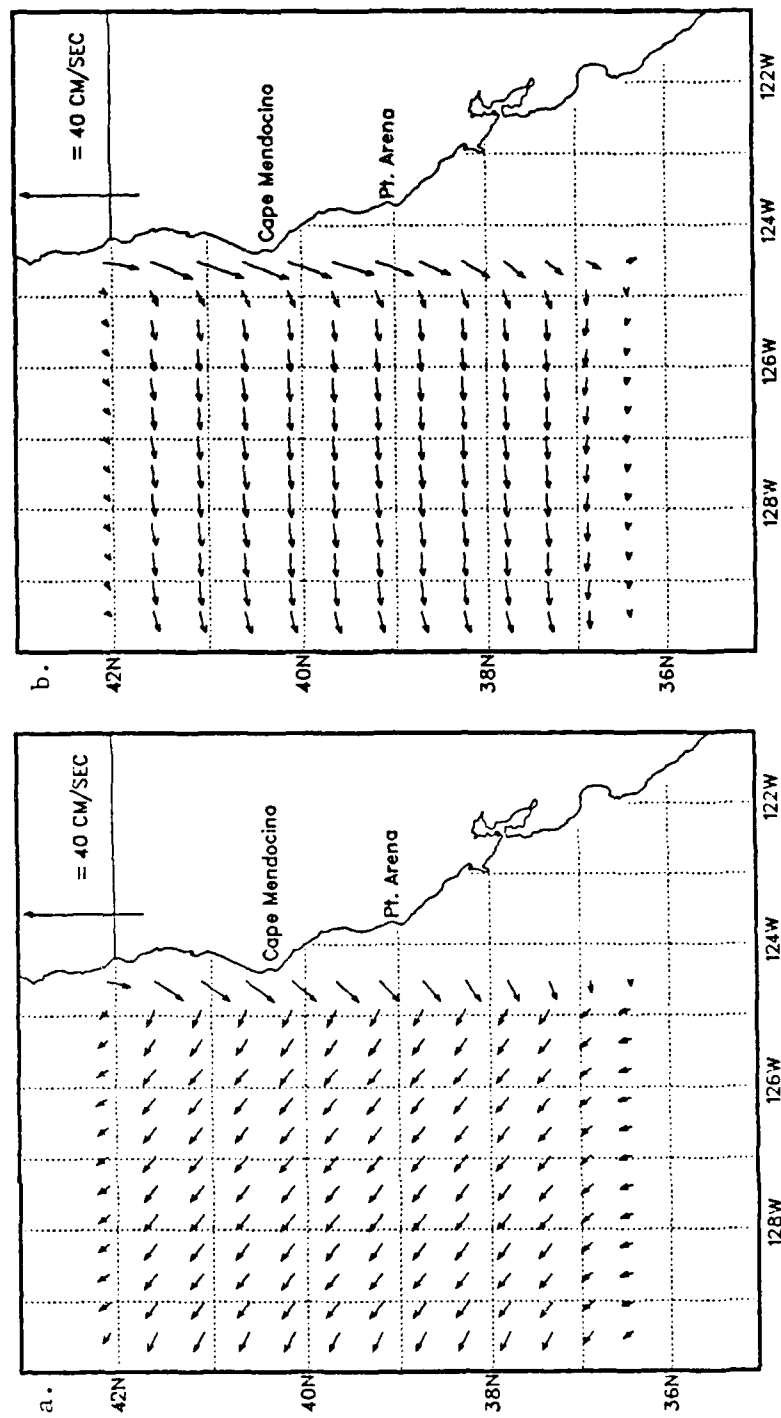
Figure 3.3   Surface current vectors for experiment 1 at (a)
              day 10, (b) day 20.

34
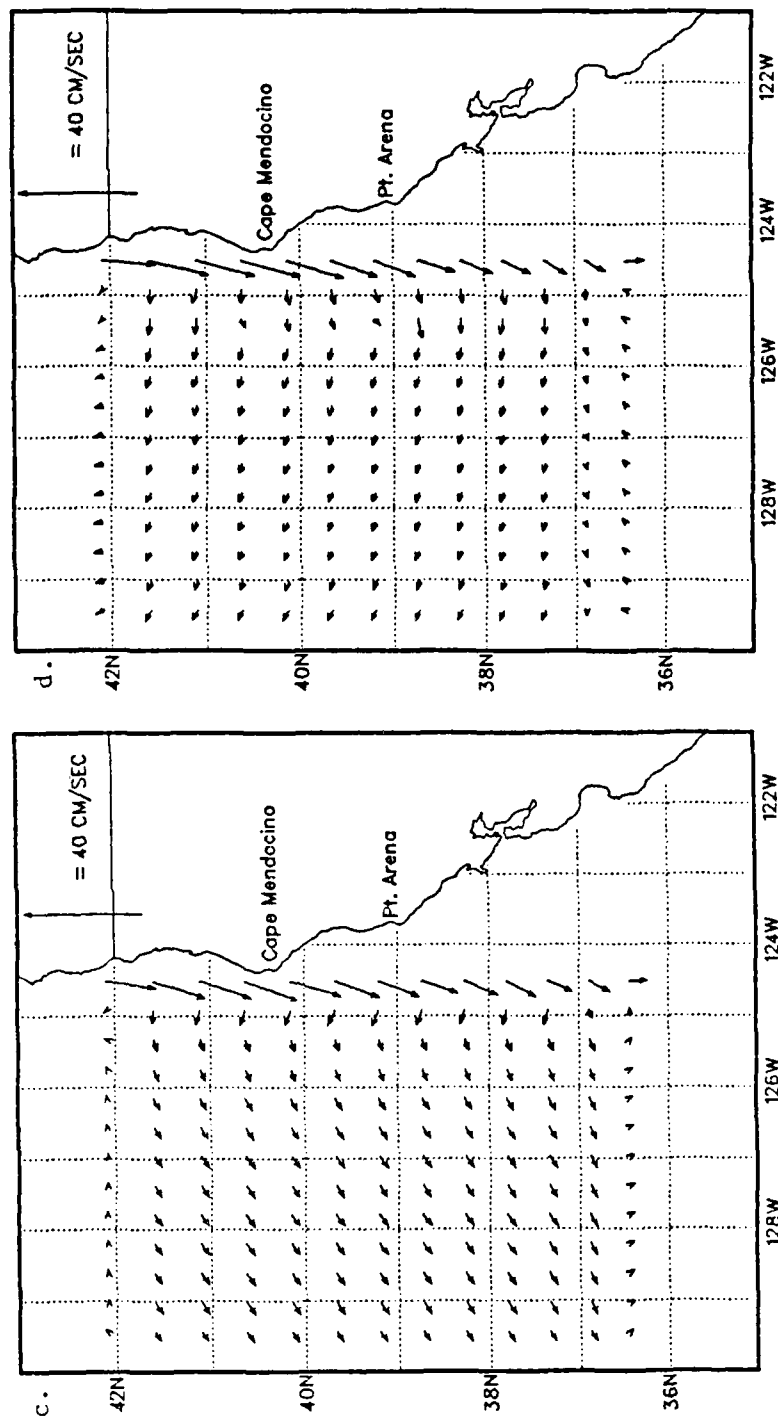
Figure 3.3   (continued) Surface current vectors for experiment 1
at (c) day 30 and (d) day 40.

35

~0.031°C/km and slightly increase with time during the 20-40 day period shown.

The steady, equatorward wind forcing resulted in an equatorward, surface coastal jet (Figure 3.5) with a maximum velocity of ~12-13 cm/sec by day 40. This nearshore surface flow is a result of geostrophy and the thermal wind equations. Gill (1982) showed that on an f-plane the coastal jet should be confined to the first internal Rossby radius of deformation, which is ~30 km for the model domain, as calculated by the method of Feliks (1985). The coastal jet axis seen in Figure 3.5 is at ~16 km, has a maximum offshore extent of ~45 km and extends to ~200 m depth. This coastal jet development correlates well with the steady wind forcing results of McCreary et al. (1987).

A weak, poleward current of ~2 cm/sec is also seen in Figure 3.5 below the coastal current at a depth of ~200-370 m. The offshore extent of the undercurrent is confined to ~10 km of the coast. McCreary (1981) found that a poleward undercurrent can develop as a result of either an alongshore pressure gradient or a variation in the wind stress, and it can be established by the radiation of Kelvin waves, and the vertical mixing of heat and momentum. McCreary (1981) described the sequence of events on the f-plane with suddenly imposed winds. First, offshore Ekman transport occurred in the area of the applied wind band. Next, an upwelling signal propagated rapidly poleward as a coastal Kelvin wave. As the Kelvin wave passed, a coastal jet was set up and provided a source of water for the Ekman transport. Philander and Yoon (1982) found that Kelvin waves also

36
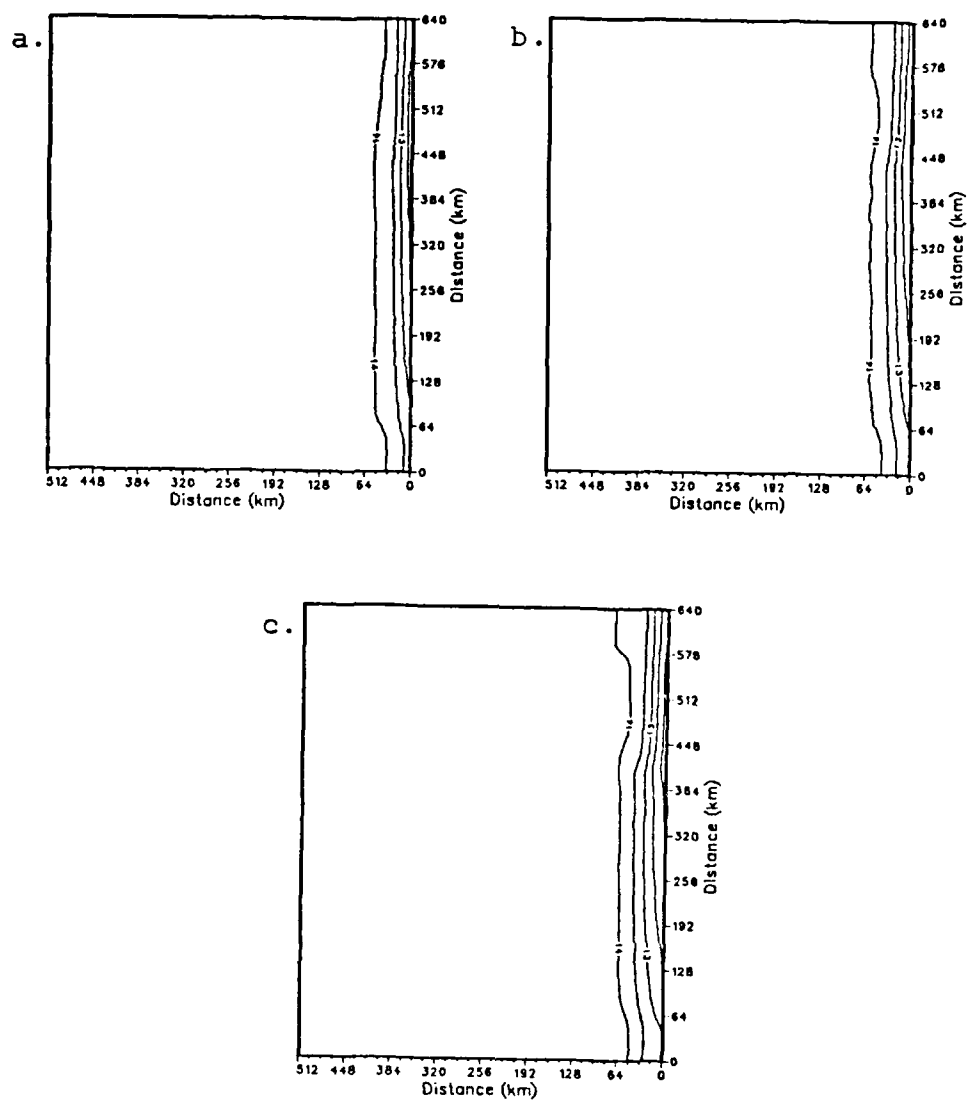
Figure 3.4   Surface contours of temperature (°C) for experiment 1
               at (a) day 20, (b) day 30 and (c) day 40. Contour
               interval is 0.5°C.

Figure 3.5   Vertical cross-shore sections of meridional (v)
               velocity (cm/sec) for experiment 1 at (a) day 20
               and (b) day 40.   Contour interval is 2.0 cm/sec.
               Dashed contours denote southern velocities.   The
               vertical cross-section was taken at y = 290 km.

introduced an undercurrent which reduced the intensity of coastal upwelling, but did not modify the zonal velocity perpendicular to the coast.

The vertical and offshore extent of the colder, upwelled waters is depicted in the vertical cross-sections of temperature (Figure 3.6). The initial conditions of a uniform, horizontal, temperature field have been changed by the presence of colder, upwelled water near the coast. Consequently, a rise of isotherms, consistent with upwelling, above ~300 m can be seen, while a slight bending down of isotherms, consistent with downwelling, below 320 m is discernible. The near-surface upwelled water extends ~120 km offshore. A comparison of Figure 3.6 with Figure 3.5 shows that these results are consistent with McCreary (1981), who found that upwelling did not reach deep depths, but was confined to above the core of the undercurrent; below the undercurrent, weak downwelling occurred.

At around day 45 of the experiment, the first evidence of developing ocean eddies can be seen in Figure 3.7 as perturbations in the zonal current near the coast at ~384 km. As will be seen in Section III.C, these eddies develop due to the presence of the unstable, coastal jet. The time-sequence of surface zonal velocity, shown in Figure 3.8, shows the continued development of these mesoscale features in the center of the model domain along the coast (between y ~160-448 km). The zonal length scale maximum for these eddies is ~70-80 km with zonal velocities greater than 15 cm/sec. The instantaneous zonal velocity field at day 90 (Figure 3.8c) depicts the location of a weak cyclonic and anticyclonic circulation at y ~320 km.
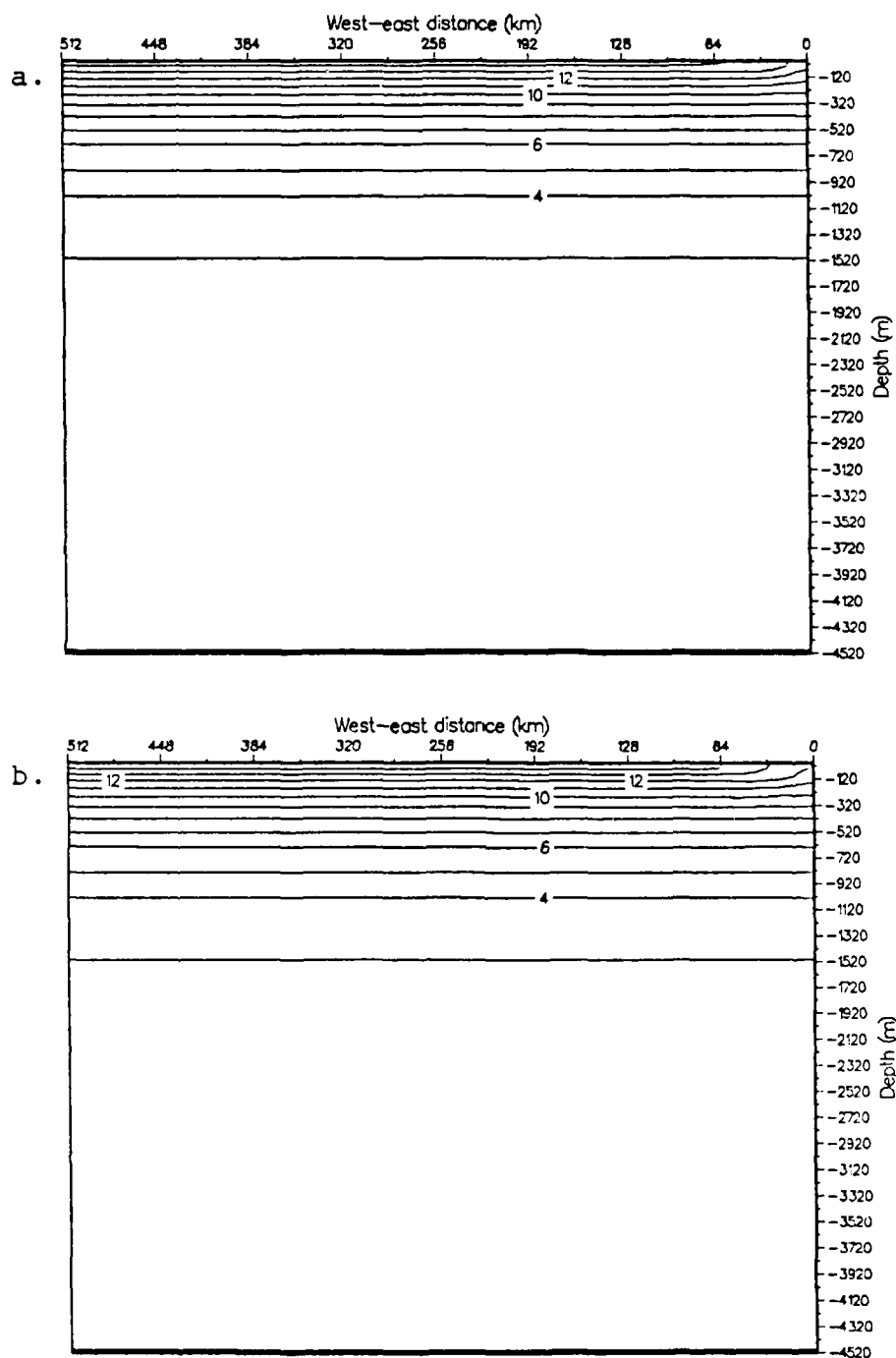
Figure 3.6   Vertical cross-shore sections of temperature (°C) for
              experiment 1 at (a) day 20 and (b) day 40. Contour
              interval is 1.0°C. The vertical cross-section was
              taken at y = 290 km.
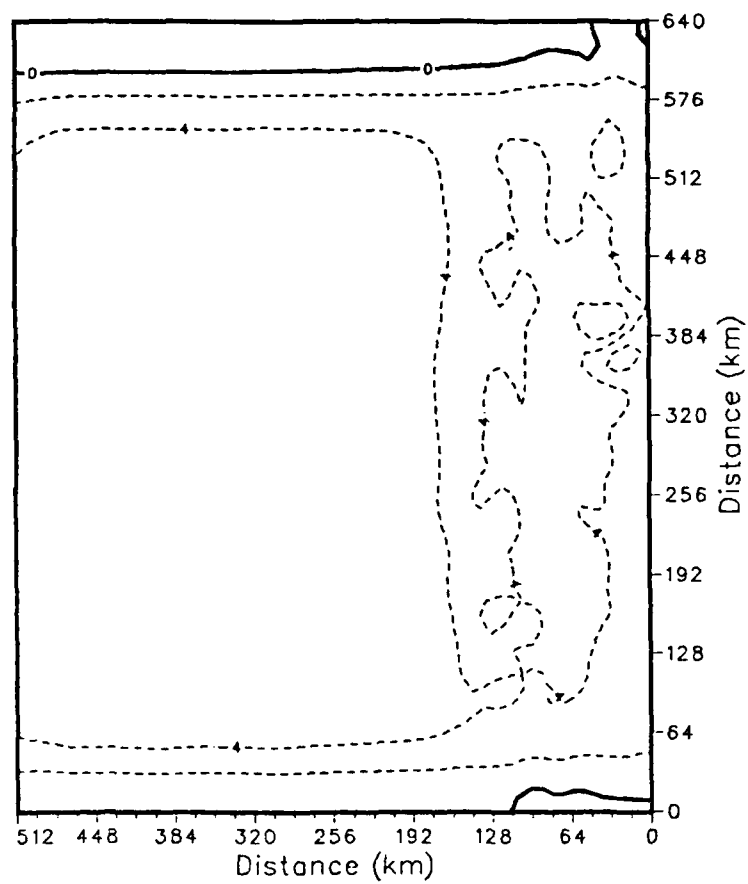
Figure 3.7   Surface contours of zonal (u) velocity (cm/sec) for
experiment 1 at day 45.   Contour interval is 2.0
cm/sec.   Dashed contours denote westward velocities.

41

Figure 3.8   Surface contours of zonal (u) velocity (cm/sec)
              for experiment 1 at (a) day 70, (b) day 80 and (c)
              day 90. Contour interval is 2.0 cm/sec for (a) and
              (b), 5.0 cm/sec for (c). Dashed contours denote
              westward velocities.

42

This type of circulation, known as a "vortex pair", is consistent with CCS observations (Bernstein et al., 1977).

The instantaneous plots of meridional velocity plots for days 70, 80 and 90 (Figure 3.9) show the intensification of the equatorward, surface coastal jet. By day 90, the maximum velocity of the jet is greater than 20 cm/sec with the core at about 30 km offshore. The maximum offshore extent is ~64 km.

The poleward undercurrent (Figure 3.10) is shown to extend to only ~16-18 km offshore. This undercurrent has a maximum core velocity of ~6-7 cm/sec at a depth of ~300 m only ~10 km from the coast. The entire undercurrent depth extends from ~60 m to 620 m. The surface coastal jet is shown to extend to ~42 km offshore, and extends to ~400 m depth offshore of the undercurrent. Offshore of the jet, at ~127 km, can be seen the signature of an eddy field at this latitude. These eddy fields contribute to the meandering of the jet, as seen in previous plots.

The surface dynamic height field, shown in Figure 3.11, was calculated from the pressure field relative to 2400 m depth. A downward slope of dynamic height towards the coast was observed, as expected. In addition, an anticyclonic eddy was seen offshore at 50 km at y ~250 km. A comparison of Figure 3.11 with Figure 3.12, which shows the corresponding temperature fields, shows that the isotherm perturbations align favorably with the generated offshore/onshore geostrophic flow of the eddies. These results, as will be shown in Section IV, compare favorably with CCS observations of cold, intense seaward flow, called squirts.

43
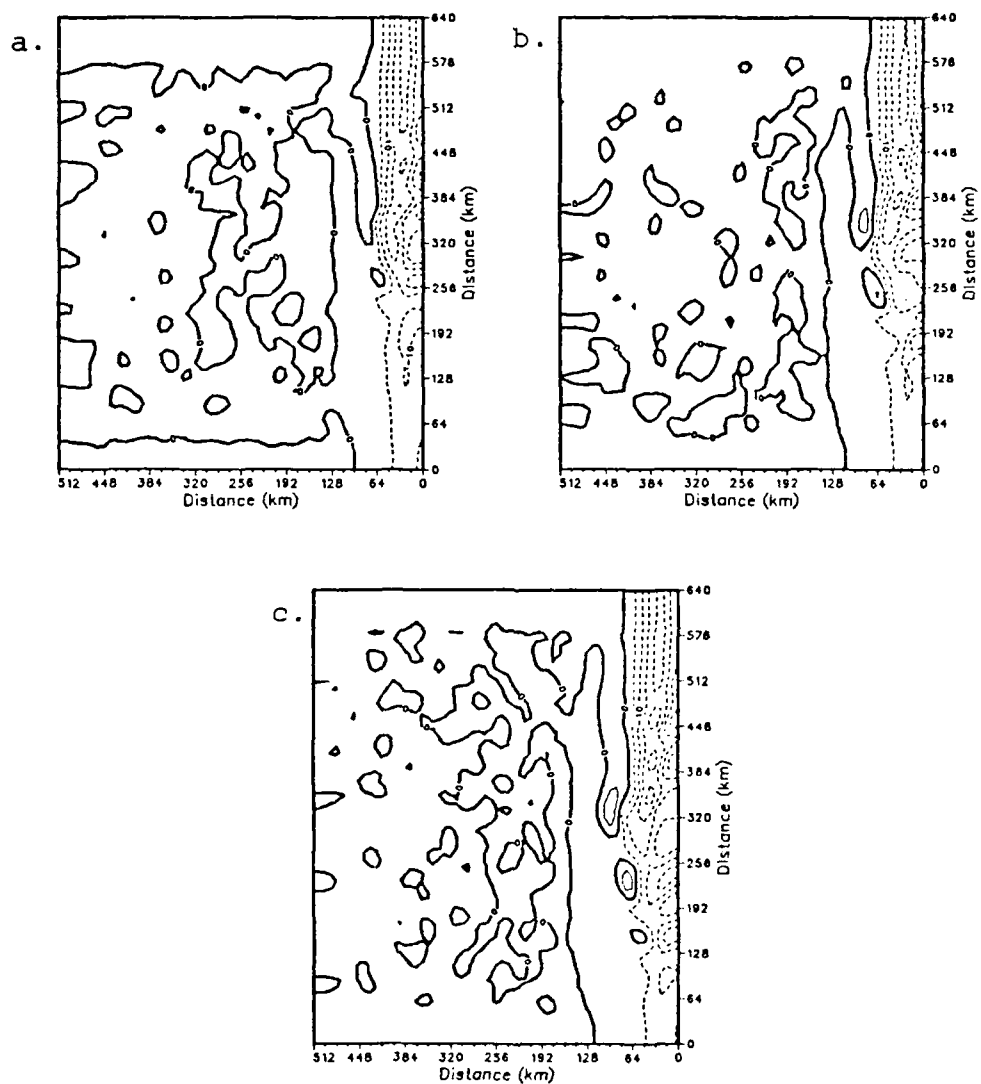
Figure 3.9   Surface contours of meridional (v) velocity
              (cm/sec) for experiment 1 at (a) day 70, (b)
              day 80 and (c) day 90.   Contour interval is 5.0
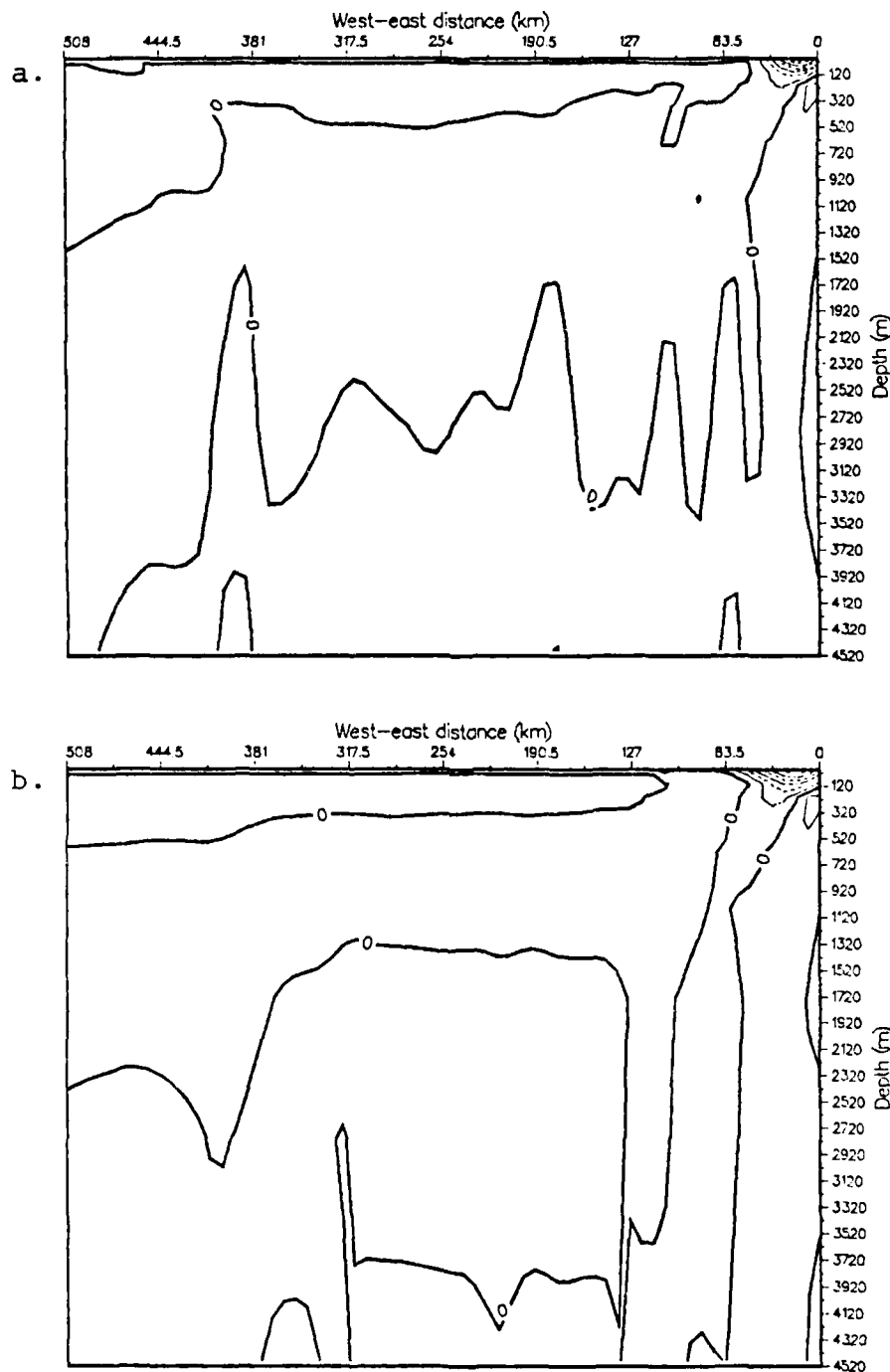   cm/sec.   Dashed contours denote southward
              velocities.
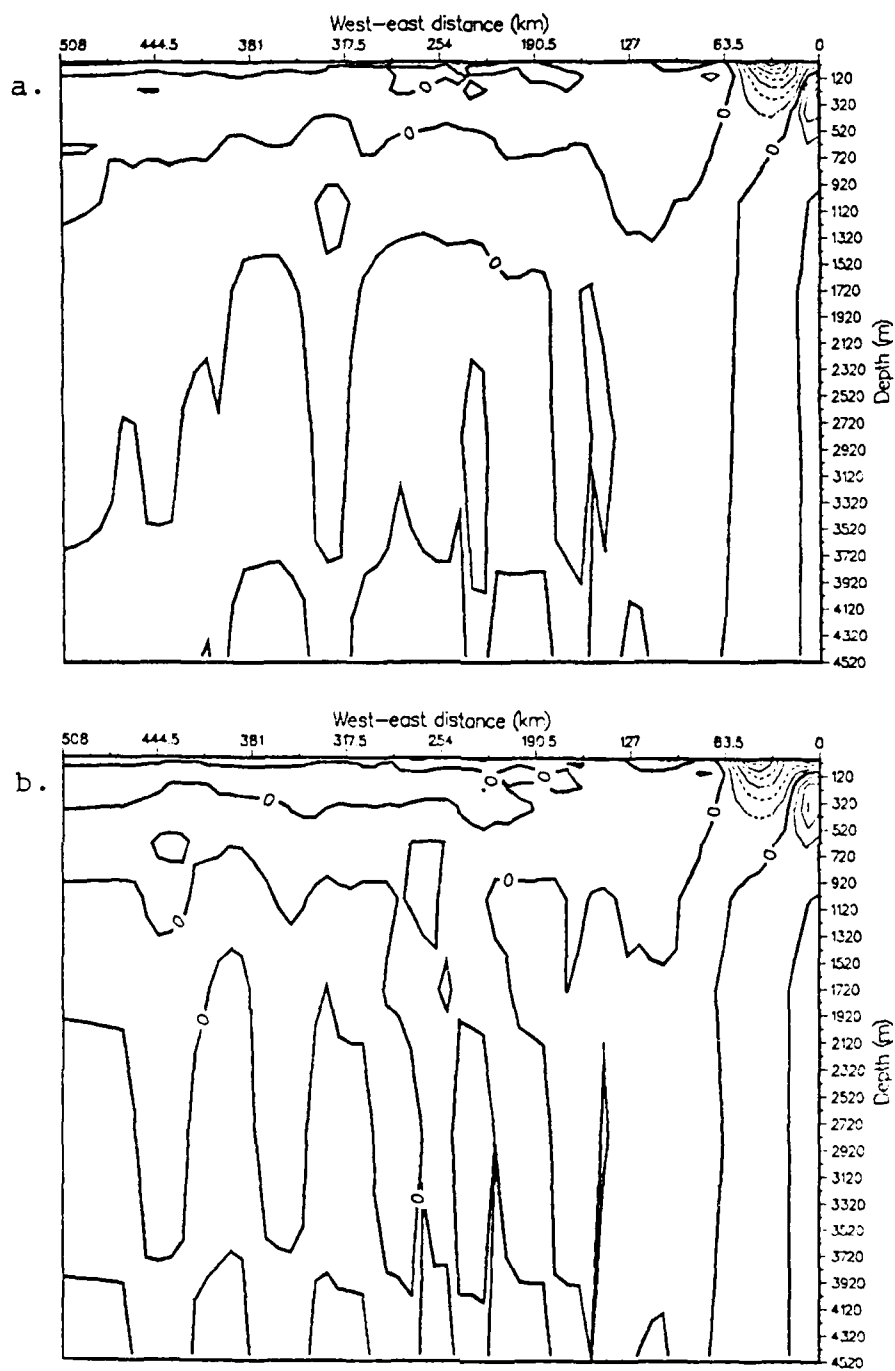
Figure 3.10   Vertical cross-shore sections of meridional
(v) velocity (cm/sec) for experiment 1 at (a)
day 70 and (b) day 80. Contour interval is
2.0 cm/sec. Dashed contours denote southward
velocities. The vertical cross-section was
taken at y = 290 km.

45

Figure 3.10   (continued) (c) Vertical cross-shore section
of meridional (v) velocity (cm/sec) for
experiment 1 at day 90.

46
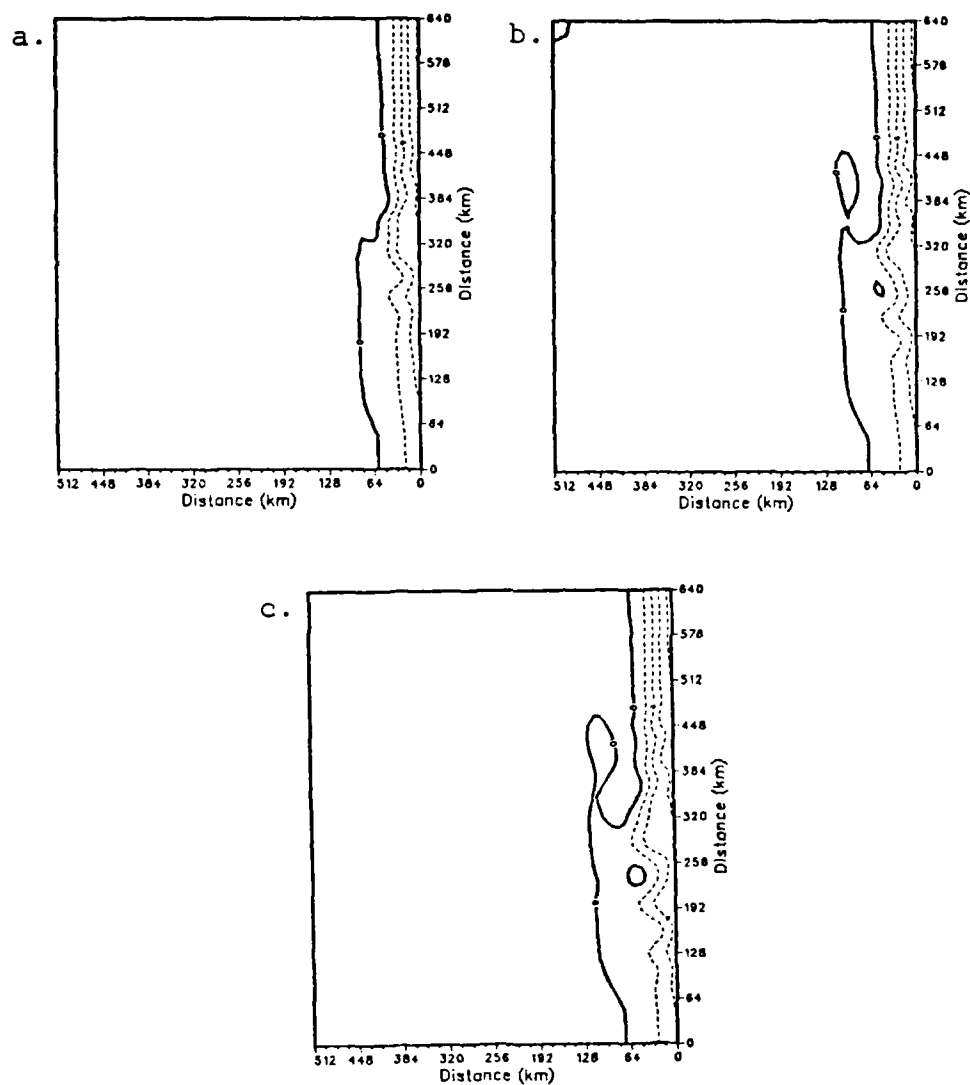
Figure 3.11   Surface contours of dynamic height (cm) for
experiment 1 at (a) day 70, (b) day 80 and (c)
day 90. Contour interval is 2.0 cm.
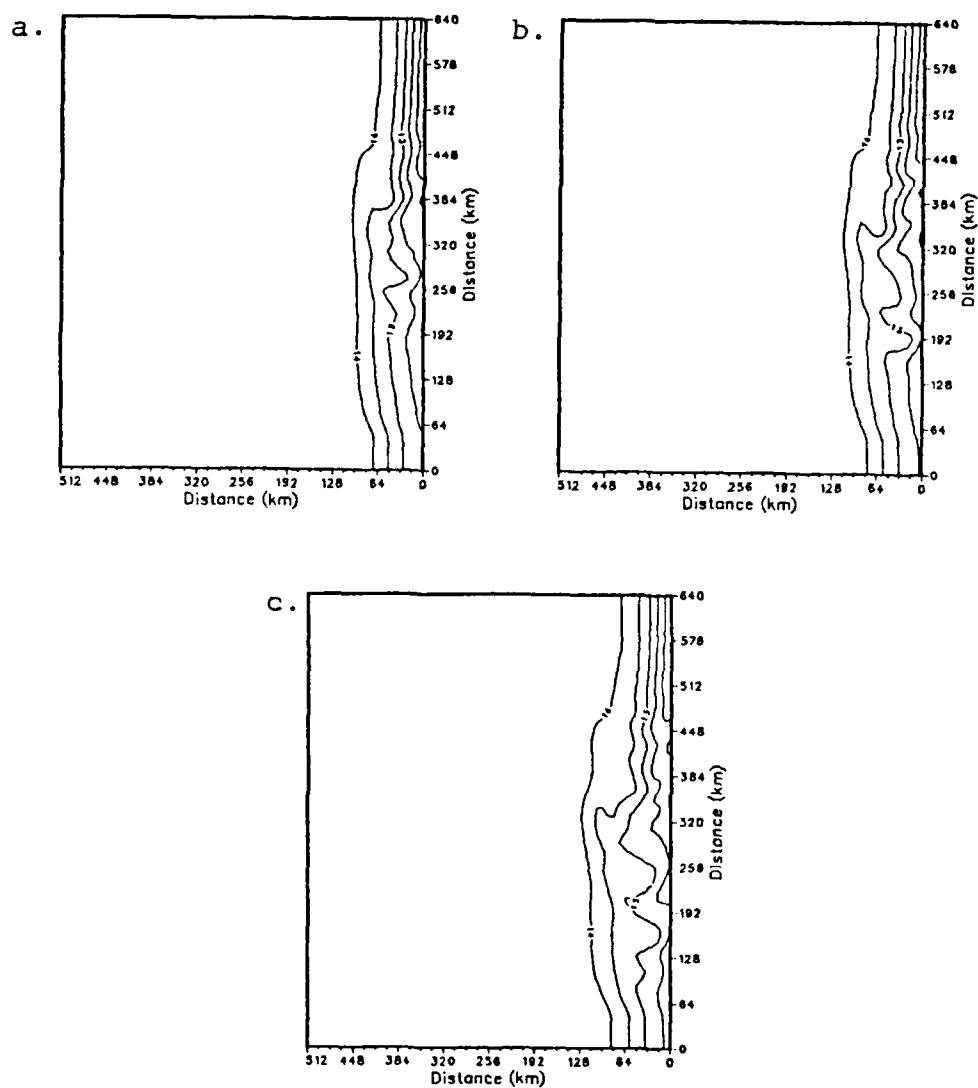
Figure 3.12   Surface contours of temperature (°C) for
               experiment 1 at (a) day 70, (b) day 80 and (c)
               day 90.   Contour interval is 0.5°C.

48

2. Experiment 2 (Wind Stress Curl)

Experiment 2 differed from experiment 1 only in that the wind stress forcing included the important effect of a curl. As discussed in Section II.B, wind field data (Figure 2.10) derived from the analytical representation of the wind stress curl (eqn. 2.7) was used to force the PE model.

The maximum wind stress (Figure 2.10) was located ~187 km offshore, which, as expected, corresponded to the zero value of wind stress curl (Figure 2.8). Wind stress curl can cause a variation in the Ekman transport leading to convergence and divergence of mass, resulting in more complex mass balances. Inshore, the positive wind stress curl along the coast caused Ekman pumping due to the horizonal mass divergence at the surface, which required water from below the surface to replace the transported fluid. Offshore, the negative curl caused horizonal mass convergence which led to the occurrence of downwelling.

The important results of experiment 2 are illustrated in the time progression of surface meridional velocity fields shown in Figure 3.13. Initially, a surface coastal jet developed as observed at day 10 (Figure 3.13a), but later (~day 40) weakened and disappeared due to the presence of a dominating poleward current. By ~day 30, a surface poleward current was generated in the southeastern portion of the domain. This current (similar to the Davidson Current) continued to develop during the entire period, so that by day ~90 (Figure 3.13d) the current had reached a velocity of ~16 cm/sec and had a core centered offshore at ~34 km. A broad, slower (~5 cm/sec), offshore,

Figure 3.13   Surface contours of meridional (v) velocity
               (cm/sec) for experiment 2 at (a) day 10, (b)
               day 30, (c) day 60 and (d) day 90. Contour
               interval is 5.0 cm/sec. Dashed contours
               denote southward velocities.

surface equatorward flow was discernible at ~day 60 (Figure 3.13c) and subsequently encompassed a greater extent of the offshore domain.

The time sequence of vertical cross-shore sections, shown in Figure 3.14, show that after ~day 10, the weak (~6 cm/sec), surface coastal jet was no longer observed. Instead, at ~day 20, a poleward surface current developed near the coast with its core located at a depth of ~150 m and a maximum velocity of ~20 cm/sec. This current extended offshore to ~60 km and to a depth of ~1100 m. At ~day 60, a broad, offshore equatorward flow appeared with a width of ~174 km and a core centered at ~120 km. McCreary et al. (1987) found similar results with his flat-bottom model. In particular, he found that, due to the presence of the steady, positive wind stress curl, both a deep, broad poleward surface current near the coast and an equatorward surface flow located farther offshore developed.

No eddies or jets developed in this experiment. As will be discussed in Section III.C, this is due to the lack of an unstable coastal surface jet overlying a poleward undercurrent.

3. Experiment 3 (Wind with Y-Variation in Wind Stress)

Experiment 3 was similar to experiment 1 with the exception of an implemented variation in the alongshore wind stress, as discussed in Section II.B. The maximum alongshore wind stress computed (Figure 2.11) was just south of the Cape Mendocino region.

The initial results of experiment 3 were quite similar to experiment 1. In particular, ocean eddies initially developed around days 40-50, and the location of the generation (Figure 3.15) of these eddies correlated well with experiment 1. As seen in Figure 3.16,

51
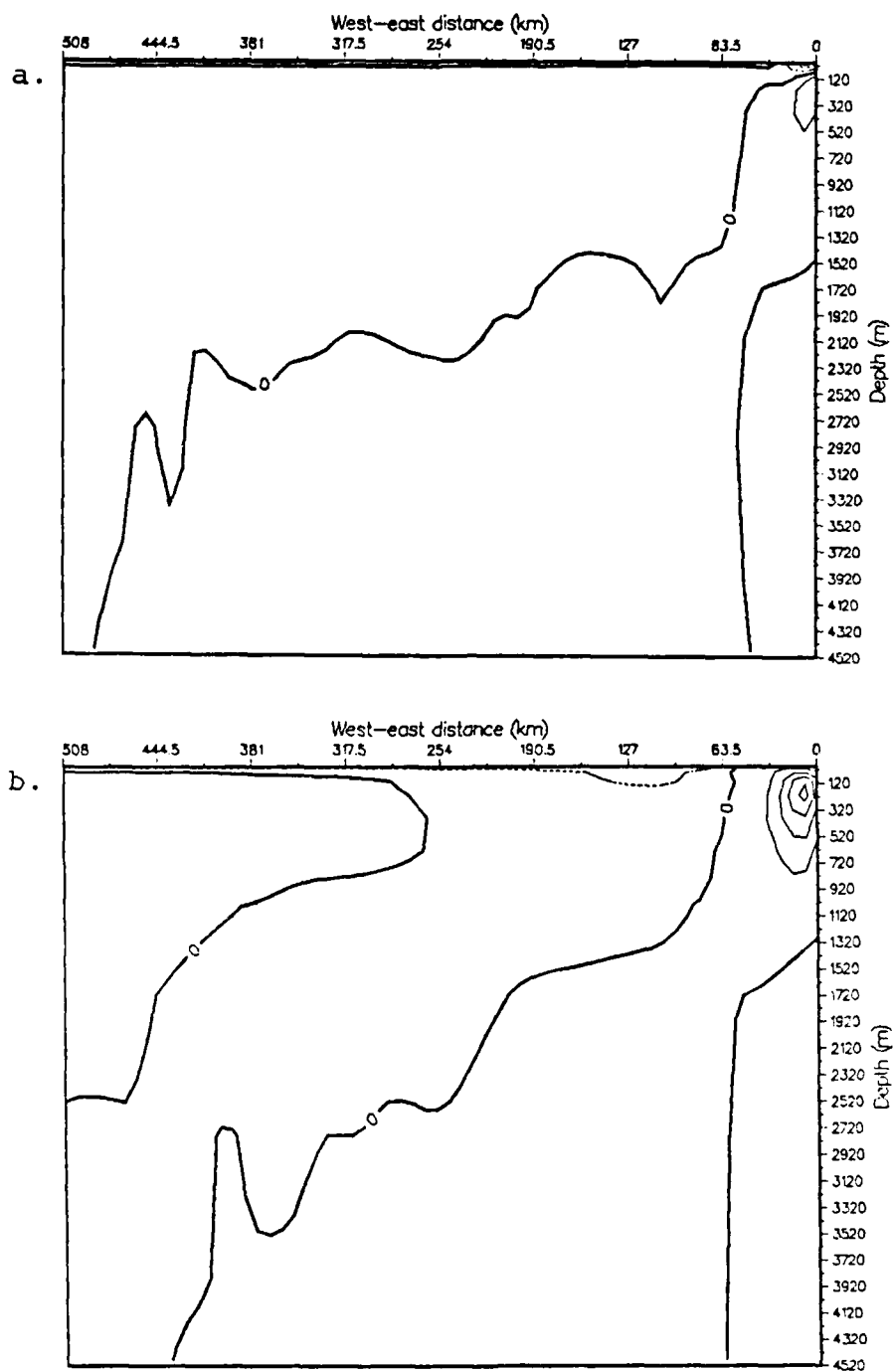
Figure 3.14   Vertical cross-shore sections of meridional
               (v) velocity (cm/sec) for experiment 2 at (a)
               day 10 and (b) day 30.   Contour interval is
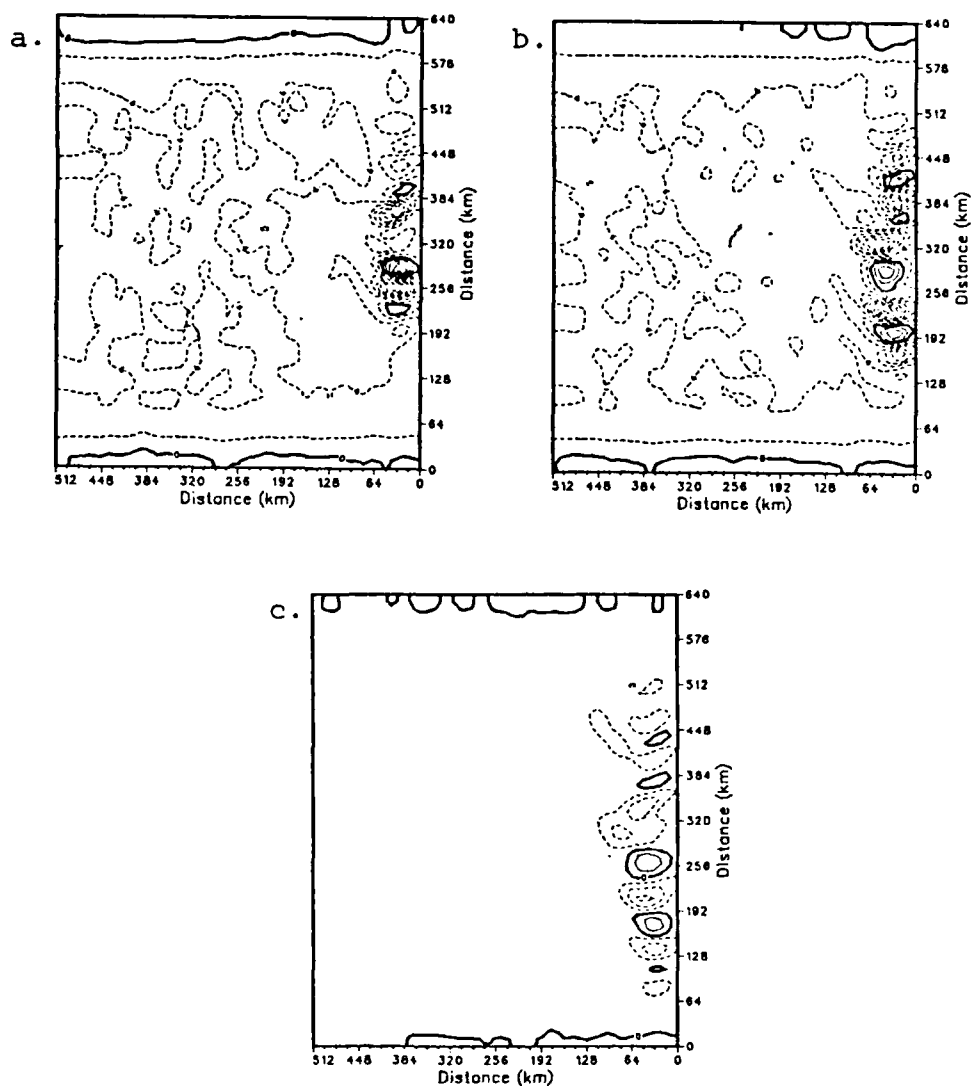   2.0 cm/sec.   Dashed contours denote southward
               velocities.   The vertical cross-section was
               taken at y = 290 km.
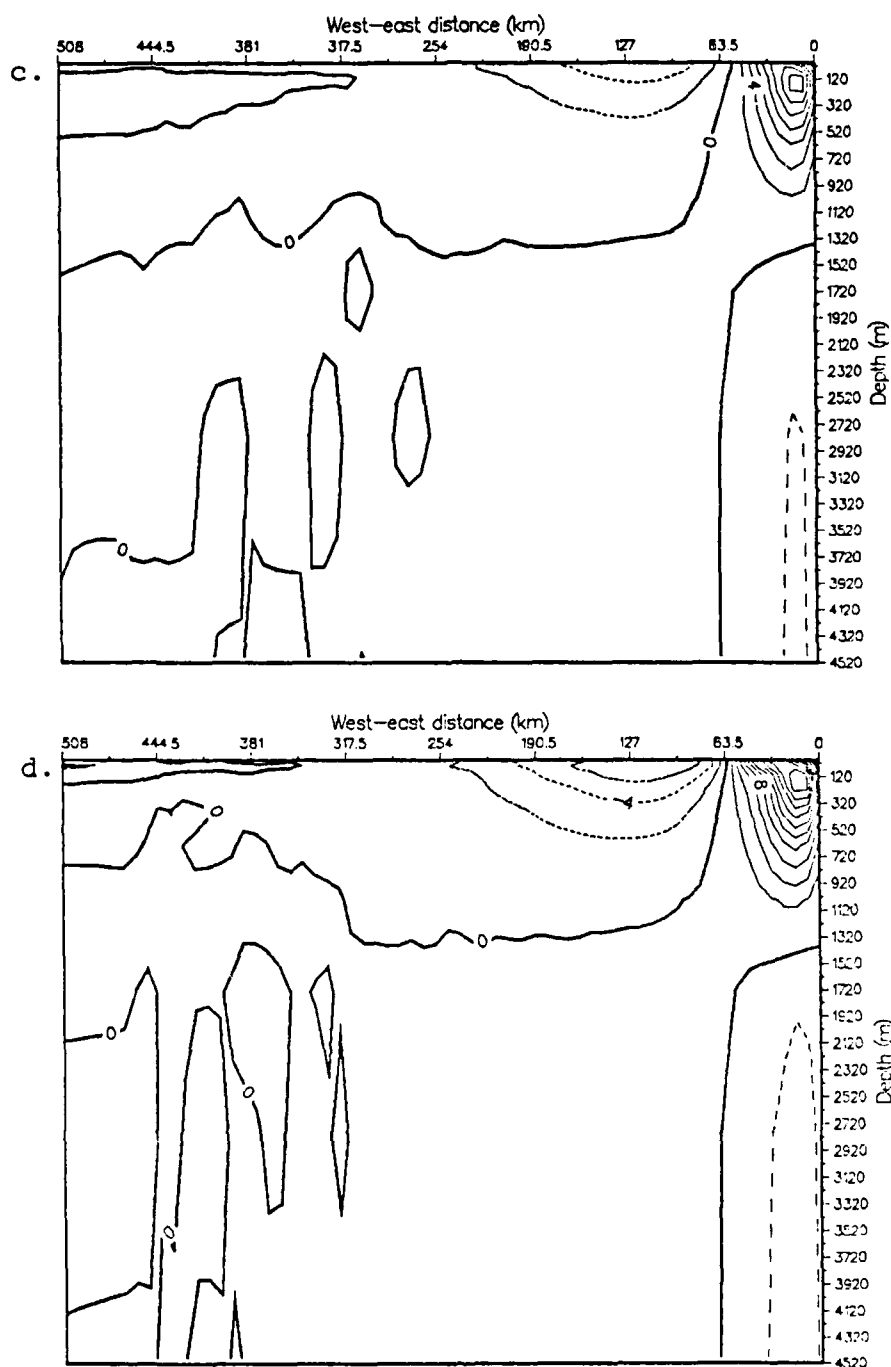
Figure 3.14   (continued) Vertical cross-shore sections of
                meridional (v) velocity (cm/sec) for
                experiment 2 at (c) day 60 and (d) day 90.

which shows surface contours of zonal and meridional velocity, dynamic height and temperature fields at day 90, the core of the equatorward coastal jet is centered ~32 km offshore with a maximum velocity of ~20 cm/sec.

A notable difference from experiment 1 was that experiment 3 did not have the eddy development occur as far north as in experiment 1, i.e., no eddies developed north of ~385 km. This was likely due to the maximum wind stress occurring south of this region. Temperature perturbations associated with offshore jets and eddies also, as expected, occurred further to the south. By ~day 45, the surface coastal jet (Figure 3.17) had intensified to ~12 cm/sec with the core ~25 km offshore. The maximum offshore extent of the jet was ~63 km. A weak poleward undercurrent (~2 cm/sec) was seen at a depth of ~200-400 m. The meridional velocity field (Figure 3.17b) at day 90 showed that the undercurrent velocity had increased slightly to ~4 cm/sec while the surface coastal jet velocity had increased to ~14 cm/sec. A weak surface poleward velocity was also observed at ~87 km offshore of the jet, which was associated with the development of an anticyclonic eddy.

This experiment showed that the variation in alongshore wind stress can play a key role in the location of the eddy development region. In particular, eddies can be generated in the localized area of maximum alongshore wind stress.

Figure 3.15   Surface contours of zonal (u) velocity
(cm/sec) for experiment 3 at day 50. Contour
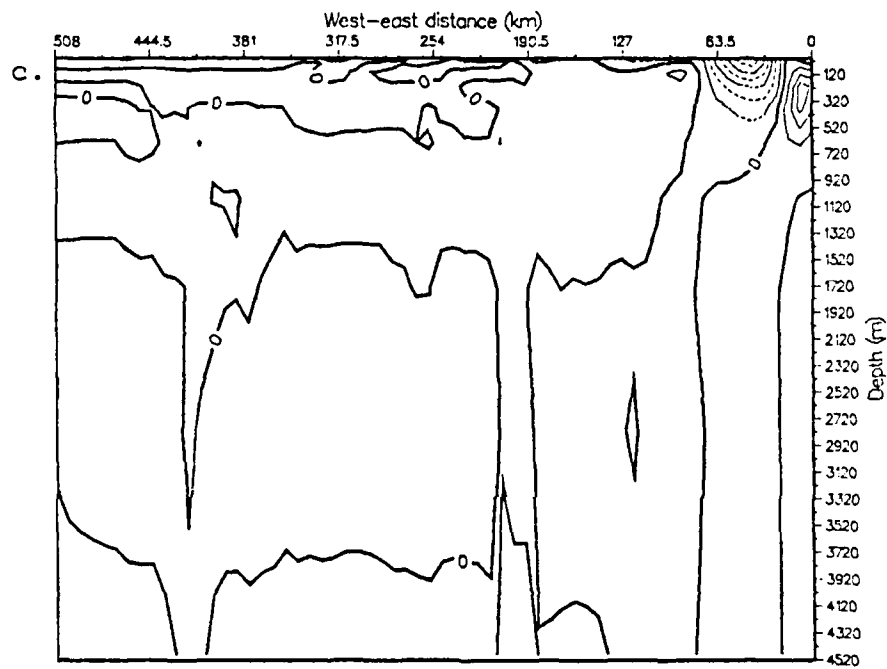interval is 2.0 cm/sec. Dashed contours
denote westward velocities.

55

Figure 3.16   Surface contours of (a) zonal (u) velocity
(cm/sec), (b) meridional (v) velocity
(cm/sec), (c) dynamic height (cm) and (d)
temperature (°C) for experiment 3 at day 90.
Contour interval for (a) and (b) is 5.0
cm/sec. Contour interval for (c) is 2.0 cm
and (d) is 0.5°C. Dashed contours denote
westward velocities in (a), southward
velocities in (b) and negative values in (c).

56

Figure 3.17   Vertical cross-shore sections of meridional
               (v) velocity (cm/sec) for experiment 3 at (a)
               day 45 and (b) day 90. Contour interval is
               2.0 cm/sec. Dashed contours denote southward
               velocities. The vertical cross-section was
               taken at y = 290 km.

B. EXPERIMENTS ON A BETA-PLANE

1. Experiment 4 (Uniform Wind Stress)

Experiment 4 used the same parameters and forcing mechanisms as in experiment 1, but used a β-plane rather than an f-plane. The Beta effect, i.e., the variation of the Coriolis parameter with latitude due to the curvature of the earth, allows the existence of freely propagating planetary waves, i.e., Rossby waves (Gill, 1982). Due to the Beta effect, the surface coastal jet is not required to be confined within a Rossby radius of deformation of the coast (McCreary et al., 1987). The offshore radiation of Rossby waves, according to McCreary (1987). can contribute to the generation of an alongshore pressure gradient field, which, as mentioned previously, can cause a poleward undercurrent to develop.

The results of experiment 4 showed the generation of eddies at ~day 40, as seen in the zonal velocity plots of Figure 3.18. The eddy perturbations were generated a little farther to the north on the β-plane than in experiment 1. Zonal eddy velocities ranged from ~5-12 cm/sec, at ~day 70 (Figure 3.18d). The time progression of the westward propagation of the faster, longer wavelength Rossby waves can be seen in Figures 3.18a-d. As expected, progressively shorter wavelength Rossby waves propagate offshore in subsequent times. Surface contour plots for instantaneous velocity, temperature and dynamic height fields at day 90 are shown in Figure 3.19. The maximum zonal velocity (Figure 3.19a) reached is ~15 cm/sec coinciding with the intense generation of an anticyclonic eddy at y~224 km (Figure

58
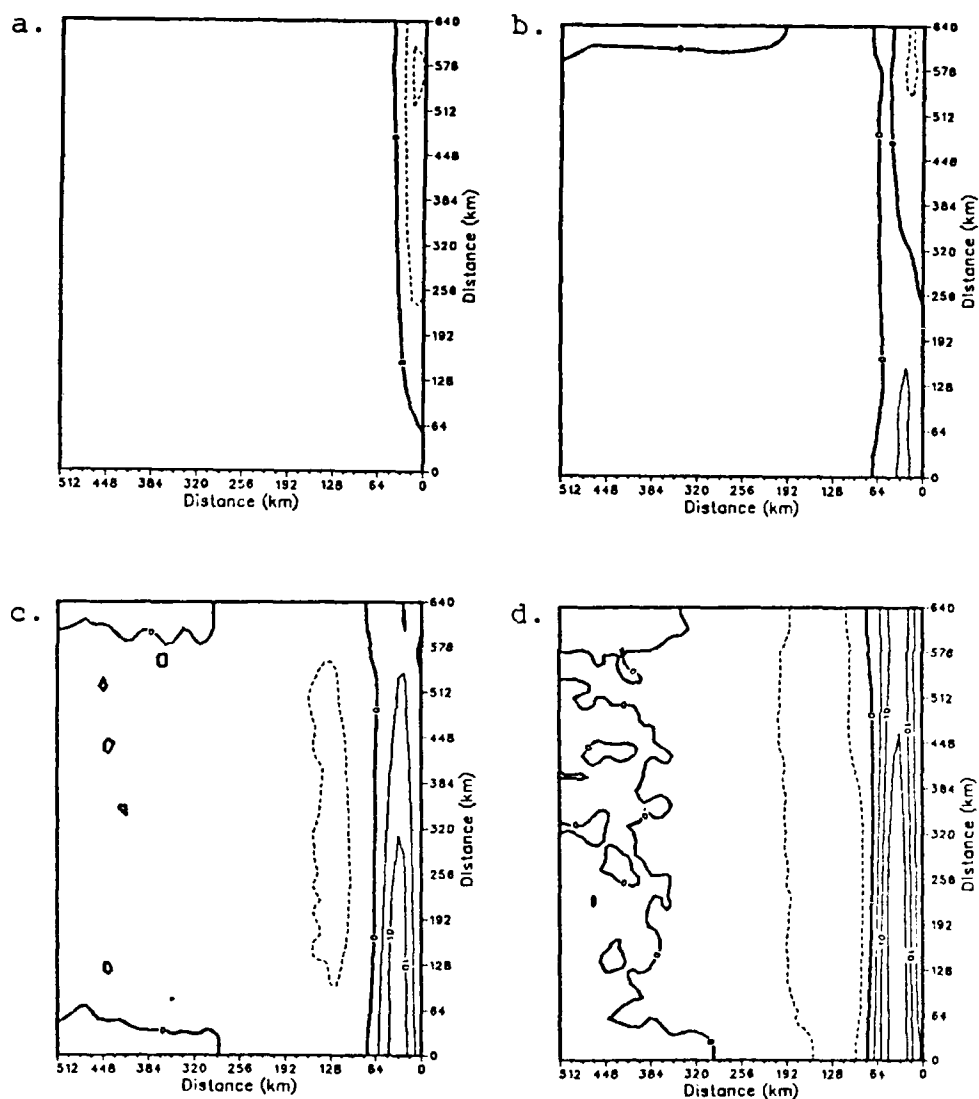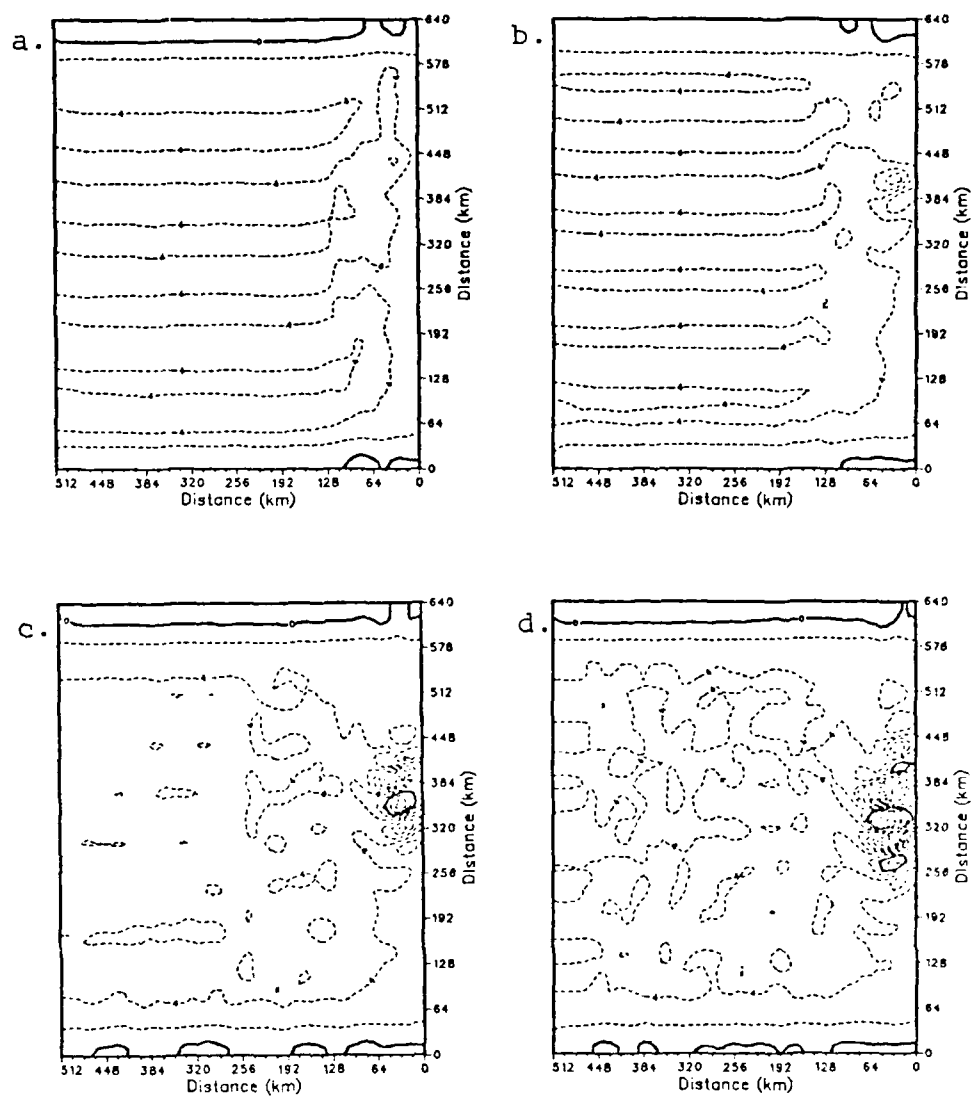
Figure 3.18   Surface contours of zonal (u) velocity
(cm/sec) for experiment 4 at (a) day 40, (b)
day 50, (c) day 60 and (d) day 70. Contour
interval is 2.0 cm/sec. Dashed contours
denote westward velocities.

3.19c). The 13.5°C temperature anomaly in the same area (Figure 3.19d) is likely associated with the warm core of this anticyclone.

The surface coastal jet with equatorward flow (Figure 3.19b) has maximum velocities of ~10-15 cm/sec which are located offshore at ~56 km. This was approximately 25 km farther offshore and 5 cm/sec weaker than the results of experiment 1. A comparison of the coastal jet in this experiment at day 90 (Figure 3.20) and that in Experiment 1 (Figure 3.10c) shows that the coastal jet is shallower and the undercurrent is deeper in this experiment. The maximum offshore extent of the undercurrent is ~30 km , which is ~10 km farther offshore than in experiment 1.

This experiment showed that, due to the Beta effect, circulation does not necessarily have to be confined within a Rossby radius of deformation of the coast. As in previous no curl experiments, a coastal jet develops within a Rossby radius of deformation of the coast (which is ~30 km, based on the method of Feliks, 1985), within which eddies develop. Due to the use of vertical mixing in the model, the Rossby waves do not advect the jet or eddies offshore. Rather, the Rossby waves propagate offshore as a packet, with longer and then shorter waves moving westward, as expected.

2. **Experiment 5 (Wind Stress Curl)**

This experiment paralleled experiment 2, but used a β-plane rather than an f-plane. Surface contours of zonal velocity, shown in Figure 3.21, depict the offshore radiation of Rossby waves, as expected with the inclusion of the beta effect, and the initial

60

Figure 3.19   Surface contours of (a) zonal (u) velocity
(cm/sec), (b) meridional (v) velocity
(cm/sec), (c) dynamic height (cm) and (d)
temperature (°C) for experiment 4 at day 90.
Contour interval for (a) and (b) is 5.0
cm/sec.   Contour interval for (c) is 2.0 cm
and (d) is 0.5°C.   Dashed contours denote
westward velocities in (a), southward
velocities in (b) and negative values in (c).

61

Figure 3.20   Vertical cross-shore sections of meridional
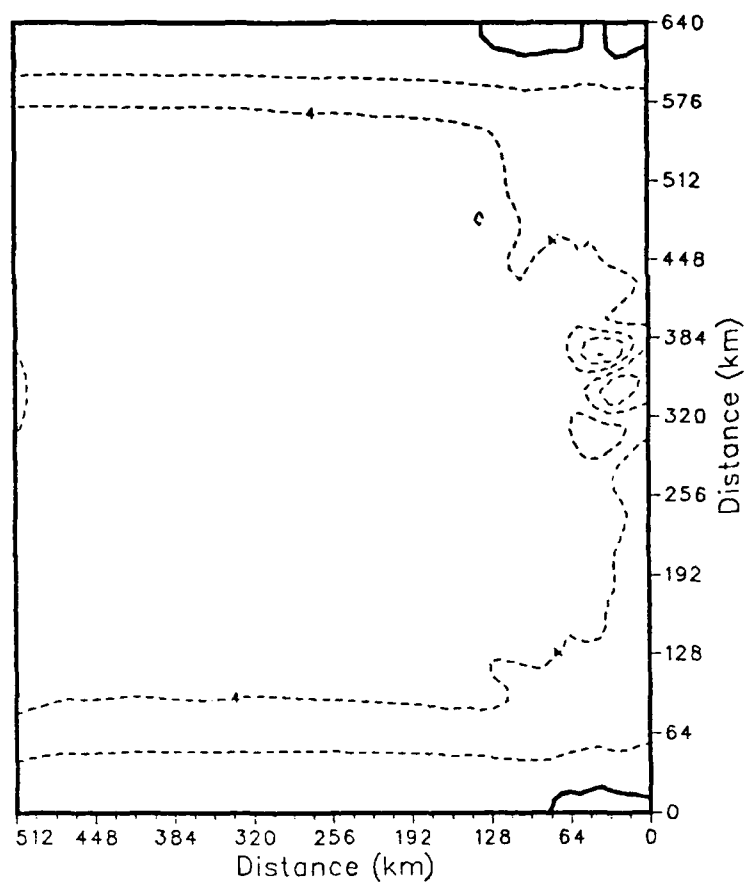   (v) velocity (cm/sec) for experiment 4 at day
               90.   Contour interval is 2.0 cm/sec.   Dashed
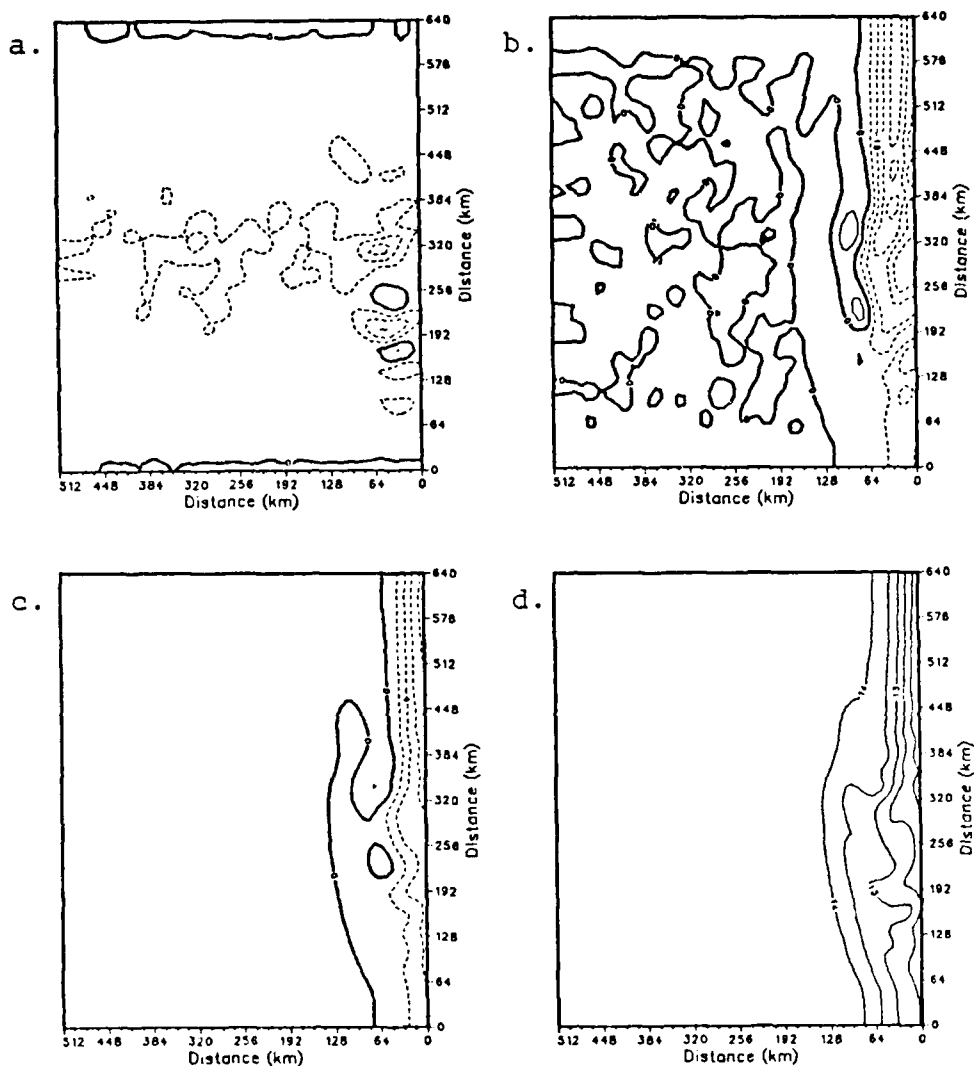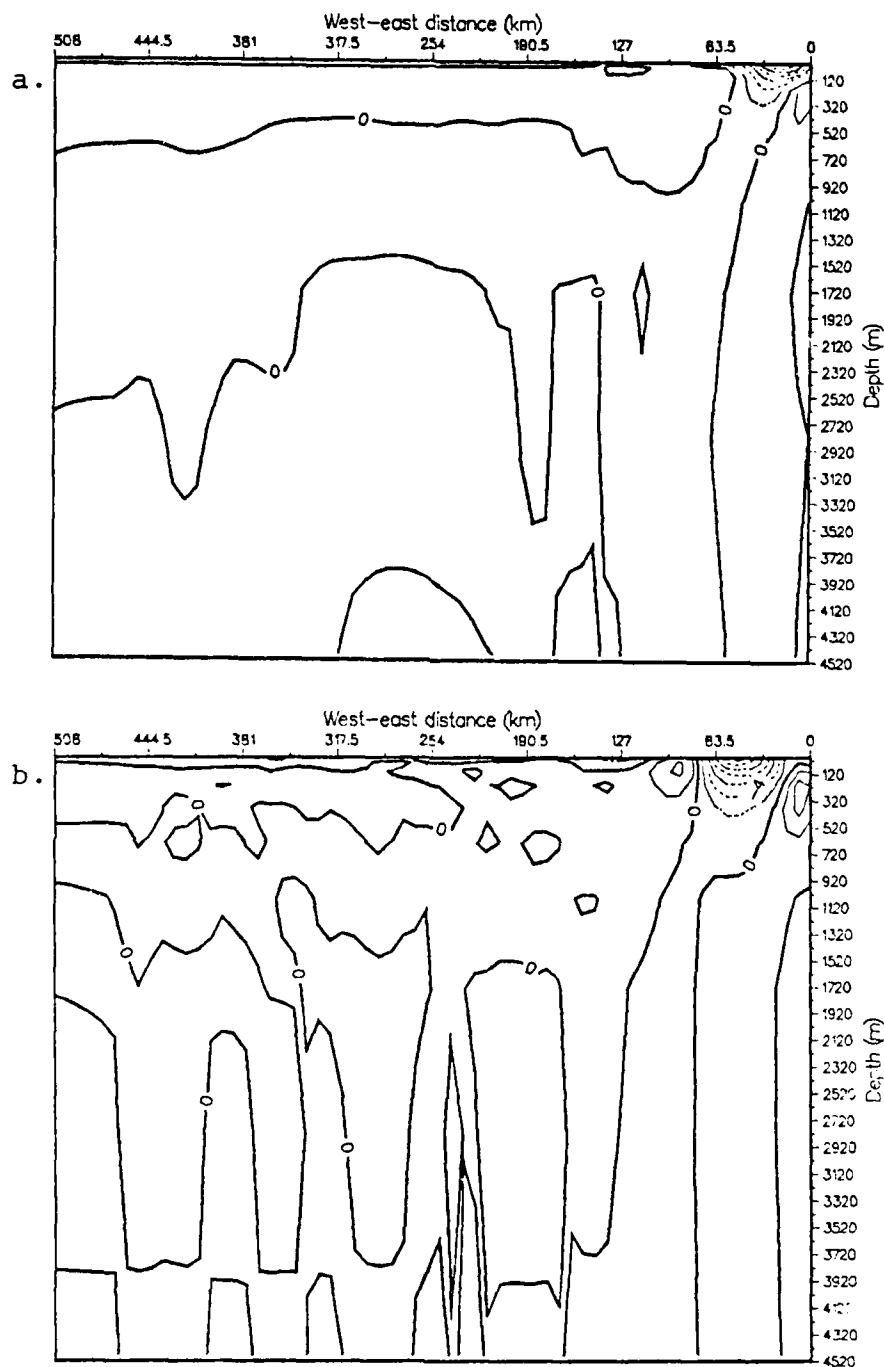   contours denote southward velocities.   The
               vertical cross-section was taken at y = 290
               km.

generation of an eddy field between y~500-575 km. This experiment differed from experiment 2 (wind stress curl on an f-plane) which had neither of these features. It also differed from experiment 1, (no curl on an f-plane) which had of course no Rossby waves, but had eddies developing much earlier (~day 45 rather than ~day 80) and farther south (~100 km). The generation of the eddies here, as in previous experiments in which eddies were generated, was due to the presence of the unstable coastal jet and undercurrent, as will be shown in Section III. C.

A time progression of surface contours of meridional velocity, shown in Figure 3.22, showed the weak surface coastal jet confined to within ~16 km from the coast in the northern portion of the domain. A poleward current surfaced at ~day 60 and extended from the northern to the southern domain boundaries by ~day 90, with a maximum velocity of ~10-12 cm/sec. This current was weaker (~5 cm/sec) and extended ~16 km farther offshore than in experiment 2(f-plane).

The broad equatorward flow at ~y = 100-200 km offshore was best observed in the vertical cross-shore sections of meridional velocity (Figure 3.23). The flow developed by ~day 30 and reached a maximum velocity of ~5 cm/sec by ~day/90. The stronger surface coastal jet weakened throughout the time period and became a weaker, near-coastal feature as the poleward undercurrent grew and surfaced. The core of the poleward current was ~8 cm/sec weaker and ~15 km wider than in experiment 2.
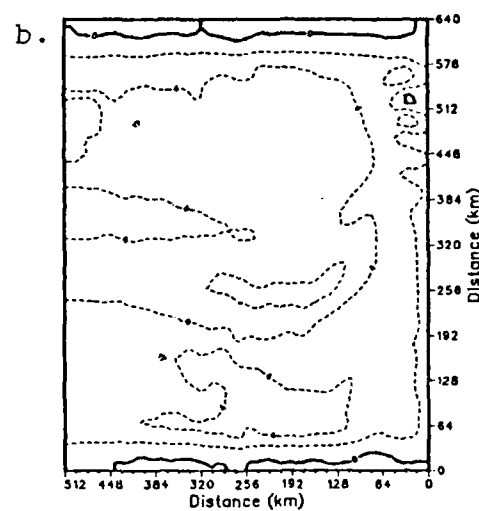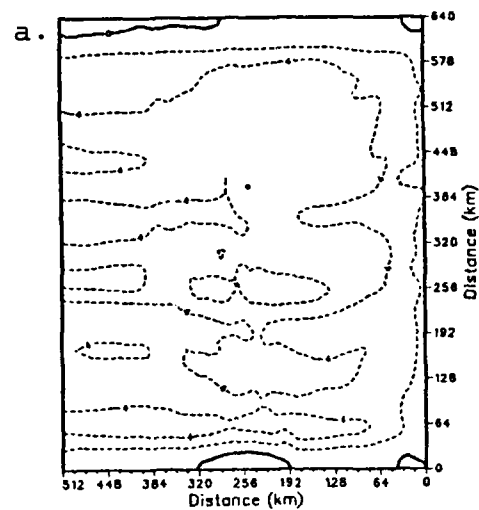
Figure 3.21   Surface contours of zonal (u) velocity
               (cm/sec) for experiment 5 at (a) day 40 and
               (b) day 80. Contour interval is 2.0 cm/sec.
               Dashed contours denote westward velocities.

64
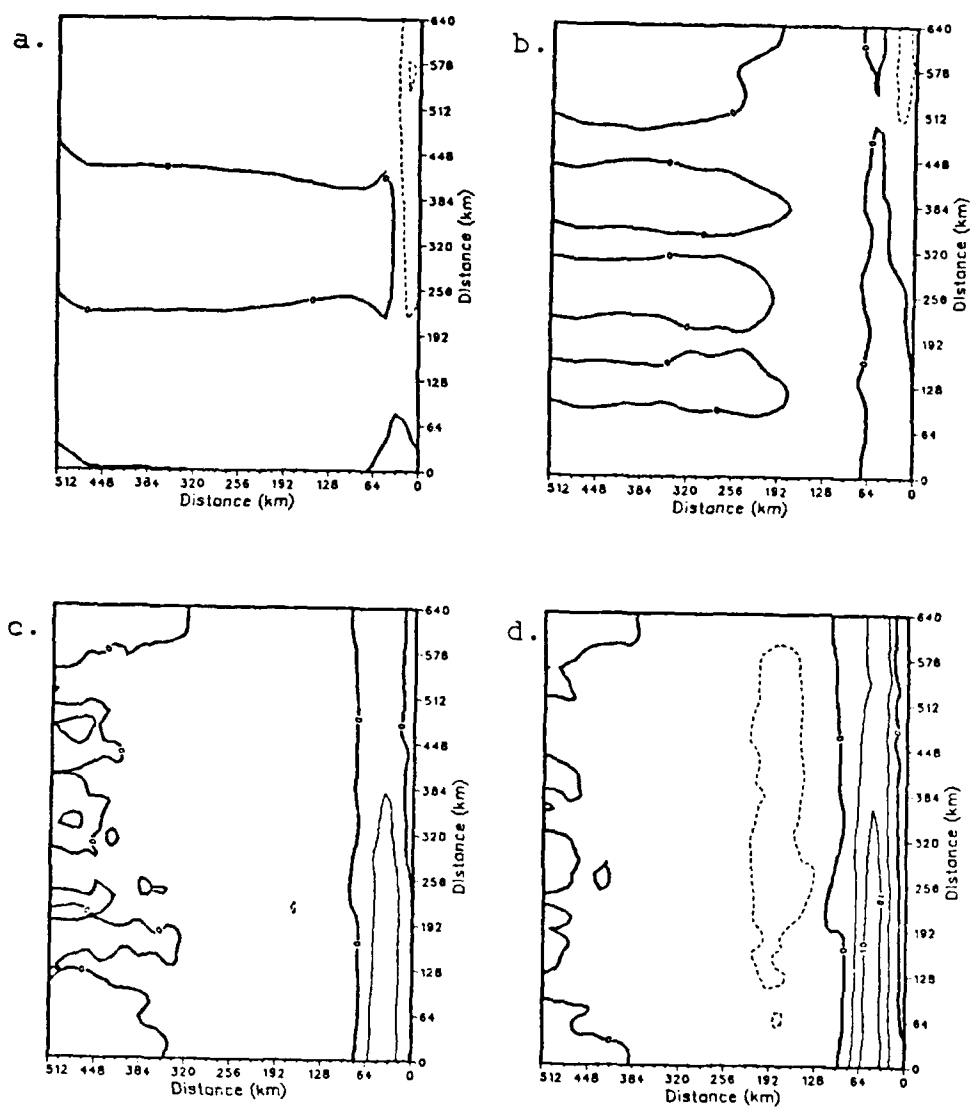
Figure 3.22   Surface contours of meridional (v) velocity
               (cm/sec) for experiment 5 at (a) day 10, (b)
               day 30, (c) day 60 and (d) day 90. Contour
               interval is 5.0 cm/sec. Dashed contours
               denote southward velocities.
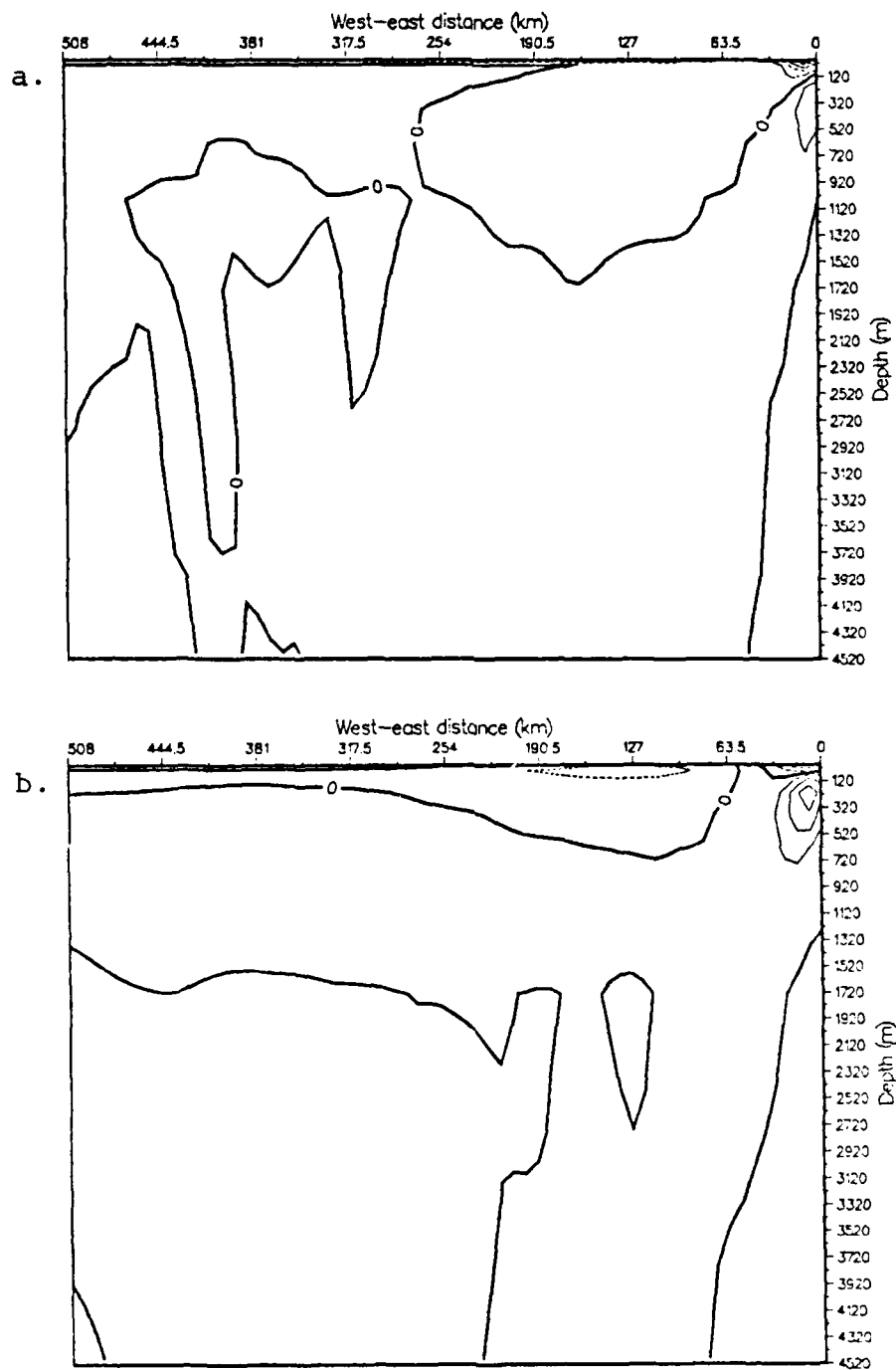
Figure 3.23   Vertical cross-shore sections of meridional
               (v) velocity (cm/sec) for experiment 5 at (a)
               day 10 and (b) day 30. Contour interval is
               2.0 cm/sec. Dashed contours denote southward
               velocities. The vertical cross-section is
               taken at y = 550 km.
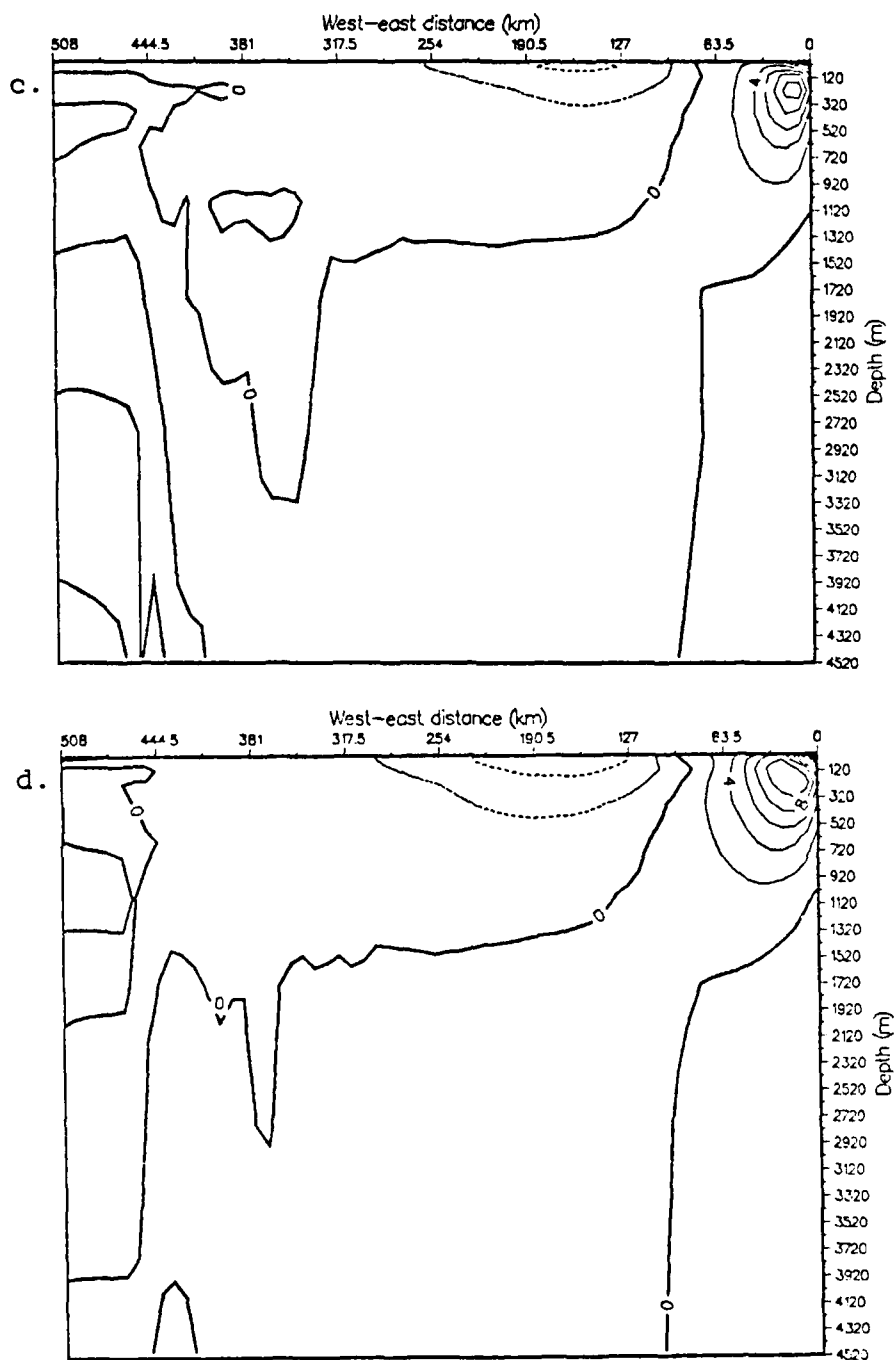
Figure 3.23 (continued) Vertical cross-shore sections of meridional (v) velocity (cm/sec) for experiment 5 at (c) day 60 and (d) day 90.

67

The offshore side of this current also had a much weaker vertical shear than that of experiment 2; however, unlike experiment 2, due to the presence of the coastal jet, eddies were generated.

This experiment showed that, due to the presence of the curl, both the Davidson Current and an equatorward flow more than 100 km offshore can develop, as in experiment 2. Due to the inclusion of the β-plane rather than the f-plane (as in experiment 2), a coastal jet inshore of the Davidson Current also develops, and within this jet, eddies are generated. Due to the Beta effect, eddies develop further north than in experiment 1, and, as expected, Rossby waves propagate offshore as a packet, with longer waves followed by shorter waves. This experiment, because of the inclusion of both wind stress curl and the β-plane, should be more representative of observations in the CCS. than in the other experiments.

3. **Experiment 6 (Wind with Y-Variation in Wind Stress)**

This experiment used the same forcing parameters as experiment 3, but used a β-plane rather than an f-plane. In general, the results (Figures 3.24, 3.25) were similar to experiment 3; however, with the β-plane, eddies, as seen in the zonal velocity fields at day 50 (Figure 3.24) developed ~20-25 km farther north, as expected. The surface coastal jet, seen in Figure 3.25, had a maximum core velocity of ~15 cm/sec and was centered offshore ~32 km in the north and ~64 km in the central part of the model domain. The maximum offshore extent of the surface jet was ~16 km farther offshore than in experiment 3. The vertical cross-shore section of meridional velocity (Figure 3.26) showed the time progression of both the coastal jet and the poleward
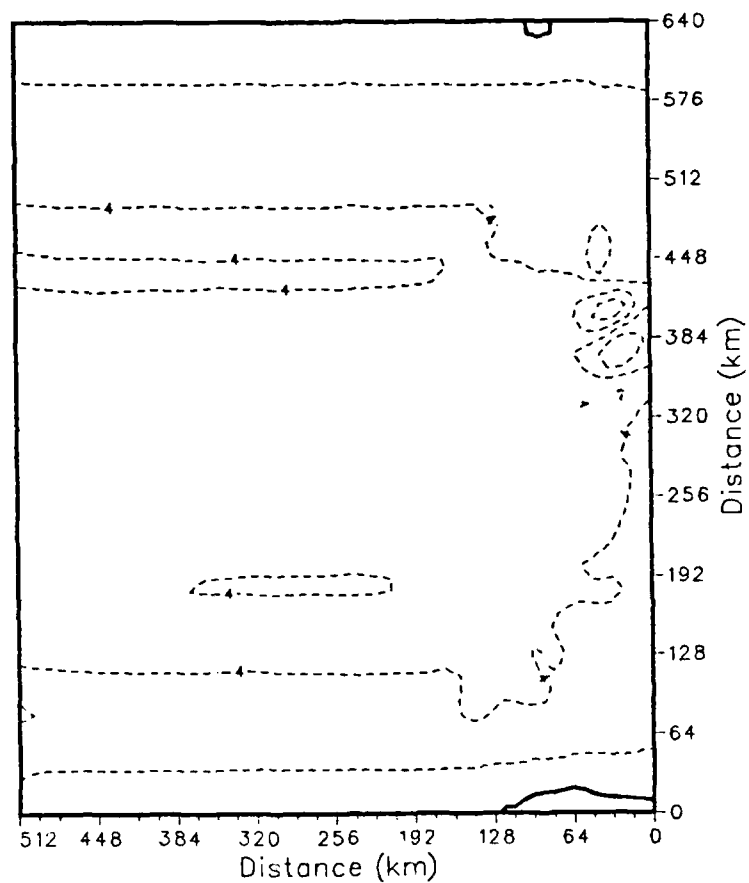
Figure 3.24   Surface contours of zonal (u) velocity
(cm/sec) for experiment 6 at day 50. Contour
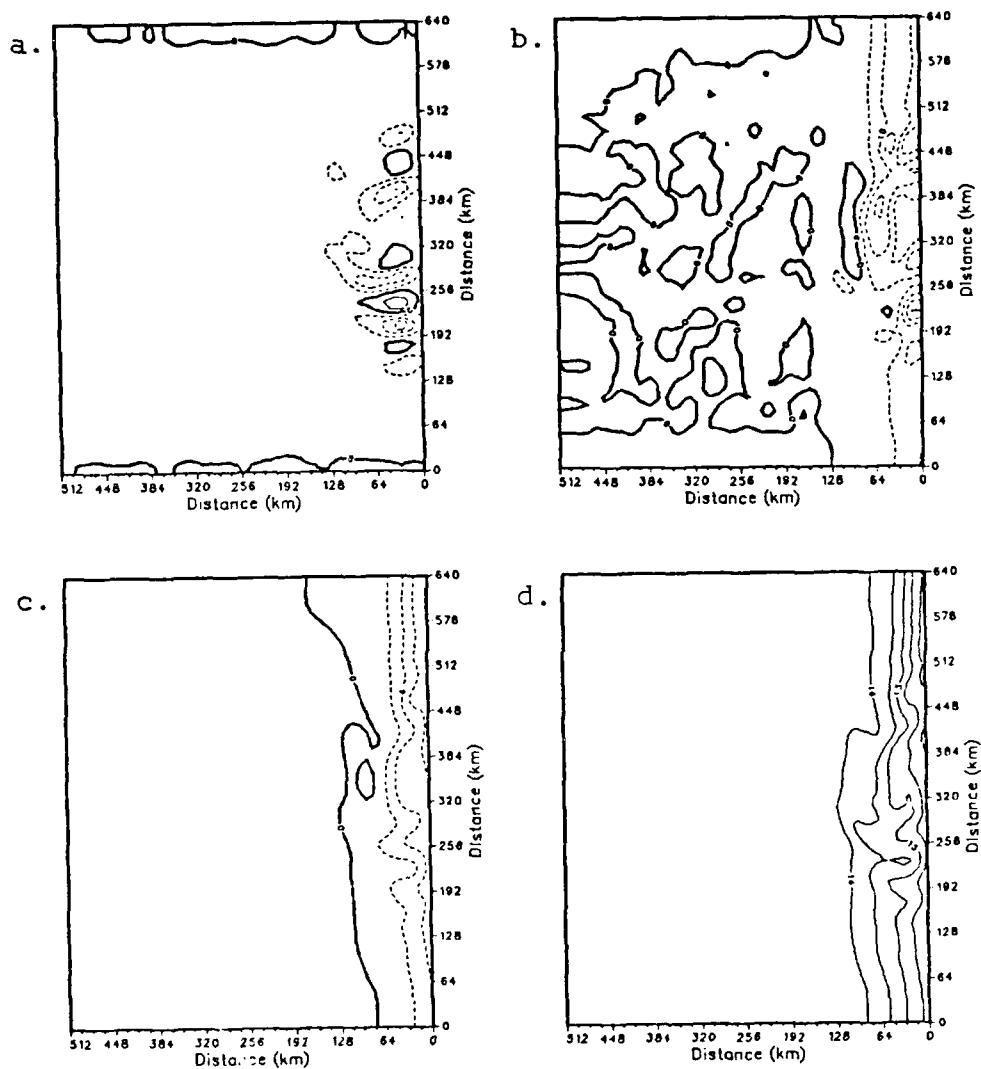interval is 2.0 cm/sec. Dashed contours
denote westward velocities.
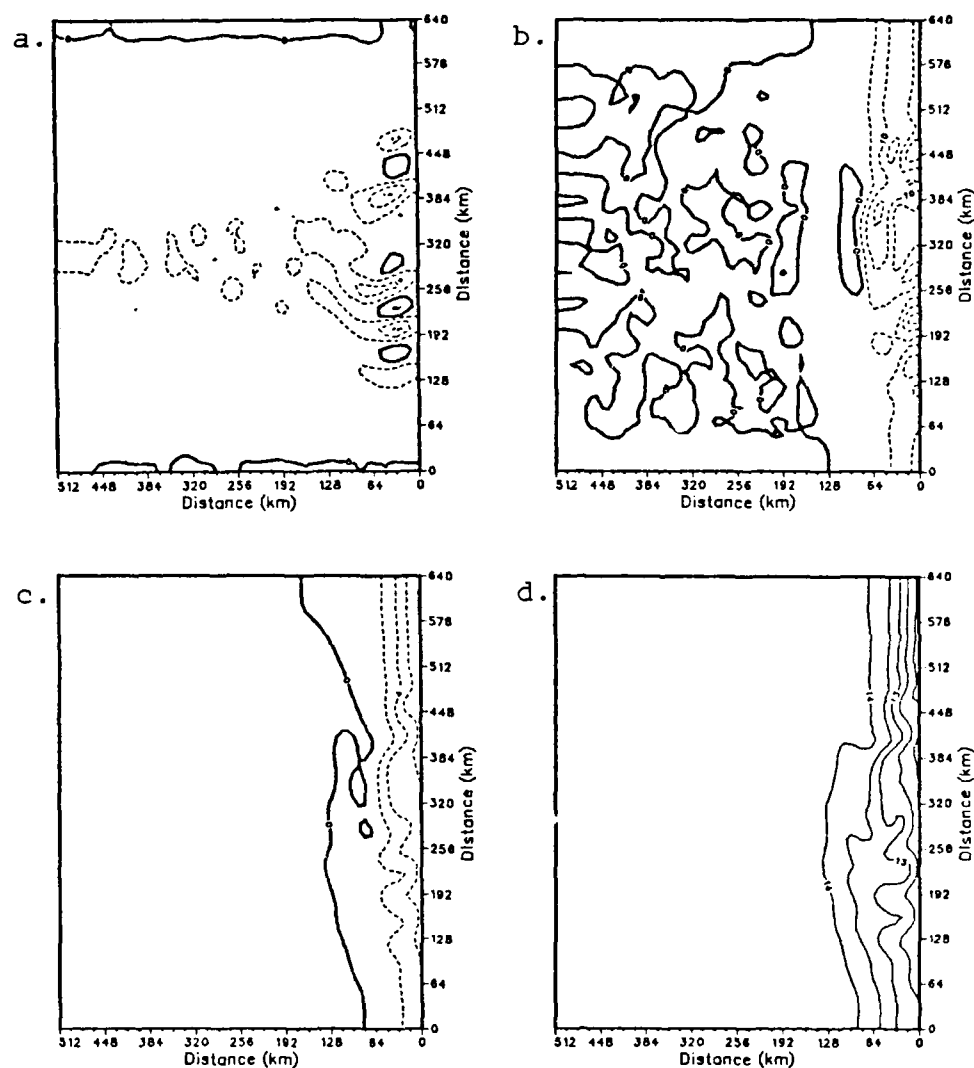
Figure 3.25   Surface contours of (a) zonal (u) velocity
(cm/sec), (b) meridional (v) velocity (cm/sec),
(c) dynamic height (cm) and (d) temperature (°C)
for experiment 6 at day 90. Contour interval for
(a) and (b) is 5.0 cm/sec. Contour interval for
(c) is 2.0 cm and (d) is 0.5°C. Dashed contours
denote westward velocities in (a), southward
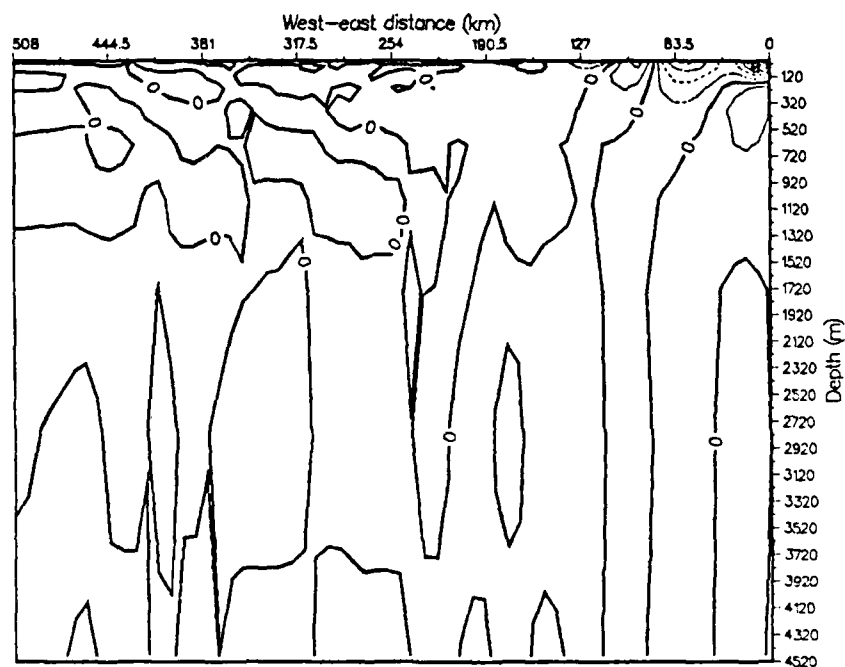velocities in (b) and negative values in (c).

70
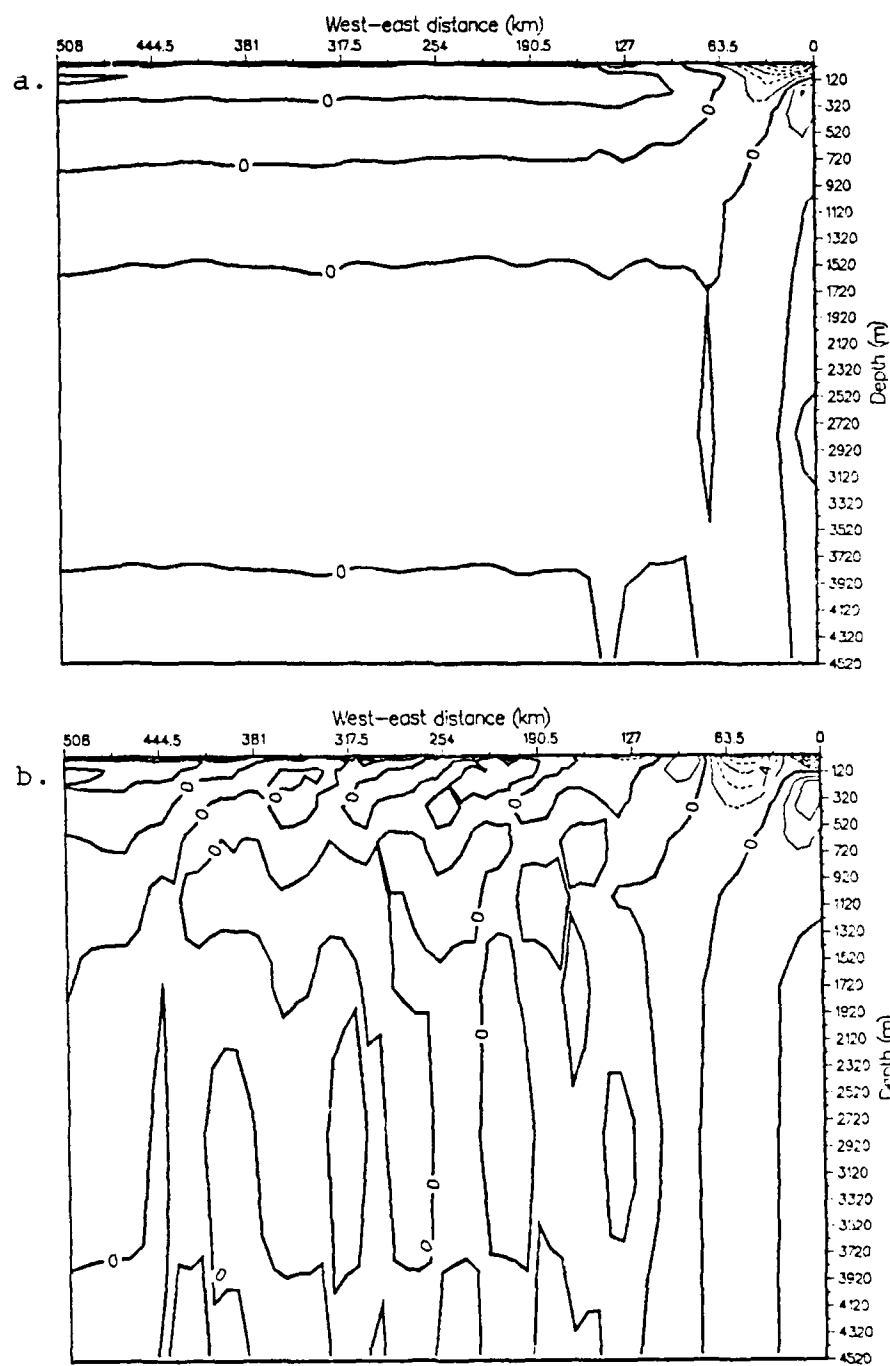
Figure 3.26   Vertical cross-shore sections of meridional (v)
                velocity (cm/sec) for experiment 6 at (a) day 45
                and (b) day 90.   Contour interval is 2.0 cm/sec.
                Dashed contours denote southward velocities.   The
                vertical cross-section was taken at y = 200.

71

undercurrent. Both currents were weaker than their counterparts in experiments 1 and 3. The core of the undercurrent was also deeper and farther offshore than in the other experiments, consistent with the β effect.

This experiment showed that both the Beta effect and the variation in alongshore wind stress can play key roles in the location of the eddy development region. When the variation in alongshore wind stress is included, eddies are generated in the localized area of maximum alongshore wind stress, which here is south of Cape Mendocino. With the addition of the Beta effect, eddies are also generated north of this area.

C. STABILITY ANALYSIS

Emery and Mysak (1980) and Thompson (1984) provided support for baroclinic instability as an important generation mechanism for eddies off Vancouver Island. Ikeda and Emery (1984) used satellite imagery off Oregon and Northern California to show the growth of coastline, cape-initiated, current meanders as a result of baroclinic instability of the surface coastal jet and California undercurrent. These meanders developed, moved offshore, were cutoff and eventually became pairs of isolated eddies or "vortex pairs" (Bernstein et al.. 1977). Mooers and Robinson (1984) showed that an intense offshore quasigeostrophic jet was often located between these cyclonic eddy-anticyclonic eddy pairs that entrained cold, upwelled water and rapidly (50 cm/sec) advected it hundreds of kilometers offshore.

Evidence for both barotropic and baroclinic processes as important generation mechanisms for eddies was provided by Thompson (1984), who

77

showed that the contribution of both instabilities was required for the generation of a cyclonic eddy off Vancouver Island. Batteen (1988a) used a simulated CCS surface coastal jet and undercurrent and showed that the generation of complex eddy and jet patterns could be attributed to the baroclinic instability created by the vertical shear between the two currents.

Despite these investigations, the dynamical reasons for the generation of the complex eddy and jet patterns of the CCS is not completely understood, and so will be examined here. First, we examine the necessary conditions to determine the potential for the flow field to become unstable and develop eddies and jets. It is known that a necessary condition for barotropic instability on an f-plane is a sign change in the velocity profile curvature (Haltiner and Williams, 1980). Since, in all the experiments of this study, a *maximum velocity core was located offshore*, either due to the equatorward, surface coastal jet or the poleward undercurrent (that surfaced in experiments 2 and 5), the necessary condition for barotropic instability to occur was satisfied.

In addition to barotropic instability, baroclinic instability could also be significant due to the available energy from the vertical shear of the coastal jet and undercurrent. Watts (1983) examined the distributions of potential vorticity in the Gulf Stream as a signature of baroclinic instability. The cross-stream distribution of potential vorticity, which is a conservative quantity (Watts, 1983), was used to evaluate the necessary conditions for instability associated with quasigeostrophic theory. Gill (1982)

stated that without these necessary conditions, the required available energy would not be released so that instability would not develop. A necessary condition for baroclinic instability to occur is that the cross-stream derivative of potential vorticity must change sign somewhere within the domain. In addition, the product of the cross-stream derivative and the basic current are required to be positive. Finally, the coastal jet must meet the requirement for linearization of a basic state current that is slowly changing in space and time (Robinson, 1983); this requirement is met by the structure of the coastal jet in this study.

Watts (1983) examined the potential vorticity (q) signature in the Gulf Stream using the following expression, in cartesian coordinates:

$$q \sim (f + \zeta) \frac{\partial T}{\partial z} - \frac{\partial T}{\partial x} \frac{\partial v}{\partial z} \qquad (3-3)$$

where

$$\zeta = \frac{\partial v}{\partial x} - \frac{\partial u}{\partial y} \qquad (3-4)$$

Following Watts, we similarly studied the coastal jet to determine its potential for instability. A cross-section plot of time-averaged (days 30-40) and meridionally averaged potential vorticity (Figure 3.27) for experiment 1 showed the tendency for potential vorticity to be uniform along isothermal surfaces and to change vertically, consistent with the offshore temperature stratification. The time-average of days 30-40 was chosen because it was the period during which the instability occurred. The range of the potential vorticity was between 0.0-2.2×10^6 °C m^{-1} s^{-1} offshore of the coastal jet. A relative minimum existed in the surface layer of the offshore region
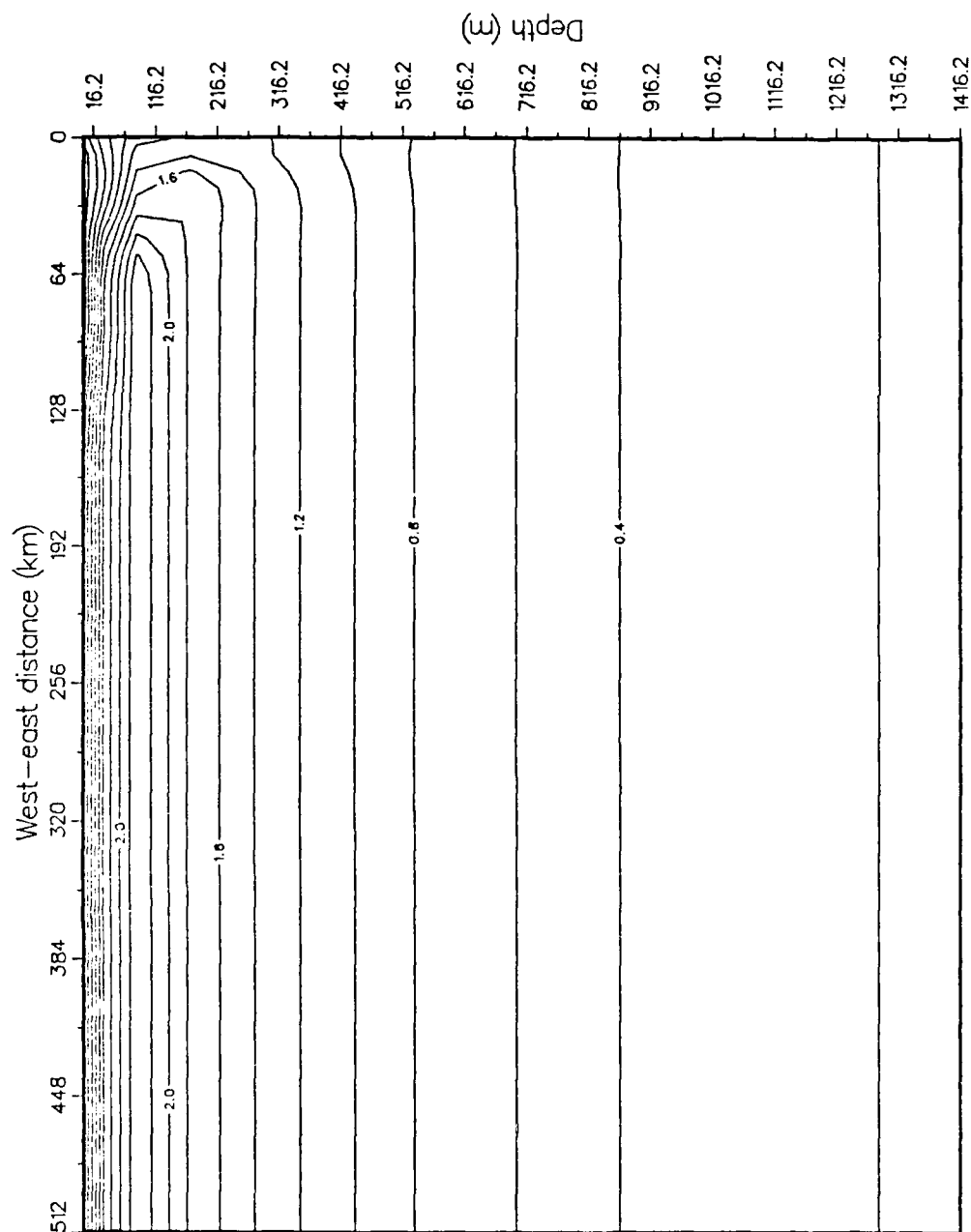
Figure 3.27   Vertical cross-section of potential vorticity
($°C \ m^{-1} \ s^{-1}$) for the time-averaged days 30-40 of
experiment 1, scaled by 10^6. Contour interval is
0.2 $°C \ m^{-1} \ s^{-1}$. The vertical cross-section was
taken at $y = 290$ km.

due to weak stratification from turbulent vertical mixing. Strong upwelling in the nearshore region caused weak stratification and deeper minimum values. A relative maximum of potential vorticity was located at a depth of ~100 m, greater than 63 km offshore, which corresponded to the "seasonal" thermocline in the model. (All experiments in this study, where instability occurred, showed similar potential vorticity results, and so will not be shown here).

The cross-stream derivative of potential vorticity was plotted (Figure 3.28) to examine the necessary condition for baroclinic instability that the cross-stream derivative of potential vorticity must change sign somewhere in the domain. The plot was obtained by first calculating the horizontal gradient $(\partial q/\partial x)$ and then multiplying by one grid length (Δx) for scaling purposes. From Figure 3.28, it is obvious that the cross-stream derivative meets the necessary condition (of a sign change) for instability in the vicinity of the coastal jet and undercurrent.

Renaud's (1986) potential vorticity analysis had similar results as this study; however, even with both barotropic and baroclinic necessary conditions met, his experiments did not show any development of instability. The boundary conditions of our study, unlike Renaud (1986), used a band of wind forcing in the middle of the domain, as described in Section II.B.3, which was important in the generation of a more realistic coastal jet and undercurrent, which resulted in the generation of mesoscale eddies and jets.

Following Renaud (1986), a simple baroclinic instability model (Holton, 1979) was used to examine the sufficient conditions for
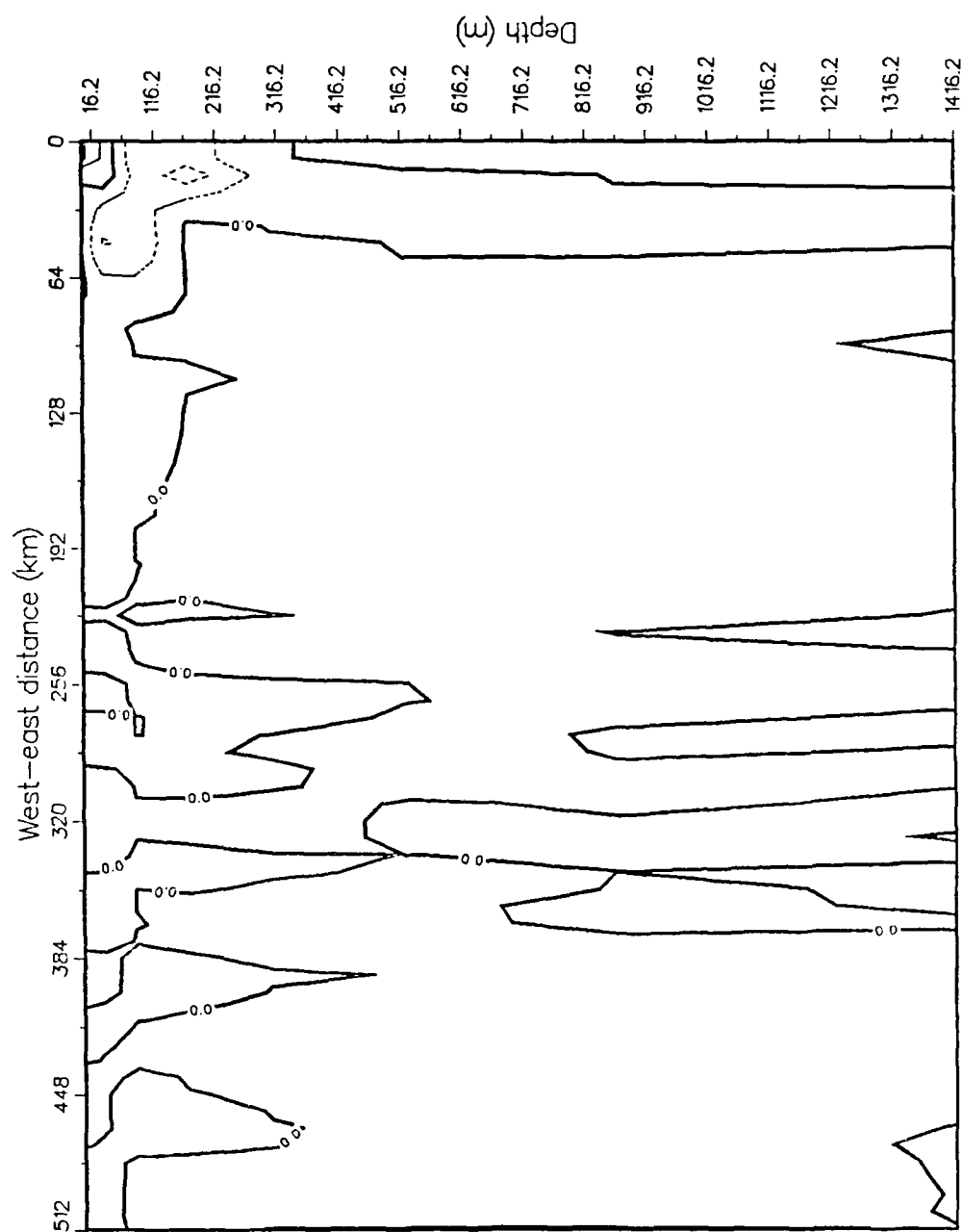
Figure 3.28   Vertical cross-section of the cross-stream
derivative of potential vorticity ($°C\ m^{-1}\ s^{-1}$) for
the time-averaged days 30-40 of experiment 1,
scaled by 10^6. Contour interval is $0.1\ °C\ m^{-1}\ s^{-1}$.
Dashed contours denote negative values. The
vertical cross-section was taken at $y = 290$ km.

77

baroclinic instability. The ocean was divided into two discrete layers. The upper layer extended from the surface to 150 m, which coincided with the bottom of the coastal jet, while the lower layer extended from 150 m to 300 m, basically to the maximum velocity core of the poleward undercurrent. The arrangement of variables in the vertical for the two-layer baroclinic model is shown in Table 3.

TABLE 3

ARRANGEMENT OF VARIABLES IN THE VERTICAL
FOR THE TWO-LAYER BAROCLINIC MODEL

0 m	_____	$w_0=0$	_____	level 0
-75 m	- - - - - - - - - - - - - -	ψ_1	- - - - - - - - - - - - - -	level 1
-150 m	_____	w_2	_____	level 2
-225 m	- - - - - - - - - - - - - -	ψ_3	- - - - - - - - - - - - - -	level 3
-300 m	_____	$w_4=0$	_____	level 4

The quasigeostrophic (QG) vorticity equation was applied at levels 1 and 3, whereas the QG thermodynamic equation was applied at level 2. The streamfunction, ψ_2 was computed by linear interpolation between levels 1 and 3. This completed a closed set of prediction equations with $\beta=0$, as in experiments 1 through 3, using the PE model of this study.

The length scale used in this model was the Rossby radius of deformation (λ^{-1}) defined by:

$$\lambda^2 \equiv \frac{f_0^2}{N^2(\Delta z)^2}, \qquad (3-5)$$

where Δz was the layer thickness (150 m) and N^2 was the stability parameter defined by equation (3-2).

Following Renaud (1986), the phase speed (c) was computed by solving the closed set of QG equations, by assuming wave-type solutions, thus

$$c = V_M \pm V_T \left[\frac{k^2 - 2\lambda^2}{k^2 + 2\lambda^2}\right]^{1/2}, \qquad (3-6)$$

where the vertically averaged current (V_M) was defined as:

$$V_M \equiv \frac{V_1 + V_3}{2} \qquad (3-7)$$

and the basic state "thermal wind" (V_T) was defined as:

$$V_T \equiv \frac{V_1 + V_3}{2} \qquad (3.8)$$

For waves with meridional wavenumbers (k) that satisfied $k^2 < 2\lambda^2$, there was an imaginary component of the phase speed (C_i). Based on this criterion, the critical wavelength (L_c) was defined as follows:

$$L_c = 2^{1/2}(\pi/\lambda) . \qquad (3-9)$$

or

$$L_c = [(\Delta z)\pi(2N^2)^{1/2}]/f_0 . \qquad (3-10)$$

For the experiments on an f-plane ($\beta=0$), the criteria for instability did not depend on the magnitude of the basic state "thermal wind" (V_T); therefore all wavelengths longer than L_c with even the slightest vertical shear were unstable.

Any wave that was longer than this critical wavelength amplified at the growth rate (δ) where:

$$\delta = k c_i . \qquad (3-11)$$

73

The growth rate (δ) depended on V_T and N^2, was a function of the meridional wavenumber (k) and was a maximum at an intermediate wavenumber ($0<k^2<2\lambda^2$). The e-folding growth time was computed by the inverse of δ.

Batten et al. (1988) investigated the generation of eddies by baroclinic instability due to an imposed initial baroclinic jet, that represented the mean CCS during the upwelling season. A comparison of this unstable jet (BCJET) was made with experiment 1 to determine the similarities or differences with a known baroclinic instability example. For the established unstable jet, computations were made using the time - (days 1-10), zonal - (within 64 km of the coast) and meridional - averaged data for two layers (0-250 m and 250-500 m). The same procedure was used for experiment one; however we time-averaged for days 1-10 (the initial establishment of the coastal jet overlying the poleward undercurrent) and days 30-40 (the period immediately preceding the generation of eddies). Additionally, since the mean currents were shallower and did not extend as far offshore, we used the two layers described earlier of 0-150 m and 150-300 m and varied the zonally averaged data to correspond to the offshore extent of the mean currents (~8-16 km). The ten-day averaged data was then input to the two layer baroclinic model to determine the baroclinicity of the flat bottom, f-plane experiments with a coastal jet and undercurrent.

Table 4 shows the internal Rossby radius of deformation (λ^{-1}), the critical wavelength (L_C), the basic state "thermal wind" (V_T) and the most unstable wavelength (L_M) with its associated e-folding time (δ^{-1})

for the unstable jet and experiment 1. A comparison of the wind forcing results with that of the unstable jet in Table 1 show that the results are comparable. The short e-folding times show that once this unstable state has been reached, eddy development should occur after about a week of model integration.

The results of experiment 1 were as expected from Table 1: that is, as the vertical shear increased with time due to the developing coastal jet and undercurrent, the shorter waves became the more unstable waves with shorter e-folding times. However, it should be noted that these e-folding times are only an approximation to the actual baroclinic growth rates since a simple two-layer baroclinic model was used for the computations.

TABLE 4

TWO-LAYER BAROCLINIC MODEL RESULTS

exp.(days)	λ^{-1}(km)	L_c(km)	V_T(cm/s)	L_m(km)	δ^{-1}(days)
BCJET(1-10)	9.60	42.7	9.3	67.7	2.05
1(1-10)	7.12	31.6	3.0	51.6	4.70
1(30-40)	6.50	28.9	3.7	43.9	3.45

The baroclinic instability growth rate of the unstable jet is shown in Figure 3.29 as a function of meridional wavelength ($L=2\pi/K$). The shorter wavelengths had the fastest growth rate compared to the longer wavelengths; however the difference in their growth rates was not that significant. The preferred growth rate occurred at the most

unstable wavelength of ~70 km, which correlates well with Table 4.
The plot of e-folding time versus meridional wavelength (Figure 3.30)
for experiment 1 of the wind forcing results showed the time
progression of the e-folding rates with the development of the coastal
jet and undercurrent. The large difference between days 1-10 and days
11-20 was due to the time for the wind field to initially set up the
mean current features (instead of being imposed in the model as in
Batteen et al., 1988). At the shorter wavelengths (below ~80 km) the
e-folding times are similar for the days 11-50, with the most unstable
wavelength of ~45 km corresponding to a growth time of ~3.5 days. The
longer wavelength shows a small growth time difference for the
specific time periods due to the aperiodic increase and decrease of
the two mean currents relative to each other as they develop both in
depth and offshore extent.

Following Renaud (1986) and Batteen et al. (1988). the damping
(e-folding) times caused by model heat and momentum diffusion was also
examined to see how they compared with the e-folding times from the
stability analysis of the mean flow. If the damping time was of the
same order as the growth rate of the unstable wave, instability of the
mean flow could be inhibited.

Both biharmonic heat and momentum, as described in Section II.A.6.
were used in the PE model. Following Holland and Batteen (1986). the
QG baroclinic mode vorticity and thermal equation had the form:

$$(\nabla^2 - \lambda^2)\psi_t = \ldots - A \nabla^6 \psi + \lambda^2 B \nabla^4 \psi. \tag{3-11}$$
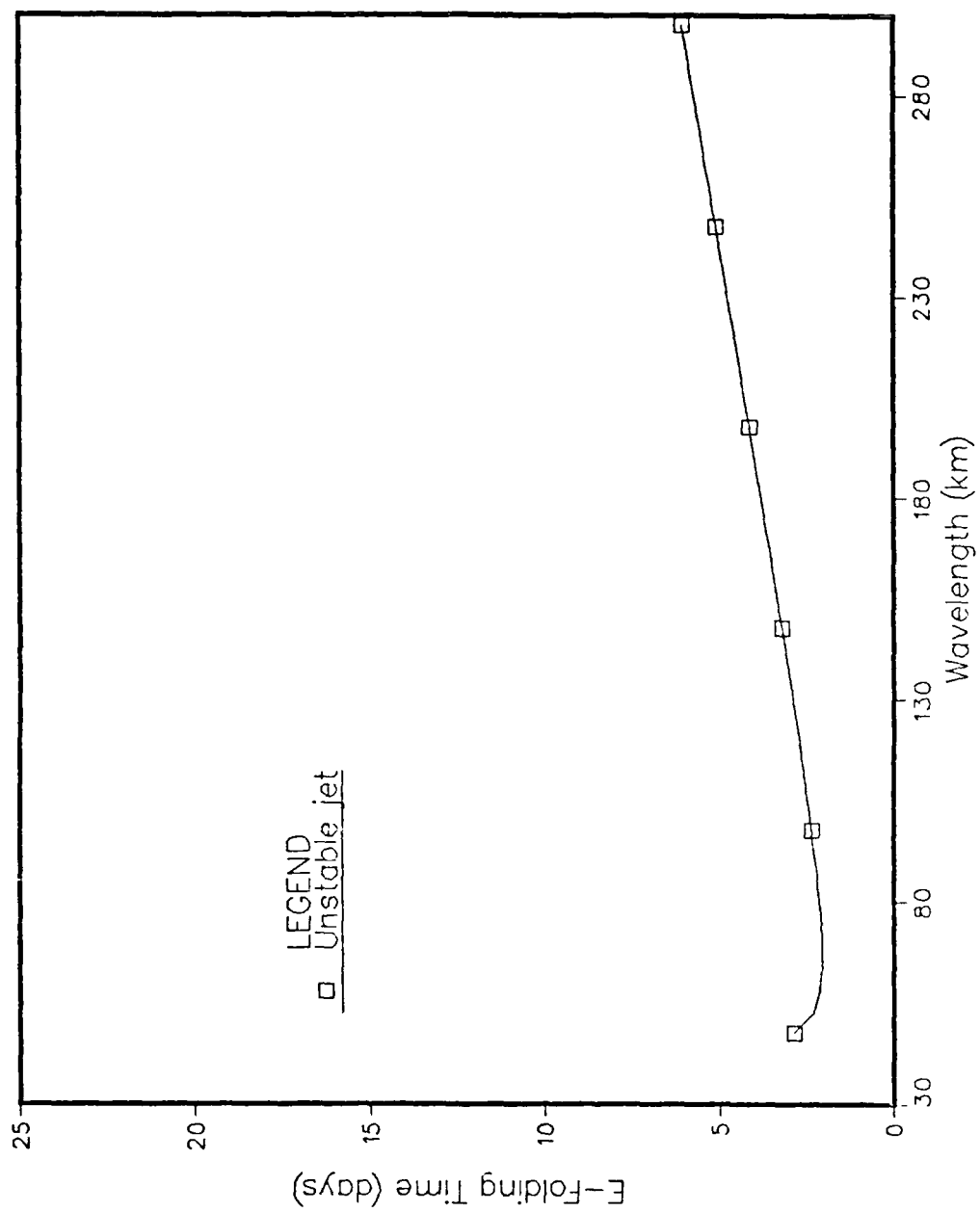
Figure 3.29   Baroclinic instability growth rate for the
unstable jet (from Batteen et al., 1988).
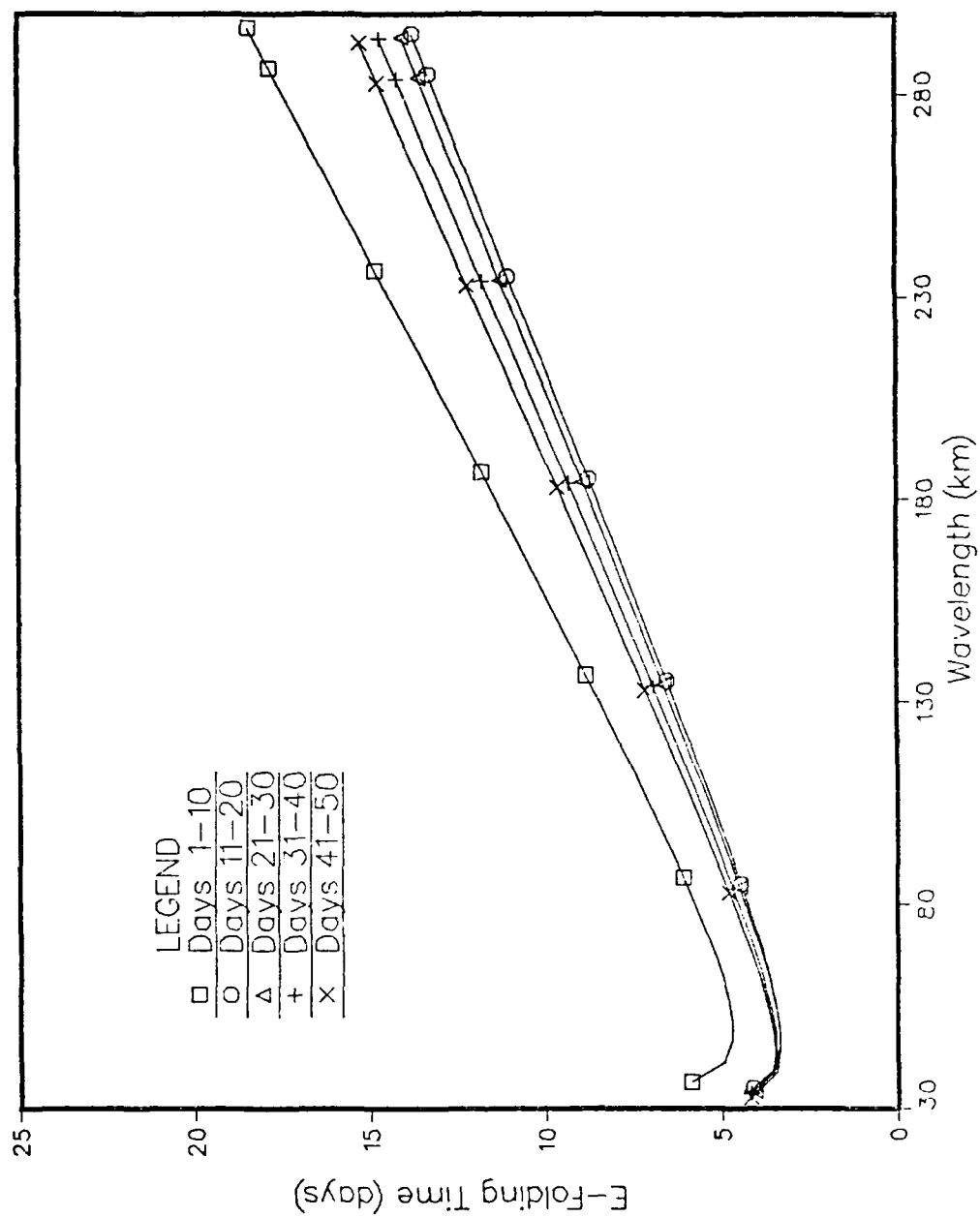
Figure 3.30   Baroclinic instability growth rate for time-averaged periods of experiment 1.

where ψ was QG "temperature" ($\psi_1 - \psi_3$ in two layer model). A was biharmonic eddy viscosity. B was biharmonic eddy diffusion. λ was inverse Rossby radius and only the damping terms were kept in eqn. (3-10).

Assuming wave numbers (k, ℓ), (3-10) became:

$$\psi_t = -\left[\frac{A(k^2 + \ell^2)^3 + \lambda^2 B(k^2 + \ell^2)^2}{k^2 + \ell^2 + \lambda^2}\right] \psi, \qquad (3-11)$$

or $\qquad \psi_t = \psi_0 e^{-\gamma t}.$ $\qquad\qquad\qquad\qquad (3-12)$

Therefore the e-folding (damping) time of baroclinic modes was:

$$\gamma^{-1} = \frac{(k^2 + \ell^2 + \lambda^2)}{A(k^2 + \ell^2)^3 + \lambda^2 B(k^2 + \ell^2)^2} \qquad (3-13)$$

The damping rates (γ^{-1}) and time scales γ for various wavelengths using values of A=B=2×10^{17} cm^4/sec. as in the PE model are shown in Table 5. The choice of values A and B are consistent with considerations given by Semtne and Mintz (1977). who found that. by using a biharmonic operator. an optimum value to use can be selected which will both control computational noise and reduce the diffusion of mesoscale features. i.e.. unrealistic damping will be reduced. except for features which are poorly resolved while the advective effects of large-scale features will be enhanced. They used the following equation to obtain damping of the smallest resolvable wave in either coordinate system (e.g.. when k=$\pi/\Delta x$ and ℓ=0):

$$B = \frac{1}{4} A (\Delta x)^2. \qquad (3-14)$$

where B was the biharmonic diffusion. A was the Laplacian diffusion and Δx was the grid length. Investigation of the Reynolds number

yielded the results that A cannot be less than 1×10^6 cm^2/sec or the Reynolds number will be too large and unable to successfully damp vorticity on a grid scale of 20 km ($2\Delta x$). This value of A produces e-folding damping times that are too short (Table 5) for observing the generation of reasonable sized mesoscale features.

From Table 5, the damping time scale of ~22 days correlated with the wavelength (~70 km) of the most unstable wave in the imposed baroclinic jet case of Batteen et al. (1988); however, the baroclinic growth rate of 2.05 days for the equivalent wavelength was much shorter. As a result, the diffusive damping should not have suppressed any development of instability. Similar results were observed for the longer wavelengths with much shorter e-folding times due to baroclinic instability than diffusive damping times.

Experiment 1 showed different results. We used the biharmonic heat and diffusion to damp the smaller scale "noise" that may have masked the larger scale eddies we wanted to observe: however, in this case the biharmonic damping may have inhibited the rapid, baroclinic growth of more intense eddies. The most unstable wavelength of time-averaged days 1-10 for experiment 1 was ~50 km with an associated baroclinic instability growth rate of ~4.7 days. This is close to the biharmonic damping time scale of 5.8 days. The wavelength of ~44 km for the time-averaged days 30-40 is even more significant with a growth rate of ~3.45 days versus the damping rate of ~3.5 days.

Comparing the baroclinic instability growth rates (Figures 3.29 and 3.30) and the damping rates (Table 5), we can conclude some interesting points about using biharmonic diffusion. In the case of

TABLE 5

DAMPING RATES FOR VARIOUS WAVELENGTHS

L(km)	PE MODEL γ (days^{-1})	PE MODEL γ^{-1} (days)	BIHARMONIC $(1 \times 10^{17} cm^4/sec)$ γ^{-1} (days)	LAPLACIAN $(1 \times 10^6 cm^2/sec)$ γ^{-1} (days)
10	1.11×10^2	.009	.02	.15
20	0.67×10^1	.15	.30	.58
30	1.33×10^0	.75	1.5	1.3
40	4.17×10^{-1}	2.4	4.7	2.4
50	1.72×10^{-1}	5.8	12	3.7
60	8.33×10^{-2}	12	24	5.3
70	4.55×10^{-2}	22	45	7.2
80	2.63×10^{-2}	38	76	9.7
90	1.64×10^{-2}	61	122	12
100	1.08×10^{-2}	93	185	15
200	6.76×10^{-4}	1480	2960	58

the unstable jet, the biharmonic diffusion damped out all developing waves ~50 km or less. Experiment 1 also had all developing waves 50 km or less damped. This, unlike Batteen et al. (1988), even included the most unstable wavelengths (~40 km). With the shorter wavelengths damped out or growth inhibited, only the longer waves (~100 km) with relatively much longer damping times will be observed. In addition, the time when they actually are observed are even longer than the e-folding baroclinic growth time due to the required model "spin-up" involved in the development of the mean currents.

Unlike Laplacian diffusion, which can damp all wavelengths considerably as noted by Holland (1978), biharmonic diffusion should damp the shorter wavelengths (of 10-30 km) in a short amount of time and the longer wavelengths (longer than 40 km) in a longer period of time. As a result, ocean models with very fine horizontal resolution will probably have shorter wavelength unstable waves damped. Thus even with biharmonic diffusion, there is a trade-off between resolution, damping times and wavelengths, and for very fine resolution (due to the short damping times) biharmonic damping may cause shorter wavelengths which are resolvable to be damped.

Experiment 3, which included the wind with y-variation in wind stress on an f-plane, had similar stability results as in experiment 1 due to the interaction of the coastal jet and undercurrent. Experiment 2 with wind stress curl incorporated did not go baroclinically unstable due to the lack of a developed coastal jet, which as showed by Batteen et al. (1988), was necessary for baroclinic instability to occur. A strong poleward undercurrent was generated

that eventually reached the surface; however, the vertical shear associated with baroclinic instability was not present so that no eddies occurred. The results of experiment 2 paralleled the results of Renaud (1986), who generated a similar, internal, poleward current that likewise did not develop any instability (despite satisfying the necessary conditions for both barotropic and baroclinic instability).

The last experiments (4, 5 and 6) were all conducted on a β-plane. Holton (1979), based on a zonal flow analysis, investigated the effect of β on the flow. He found that the Beta effect strongly stabilizes the long wavelengths and, as expected, the flow was always stable for wavelengths shorter than the critical wavelength, L_c. The long wave stabilization that was associated with the Beta effect, was a result of the rapid westward propagation of packets of long Rossby waves.

Olivier (1987) demonstrated that there is a difference in flow behavior between a non-zonal and zonal flow. He found that for a meridional flow, as in this study (representative of the CCS), energy can be released without any component of β acting on it; therefore any shear above the dissipation level may produce instability.

Basic instability did occur in the β-plane experiments 4, 5 and 6, which each had a coastal jet overlying a poleward undercurrent with the subsequent development of eddies and jets. These and the previous experiments provide evidence that the generation of complex eddy and jet patterns could be attributed to the instability created by the shear between the coastal jet and the poleward undercurrent.

IV. COMPARISON OF MODEL RESULTS WITH OBSERVATIONS

A. BRIEF BACKGROUND ON THE CCS

Huyer (1983) described the classical features of the CCS as consisting of a baroclinic alongshore coastal upwelling jet with the strongest equatorward velocities at the surface over the midshelf or outer shelf and a poleward undercurrent over the shelf break. Kosro (1986), Kosro (1987), Huyer and Kosro (1987) and Lynn and Simpson (1987), however, found that the instantaneous near-surface currents often deviated substantially from the time-averaged, classical currents. In particular, Kosro (1987) examined synoptic maps of the coastal current field off Northern California during CODE (Coastal Ocean Dynamics Experiment) and found a qualitative correlation between complex temperature patterns in satellite imagery and intense current structures such as squirts, eddies and jets. Davis (1985) investigated CODE drifter buoy results and concluded that it was difficult to think of the California coastal circulation as a simple wind-driven alongshore current with cross-shelf Ekman-driven circulation; instead, he found that various mesoscale motions could be primary features for cross-shelf transport. Other observations have shown that highly energetic, mesoscale eddies and meandering jets can be superimposed on the broad, slow climatological mean flow in the CCS (Bernstein et al., 1977; Mooers and Robinson, 1984; Rienecker et al., 1985, 1988). The location of these features from shore and their

intensity can also vary greatly, depending on the author and location of the observation along the west coast of the United States.

B. COMPARISONS

A comparison of model results with available observations was carried out to see if both time-averaged and instantaneous model simulations of the coastal jet, undercurrent and eddies were consistent with available observational data. The time-averaged (over days 30 to 40) comparisons, prior to the generation of eddies, are shown in Table 6, while the instantaneous comparisons to highlight specific characteristics of the currents and eddies are shown in Table 7. The observations used in both Tables 6 and 7 are from Huyer and Kosro (1987), denoted by HK in column 1. Table 6 also includes the seasonal observations from Ikeda and Emery (1984), denoted by IE in column 2. The time-averaged results of Huyer and Kosro (1987) was obtained from a set of synoptic data during CODE that included both strong wind events and relaxations. These observations may or may not be representative of mean climatological conditions in the CCS, therefore the comparison between the observed model results (using climatological winds) and these time-averaged CCS observations can be different. In this study the wind forcing was steady with either an offshore or alongshore variation to systematically investigate forcing of the model, however the actual ocean regime is subject to both the offshore and alongshore variation and could produce CCS currents with slightly different characteristics. The letter designations used in the tables have the following meanings:

91

A. Maximum coastal jet velocity (cms^{-1})

B. Offshore location of coastal jet (km)

C. Offshore extent of coastal jet (km)

D. Depth of inshore coastal jet (m)

E. Maximum vertical shear of coastal jet ($\times 10^{-3}$ s^{-1})

F. Maximum undercurrent velocity (cms^{-1})

G. Offshore location of undercurrent axis (km)

H. Width of undercurrent (km)

I. Depth of undercurrent axis (m)

J. Maximum zonal eddy diameter (km)

K. Maximum zonal eddy velocity (cms^{-1}).

Most of the time-averaged model results of experiment 1 (wind stress without curl and on an f-plane), as shown in Table 6, compare quite favorably with CCS observations. The only discrepancies are the following. The coastal jet is slightly deeper and weaker than the observations, and the poleward undercurrent velocity is ~10 cm/sec weaker with its axis location ~10 km closer to shore.

The utilization of a flat-bottom in the model for all experiments versus a topography including a shelf and slope could have affected these model results. McCreary et al. (1987) found that the presence of a shelf tends to strengthen the coastal jet and weaken the undercurrent. In addition, transient rather than steady wind forcing could result in a more realistic undercurrent (McCreary, 1987). Moreover, our value for the average alongshore wind stress for experiment 1, using data from Nelson (1977) was ~1 dyne/cm^2, which was ~33% lower than the calculated values used by Huyer and Kosro (1987).

TABLE 6

TIME-AVERAGED COMPARISON OF MODEL EXPERIMENTS (EXP.) WITH OBSERVATIONS (OBS.) OF THE CCS

	OBS. (HK)	OBS. (IE)	EXP. 1	EXP. 3	EXP. 4	EXP. 6
A.	15	20	14	14	12	12
B.	15-30	-	20-25	20-25	20-25	20-25
C.	>40	-	70	60	60	75
D.	90	150	150	150	130	140
E.	<2.5	-	.9	.9	.9	.9
F.	5-10	15-20	2	2	4	4
G.	20-25	-	10	10	10	10
H.	10-20	-	10-20	15-20	20-25	20-25
I.	200-300	300	300	300	300	300

TABLE 7

INSTANTANEOUS COMPARISON OF MODEL EXPERIMENTS (EXP.) AT Y = 290 KM WITH OBSERVATIONS (OBS.) OF THE CCS

	OBS. (HK)	EXP. 1	EXP. 3	EXP. 4	EXP. 6
A.	30-50	20	20	15	15
B.	25	25-35	25-35	25-35	25-35
C.	>40	70	70	75	75
D.	100	150	150	140	140
E.	<2.9	.8	.8	.9	.9
F.	5-15	6	4	4	4
G.	10-40	10	5-10	5-10	10
H.	10-20	15	15	20-30	20-25
I.	200-300	300	300	300-330	300-330
J.	10-100	50	50	60	60
K.	50	15	14	15	14

This lower value for wind stress would also contribute to a weaker undercurrent than what Huyer and Kosro (1987) observed.

The instantaneous model results comparison of experiment 1, as shown in Table 6, also shows good agreement with CCS observations. Although the simulated coastal jet is still deeper and weaker compared with observations, the model poleward undercurrent is more consistent with the instantaneous observations. The largest difference between experiment 1 model results and CCS observations is in the maximum zonal eddy velocities. CCS observations show eddy velocities of ~50 cm/sec while the model shows maximum velocities of ~15 cm/sec. This disagreement could likely be attributed to the difference between the seasonal wind forcing of the model and the transient event wind forcing observed during CODE.

All of the model experiment results which did not include wind stress with curl are also shown in Tables 6 and 7. As expected, each of the experiment results compare favorably with observations, since overall the values for each comparison are consistent with those of experiment 1.

Since the wind with curl experiments, i.e., 2 and 5, did not develop prominent surface coastal jets, they were not included in Tables 6 and 7; however, experiment 5 did show evidence of a very weak (~2 cm/s) coastal jet within 5 km of the coast near the end of the model simulation time. The dominant current features of both the time-averaged and instantaneous meridional velocity fields were a surface, poleward current similar to the Davidson Current and a broad surface, equatorward flow ~100 km offshore. These results are

95

c sistent with the flat-bottomed, wind stress with curl forcing model results of McCreary et al. (1987).

Even though the model results compare favorably both with available observations (such as Huyer and Kosro, 1987) and with other model results (McCreary et al., 1987), it is difficult to establish which experiment is the best simulation of the CCS. Based on these results, probably the best simulation of the CCS would incorporate both the climatological offshore and alongshore variation of wind stress, but differences may still occur if the wind stress is assumed to be time-independent. Observations show that the coastal jet, undercurrent, eddies and Davidson Current can vary greatly both spatially and temporally. A model that can correctly simulate the CCS and its complex features would require accurate observational data, parameterizations, boundary conditions and a host of other conditions too numerous and complex for the scope of this study.

V.   SUMMARY AND RECOMMENDATIONS

A.   SUMMARY

This study used a high-resolution, multi-level PE ocean model to investigate wind forcing as a possible generation mechanism for mesoscale eddies and jets in the CCS.   A band of seasonal, steady winds, either with or without wind stress curl, and either with or without alongshore variability, was used as model forcing on either an f-plane or a β-plane in an idealized, flat-bottomed oceanic regime along an eastern ocean boundary.   In addition, a stability analysis was made to determine if both the necessary and sufficient conditions for instability processes to occur were satisfied.   The analysis showed that the necessary condition for barotropic instability and both the necessary and sufficient conditions for baroclinic instability were satisfied in some of the experiments.

The model results of experiment 1, which included wind stress without curl on an f-plane, showed the development of an equatorward coastal jet and poleward undercurrent.   Baroclinic instability due to the unstable jet and undercurrent occurred after ~40 to 45 days resulting in the generation of cyclonic and anticyclonic eddies and jets.   Similar results occurred in experiment 4, which had the same form of wind stress as in experiment 1, but used a β-plane rather than an f-plane.   Due to the Beta effect, Rossby waves propagated offshore as a packet, with longer followed by shorter waves moving westward. Due to the use of vertical mixing in the model, consistent with

McCreary et al. (1987), the Rossby waves did not advect either the coastal jet or eddies offshore.

Experiment 2, which included wind stress with curl on an f-plane, showed initially the development of a coastal jet. The implementation of a steady, positive wind stress curl near shore resulted in the generation of both a deep, broad poleward surface current near the coast, similar to the Davidson Current, and an equatorward surface flow located farther offshore. No eddies or jets developed in experiment 2 due to the lack of an unstable vertical shear between a coastal surface jet (which was replaced by the poleward undercurrent) overlying a poleward undercurrent. Experiment 5 also incorporated wind stress curl, but used a β-plane rather than an f-plane. Due to the presence of the β-plane, a coastal jet inshore of the Davidson Current developed late in the model simulation time and within this jet, eddies were generated. As expected with the Beta effect, a packet of Rossby waves propagated offshore, as in experiment 4.

The model results of experiment 3, which had a y-variation in the alongshore wind stress without curl on an f-plane, were comparable to experiment 1. The variation in alongshore wind stress played a key role in determining the location of the eddy development region. In particular, eddies were generated in the localized area of maximum alongshore wind stress just south of the Mendocino region. Experiment 6 also incorporated a y-variation in the alongshore wind stress, but used a β-plane rather than an f-plane. The fact that eddies developed further north of the localized eddy generation area of experiment 3

showed that the Beta effect can also play a key role in determining the location of eddy generation regions.

A comparison of model results with available observations showed that both time-averaged and instantaneous model simulations of the coastal jet, undercurrent and eddies were consistent with available CCS observations (e.g., Huyer and Kosro, 1987) and other model results (McCreary, et al., 1987). The instantaneous model simulations of the CCS duplicated the great variability in time and space of the observed CCS while the time-averaged, simulations showed a classical two-dimensional coastal jet.

B. RECOMMENDATIONS

The results from these experiments strongly support the hypothesis that wind forcing can be a significant generation mechanism for eddies and jets. It should be noted, however, that this study employed the constraints of a regular, straight coastline and a flat-bottom. It also made use of steady, idealized wind stress patterns. Batteen et al. (1988), using the same PE model, imposed a climatological mean coastal jet and undercurrent over an idealized Mendocino Escarpment and Ridge complex, and showed that topography can influence the characteristics of eddies. McCreary et al. (1987), found that the presence of a coastal shelf in an ocean model can strengthen the coastal jet and weaken the undercurrent. Ikeda and Emery (1984) concluded that current meanders could be triggered by alongshore variations (capes) in the coastline of California and Oregon, and grow due to baroclinic instability of the mean currents. Based on the

99

results from these studies, future studies should include both an irregular coastline and bottom topography.

In addition, different open boundary conditions as discussed by Røed and Cooper (1985), should be incorporated and tested in the model. In particular, wind forcing with both a local solution and a global solution (Røed and Smedstad, 1984) could be implemented and tested. This latter incorporation may permit the wind forcing to be applied over the _entire_ domain (even at the open boundaries), while still allowing the free propagation of waves from the boundaries through the computational domain.

Time-dependent wind forcing, such as wind events and relaxations, should also be systematically investigated to see if transient wind forcing can be an important eddy generation mechanism. McCreary _et al_. (1987) has shown that the inclusion of both annually periodic and remote winds can significantly influence the mean flow currents of the CCS. Future studies therefore should include time-dependent winds along with remote forcing.

Future experiments should also include not only the alongshore variation in wind stress, but also the offshore variation in wind stress. The recent higher resolution wind data of Bakun (1988) could be incorporated as the wind forcing and systematically investigated. This should result in even more favorable model comparisons with available CCS observations.

LIST OF REFERENCES

Anderson, D.L.T, and A.E. Gill, 1975: Spin-up of a stratified ocean with applications to upwelling. _Deep Sea Res._, _22_, 583-596.

Arakawa, A., and V.R. Lamb, 1977: Computational design of the basic dynamical processes of the UCLA general circulation model. _Methods in Computational Physics_, (J. Chang, Ed.), Academic Press, _17_, 173-265.

_____, and M.J. Suarez, 1983: Vertical differencing of the primitive equations in sigma coordinates. _J. Atmos. Sci._, _111_, 34-45.

Bakun, A., 1988: _Applications of maritime data to the study of surface forcing of seasonal and interannual ocean variability in eastern boundary regions_, Ph.D. Dissertation. Oregon State University, Corvallis, OR, 226 pp.

Batteen, M.L., 1988a: Model simulations of a coastal jet and undercurrent in the presence of eddies and jets in the California Current System. _The Springer-Verlag Lecture Note Volume_, (Submitted).

_____, 1988b: On the use of sigma coordinates in large-scale ocean circulation models. _Ocean Modelling_, _77_ (In press).

_____, and Y.-J. Han, 1981: On the computational noise of finite-difference schemes used in ocean models. _Tellus_, _33_, 387-396.

_____, R.L. Haney, and P.G. Renaud, 1988: Mean flow instability and topographic influences on eddy formations in the central California Current System. (In preparation).

Bernstein, R.L., L.C. Breaker, and R. Whritner, 1977: California Current eddy formation: ship, air and satellite results. _Science_, _195_, 353-359.

Blumberg, A.F., and G.L. Mellor, 1987: A description of a three-dimensional coastal ocean circulation model. _Three-dimensional Coastal Ocean Models_, (N. Heaps, Ed.), American Geophysical Union, _4_, 1-16.

Breaker, L.C., and C.N.K. Mooers, 1986: Oceanic variability off the central California coast. _Prog. in Oceanogr._, _17_, 61-135.

Brink, K.H., 1983: The near-surface dynamics of coastal upwelling. _Prog. in Oceanogr._, _12_, 223-257.

Bryan, K., and P. Ripa, 1978: The vertical structure of North Pacific temperature anomalies. _J. Geophys. Res._, _83_, 2419-2429.

Camerlengo, A.L., and J.J. O'Brien, 1980: Open boundary conditions in rotating fluids. _J. Comput. Physics_, _35_, 12-35.

Carton, J.A., 1984: Coastal circulation caused by an isolated storm. _J. Phys. Oceanogr._, _14_, 114-124.

_____, and S.G.H. Philander, 1984: Coastal upwelling viewed as a stochastic process. _J. Phys. Oceanogr._, _14_, 1499-1509.

Chapman, D.C., 1985: Numerical treatment of cross-shelf open boundaries in a barotropic coastal ocean model. _J. Phys. Oceanogr._, _15_, 1060-1075.

Chelton, D.B., 1984: Seasonal variability of alongshore geostrophic velocity off central California. _J. Geophys. Res._, _89_, 3473-3486.

Davis, R.E., 1985: Drifter observations of coastal surface currents during CODE: The method and descriptive view. _J. Geophys. Res._, _90_, 4741-4755.

Ekman, V.W., 1905: On the influence of the earth's rotation on ocean currents. _Arkiv for Matematik Astronomi och Fysik_. _2_. No. 11, p. 52.

Emery, W.J., and L.A. Mysak, 1980: Dynamical interpretations of satellite-sensed thermal features off Vancouver Island. _J. Phys. Oceanogr._, _10_, 961-970.

Feliks, Y., 1985: Notes and correspondence on the Rossby radius of deformation in the ocean. _J. Phys. Oceanogr._, _15_, 1605-1607.

Gill, A.E., 1982: _Atmosphere-Ocean Dynamics_. Academic Press, 662 pp.

Haltiner, G.J., and R.T. Williams, 1980: _Numerical Prediction and Dynamic Meteorology_, Second edition, John Wiley and Sons Inc., 477 pp.

Haney, R.L., 1971: Surface thermal boundary condition for ocean circulation models. _J. Phys. Oceanogr._, _1_, 241-248.

_____, 1985: Midlatitude sea surface temperature anomalies: A numerical hindcast. _J. Phys. Oceanogr._, _15_, 787-789.

_____, W.S. Shiver, and K.H. Hunt, 1978: A dynamical-numerical study of the formation and evolution of large-scale ocean anomalies. _J. Phys. Oceanogr._, _8_, 952-969.

Hickey, B.M., 1979: The California Current System - hypothesis and facts. _Prog. in Oceanogr._, _8_, 191-279.

Holland, W.R., 1978: The role of mesoscale eddies in the general circulation of the ocean-numerical experiments using a wind-driven quasi-geostrophic model. _J. Phys. Oceanogr._, _8_, 363-392.

_____, and M.L. Batteen, 1986: The parameterization of subgrid scale heat diffusion in eddy-resolved ocean circulation models. J. Phys. Oceanogr., 16, 200-206.

Holton, J.R., 1979: An Introduction to Dynamic Meteorology, 2nd edition. Academic Press, 391 pp.

Huyer, A., 1983: Coastal upwelling in the California Current System. Prog. in Oceanogr., 12, 259-284.

_____, and P.M. Kosro, 1987: Mesoscale surveys over the shelf and slope in the upwelling region near Point Arena, California. J. Geophys. Res., 92, 1655-1681.

Ikeda, M., and W.J. Emery, 1984: Satellite observations and modeling of meanders in the California Current system off Oregon and Northern California. J. Phys. Oceanogr., 14, 1434-1450.

Kosro, P.M., 1986: CTD and velocity surveys of seaward jets off Northern California, July 1981 and 1982. J. Geophys. Res., 91, 7680-7690.

_____, 1987: Structure of the coastal current field off Northern California during the Coastal Ocean Dynamics Experiment. J. Geophys. Res., 92, 1637-1654.

Lynn, R.J., and J.J. Simpson, 1987: The California Current System: the seasonal variability of its physical characteristics. J. Geophys. Res., 92, 947-966.

McCreary, J.P., Jr., 1981: A linear stratified ocean model of the coastal undercurrent. Phil. Trans. Roy. Soc., London, A 302, 385-413.

_____, 1987: A hierarchy of models of the coastal undercurrent. J. Mar. Res. (Submitted).

_____, P.K. Kundu, and S.-Y. Chao, 1987: On the dynamics of the California Current System. J. Mar. Res., 45, 1-32.

Miller, R.N., A.R. Robinson, and D.B. Haidvogel, 1983: A baroclinic quasigeostrophic open ocean model, Journal of Computational Physics. 50(1), 38-70.

Mooers, C.N.K., C.A. Collins, and R.L. Smith, 1976: The dynamic structure of the frontal zone in the coastal upwelling region off Oregon. J. Phys. Oceangr., 6, 3-21.

_____, and A.R. Robinson, 1984: Turbulent jets and eddies in the California Current and inferred cross-shore transports. Science, 223, 51-53.

Nelson, C.S., 1977: Wind stress and wind stress curl over the California Current. NOAA Tech. Rep. NMFS SSRF-714. U.S. Dept. Commerce, 87 pp.

O'Brien, J.J., 1986: <u>Advanced Physical Oceanographic Numerical Modeling</u>. D. Reidel Publishing Company, 608 pp.

Olivier, D.A., 1986: <u>Numerical simulations of the California Current: filament formation as related to baroclinic instability</u>, Master's Thesis. Naval Postgraduate School, Monterey, CA, 68 pp.

Pares-Sierra, A.. 1987: <u>Interannual variability of the California Current System: a numerical model</u>, Ph.D. Dissertation, Florida State University, Tallahassee, FL, 125 pp.

Philander, S.G.H., and J.-H. Yoon, 1982: Eastern boundary currents and coastal upwelling. <u>J. Phys. Oceanogr.</u>, <u>12</u>, 862-879.

Renaud, P.G., 1986: <u>Wind Forcing Experiments in the California Current System</u>, Master's Thesis. Naval Postgraduate School, Monterey, CA, 87 pp.

Rienecker, M.M., C.N.K. Mooers, D.E. Hagan, and A.R. Robinson, 1985: A cool anomaly off Northern California: An investigation using IR imagery and in situ data. <u>J. Geophys. Res.</u>, <u>90</u>, 4807-4818.

Rienecker, M.M., C.N.K. Mooers, and R.L. Smith, 1988: Mesoscale variability in current meter measurements in the California Current System off Northern California. <u>J. Geophys. Res.</u> (Submitted).

Robinson, A.R., 1983: <u>Eddies in Marine Science</u>, Springer-Verlag. New York. 609 pp.

Røed, L.P., and O.M. Smedstad, 1984: Open boundary conditions for forced waves in a rotating fluid. <u>SIAM J. Sci. Stat. Comput.</u>, <u>5</u>, 414-426.

_____, and C.K. Cooper, 1985: Open boundary conditions in numerical ocean models. <u>Advanced Physical Oceanographic Numerical Modeling</u>. (J.J. O'Brien, Ed.), D. Reidel Publishing Company, 411-436.

Semtner, A.J., Jr., and Y. Mintz, 1977: Numerical simulation of the Gulf Stream and mid-ocean eddies. <u>J. Phys. Oceanogr.</u>, <u>7</u>, 208-221.

Thomson, R.E., 1984: A cyclonic eddy over the continental margin off Vancouver Island: Evidence for baroclinic instability. <u>J. Phys. Oceanogr.</u>, <u>14</u>, 1326-1348.

Watts, D.R. and W.E. Johns, 1982: Gulf Stream meanders: Observations on propagation and growth. <u>J. Geophys. Res.</u>, <u>87</u>, 9467-9476.

INITIAL DISTRIBUTION LIST

No. Copies

1. Defense Technical Information Center   2
   Cameron Station
   Alexandria, VA   22304-6145

2. Library, Code 0142   2
   Naval Postgraduate School
   Monterey, CA   93943-5002

3. Chairman (Code 68Co)   1
   Department of Oceanography
   Naval Postgraduate School
   Monterey, CA   93943-5000

4. Chairman (Code 63Rd)   1
   Department of Meteorology
   Naval Postgraduate School
   Monterey, CA   93943-5000

5. Prof. M. L. Batteen (Code 68Bv)   2
   Department of Oceanography
   Naval Postgraduate School
   Monterey, CA   93943-5000

6. Prof. R. L. Haney (Code 63Hy)   2
   Department of Meteorology
   Naval Postgraduate School
   Monterey, CA   93943-5000

7. Prof. D. C. Smith, IV (Code 68Si)   1
   Department of Oceanography
   Naval Postgraduate School
   Monterey, CA   93943-5000

8. LCDR Terrance A. Tielking, USN   2
   Operations Department
   U.S.S. MIDWAY (CV-41)
   FPO San Francisco, CA   96631-2710

9. Director Naval Oceanography Division   1
   Naval Observatory
   34th and Massachusetts Avenue NW
   Washington, DC   20390

105

10. Commander 1
    Naval Oceanography Command
    NSTL Station
    Bay St. Louis, MS   39522

11. Commanding Officer 1
    Naval Oceanographic Office
    NSTL Station
    Bay St. Louis, MS   39522

12. Commanding Officer 1
    Fleet Numerical Oceanography Center
    Monterey, CA   93943

13. Commanding Officer 1
    Naval Ocean Research and Development Activity
    NSTL Station
    Bay St. Louis, MS   39522

14. Office of Naval Research (Code 1122PO) 1
    800 N. Quincy Street
    Arlington, VA   22217

15. Commanding Officer 1
    Naval Environmental Prediction Research Facility
    Monterey, CA   93943

16. Chairman, Oceanography Department 1
    U.S. Naval Academy
    Annapolis, MD   21402

17. Scientific Liaison Office 1
    Office of Naval Research
    Scripps Institution of Oceanography
    La Jolla, CA   92037

18. Commander 1
    Oceanographic Systems Pacific
    Box 1390
    Pearl Harbor, HI   96860

19. Commanding Officer 1
    Naval Eastern Oceanography Center
    Naval Air Station
    Norfolk, VA   23511

20. Commanding Officer 1
    Naval Western Oceanography Center
    Box 113
    Pearl Harbor, HI   96860

21. Commanding Officer   1
    Naval Oceanography Command Center, Rota
    Box 31
    FPO New York, NY   09540

22. Commanding Officer   1
    Naval Oceanography Command Center, Guam
    Box 12
    FPO San Francisco, CA   96630

23. Dr. T. Spence, Director   1
    Physical Oceanography Program
    National Science Foundation
    Washington, DC   20550

24. Dr. C. N. K. Mooers, Director   1
    Institute for Naval Oceanography
    Bldg. 1100, room 311
    NSTL Station
    Bay St. Louis, MS   39529

25. Director of Research Administration   1
    Code 012
    Naval Postgraduate School
    Monterey. CA   93943